Key Engineering Materials
ISSN: 1662-9795, Vol. 895, pp 139-146

Submitted: 2021-03-02
Revised: 2021-03-09
Accepted: 2021-04-12
Online: 2021-08-03

Assessment of Asphalt Mixture Behaviour Containing Recycled Concrete Aggregates

Sarah Safaaldeen Musa[1,a], Noorance Al-Mukaram[1,b*] and Mohammed Bally Mahdi[1,c]

[1]Civil Engineering Department, Al-Muthanna University, Samawah, Iraq

[a]almusawysarah@mu.edu.iq, [b]noorance@mu.edu.iq, [c]engmohbaly@mu.edu.iq

Keywords: Asphalt concrete mixture, concrete waste, recycled concrete aggregates (RCA), construction and demolition waste (CDW).

Abstract. Recently, the construction industry uses the Recycled Concrete Aggregates (RCA) resulting from construction and demolition waste (CDW) to achieve sustainable requirements and economic benefits. In this paper, asphalt paving mixes were prepared with RCA instead of natural aggregates for the base course in flexible road pavements and walking areas used by pedestrians and cyclists. Different asphalt mixes samples were prepared with different asphalt contents to meet the required specifications. Additionally, several laboratory tests were carried out to assess mixture behavior including the Marshall test. The results indicated that the mixture made with aggregates of CDW have met all the requirements of Iraqi specifications of roads and bridges (SORB/R9). This investigation could be a useful guide for road engineers in designing asphalt mixtures from RCA.

Introduction

Construction and demolition waste (CDW) are one of the majority of environmental pollutants. The CDW accounts for approximately 30% and 75% of all generated waste in the EU and US, respectively [1]. However, it can be considered as a valuable resource of recovered materials. For example, recycled concrete aggregate (RCA) is produced from raw construction materials such as crushed concrete slabs, curbs, foundations, and columns. As usual, the recycling process includes breaking and crushing existing concrete after removing reinforcing steel, wood, and other embedded items. Finally, the recycled aggregates will be ranged based on particle size and quality for reuse. Accordingly, the cost of using RCA in mixtures is 40% less compared to mixtures that include natural aggregates [2]. Also, about 35% of RCA is reused in producing asphalt paving mixes and the remaining is used for road soil improvement in the lower layers particularly base and sub-base courses [3,4,5,6,7,8].

Many research has been conducted to assess the performance of bituminous mixtures that containing RCA from CDW materials. Most studies have concluded that hot mix asphalt (HMA) made with RCA show less quality and less water damage resistance than conventional mixtures. Weak adhesion contact between bitumen and recycled aggregates must be considered because of the low density and porous surface of RCA [9,10,11,12]. Other researchers indicated that the high pH value of RCA may result in a weak bond between the bitumen and the surface of RCA [13]. Also, the optimum asphalt content is affected by the content of RCA in the mix. Studies indicated that as the percentage of RCA increases, the optimum asphalt content (OAC) increases gradually as well. Specifically, a study highlighted that adding a fine fraction of RCA may increase bitumen consumption [14]. This is logical because of the large specific surface area which may lead to an increase in the bitumen content [12,15]. For economic purposes, high asphalt content can be reduced by adding RCA in the coarse fraction [16].

Otherwise, previous studies demonstrated that some treatments for HMA including RCA show significant results to improve the behavior of these mixtures [11,13,17,18]. Researchers from Spain demonstrated that the moisture damage resistance of HMA can be improved by curing the mix for a sufficient time in the oven at high temperatures before compaction. It was indicated that Marshall stability and water damage resistance are shown significant improvements by allowing HMA samples with 30% of RCA for 4 hours in the oven for the base course in flexible pavements [15].

Furthermore, more investigations are required to acquire a better understanding of treatments that can improve the properties of HMA made with RCA. With regards to HMA design, it is worth mentioning that better mix design and quality can be achieved by taking into consideration not only the OAC and absorbed asphalt content but also the proportions of filler and non-absorbed asphalt by aggregate pores [19].

Finally, the objective of the current work is to investigate the behavior of asphalt mixture using RCA instead of natural aggregate for paved base course of roads. This work could be of interest of providing jobs, investment, and infrastructure for recycling CDW materials. The next section presents the methodology used in the current study.

Methodology

Materials. Three materials were provided for preparing asphalt concrete mixtures. They are locally available in Iraq as follows:

1- Bitumen binder: One bitumen type of penetration grade 40/60 was used in the current work produced in the Samawah refinery. The physical properties of the bitumen used can be shown in Table 1.

2- Recycled aggregates: These materials were selected from a destroyed concrete building. After removing reinforcing and other embedded items, recycled concrete aggregates were separated into different sizes by sieving as illustrated in Fig. 1. For this study, the RCA mix design was prepared by combining desired RCA sizes with filler to meet the requirements of Iraqi specification SORB/R9 [20] of paved base course as shown in Table 2.

3- Filler: Cement was used as filler material in the existing work, which is manufactured in the Samawah factory. The physical properties can be presented in Table 3.

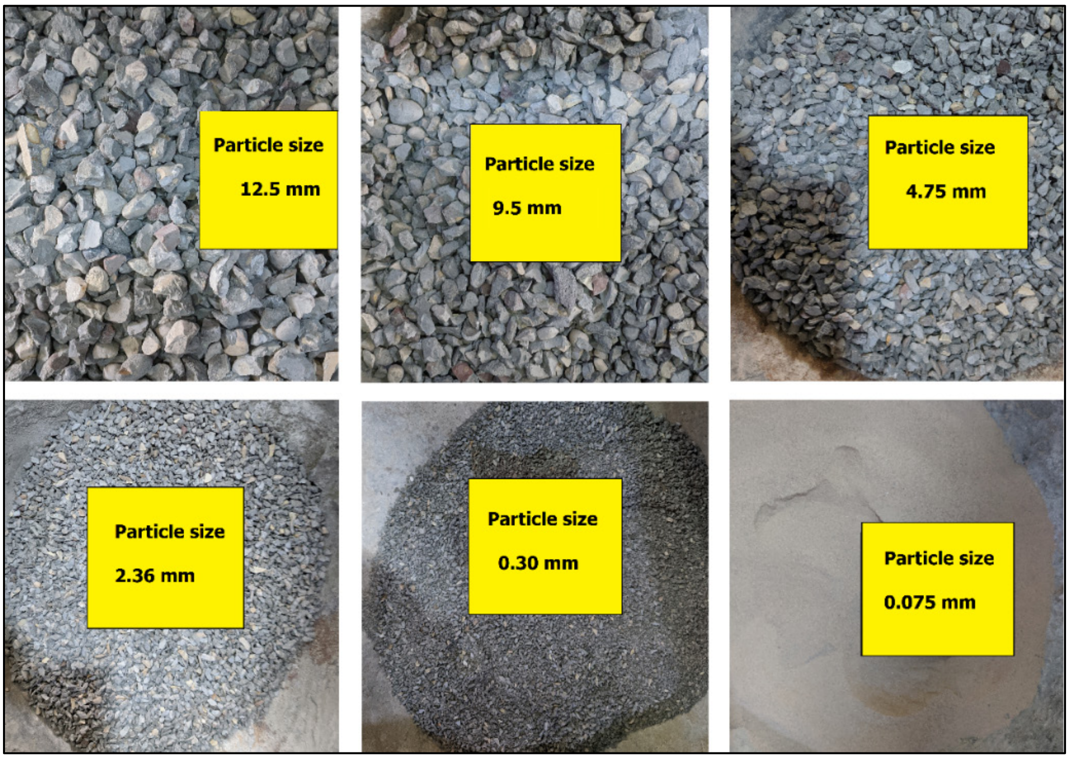

Figure 1. Recycled concrete aggregates used in the current work

Table 1. Physical properties of asphalt binder used

Test	Unit	Penetration Grade (40/50)	ASTM	Reference
Penetration 100 gm , 25° C , 5 sec	1/100 mm	43	D5	[21]
Absolute Viscosity at 60° C	Poise	3268	D88	[22]
Kinematic Viscosity at 135° C	C st	403	D88	[22]
Ductility 5 cm/min , 25° C	cm	130	D113	[23]
Softening Point (Ring & Ball)	C°	56.7	D36	[24]
Specific Gravity at 25° C	-----	1.02	D70	[25]
Flash Point (Cleveland Open Cup)	C°	253	D92	[26]

Table 2. RCA mix design according to Iraqi specification SORB/R9 for asphalt concrete base course

Sieve size (mm)	Passing %					Combined Gradation	Iraqi SORB/R9 Ranges [20]
	RCA > 1 1/2″ (15%)	RCA > 1/2″ (10%)	RCA > No.4 (35%)	Natural Sand (35%)	Filler (5%)		
50	100	100	100	100	100	100.0	100
37.5	100	100	100	100	100	100.0	100
25	51.7	100	100	100	100	92.8	90 – 100
19	2.4	98.8	100	100	100	85.2	76 – 90
12.5	0.7	28.4	90.8	100	100	74.7	56 – 80
9.5	0.5	3.2	64.6	99.3	100	62.8	48 – 74
4.75	0	0	1	90.5	100	37.0	29 – 59
2.36	0	0	0	77.3	100	32.1	19 – 45
0.3	0	0	0	20	100	12.0	5 – 17
0.075	0	0	0	0	94	4.7	2 – 8

Table 3. Physical properties of cement

Properties	Results	Specification	Reference
% Passing Sieve No. 200	100%	ASTM C117	[27]
Liquid limit (L.L %)	25%	SORB/R9	[20]
Plasticity index (P.I%)	3.4%	SORB/ R9	[20]

Preparation of asphalt concrete mixture. After preparing the required materials as described in the previous section, the preparation of asphalt mixture was based on ASTM D6926 [28]. The combined RCA was firstly oven-dried before the mixing process. Next, fifteen mixtures were prepared using five bitumen contents 4.0, 4.5, 5.0, 5.5, and 6.0% (i.e. three specimens for each asphalt content). The combined RCA was then heated to 155 °C before mixing with the bitumen. As well, the asphalt binder was heated to the temperature that produces a kinematic viscosity of (170 ± 20) centistokes (up to 163 °C as an upper limit). Next, the asphalt binder was weighted to the desired amount to be mixed until all crushed concrete particles (i.e. heated RCA) were coated by bitumen.

Following that, a clean mold of 101.6 mm diameter and 76.2 mm height with extension collar and base plate was prepared for placing the hot mix in. Next, the mold was placed in the compaction pedestal and applied 75 blows from a hummer falling 457.2 mm distance perpendicularly to the upper mold base. The compaction method from falling hummer can be repeated with 75 blows on the bottom base after removing the plate and collar. Each produced specimen was weighted on about 1200 gm after the compaction process.

Tests of asphalt concrete mixture. In this work, two tests were conducted on the prepared asphalt concrete mixtures. These can be described in the following subsections:

Marshall test for base course. Marshall test was implemented to find out the optimum asphalt content (OAC) in the mix according to ASTM D6927 [29]. Before placing a specimen in the Marshall apparatus, several measurements were carried out to determine the density and specific gravity. The procedures include recording the weight of each specimen before and after immersing in water for three minutes. Then, it was placed in a water bath at 60 ±1°C for 30-40 minutes, or in an oven for two hours at least until the temperature of the model reached 60 °C. After drying the specimen, it was tested in the Marshall apparatus for recording the stability and flow values at maximum load before deformation occurred. Finally, the resistance to plastic flow can be expressed by Marshall stiffness which can be determined from the following formula:

$$Marshall\ Stiffness = Marshall\ Stability\ /\ Marshall\ Flow \tag{1}$$

Immersion compression ratio test. This test was performed as per ASTM D1075 [30] to measure the loss of compressive strength due to the water effect on compacted specimens. Six specimens were prepared for the compressive strength test after obtaining the optimum bitumen content (OAC) from the Marshall test. Three of them were tested after 4 hours of storing in an air bath at 25 °C. While the others were placed in a water bath for 96 hours at 50 °C, then transferred to another water bath at 25 °C for 2 hours before testing for compressive strength. The numerical index that calculated the loss of strength can be expressed in the following formula:

$$IRS\ \% = \frac{S_2}{S_1} \times 100 \tag{2}$$

Where *IRS* is the index of retained strength in percent, S_1 and S_2 are the compressive strengths of dry and immersed specimens, respectively.

Results and Discussion

Resistance to plastic flow (Marshall test). The results of the Marshall test can be illustrated in Fig. 2. As shown in Fig. 2a, the stability values decrease as the asphalt contents increase. The asphalt content was 4.4% that achieved maximum stability at 9.25 kN. Also, the results presented that the stability values were within the allowable limit that should not be less than 5 kN for the base course according to the Iraqi specifications of roads and bridges SORB/R9 [20].

On the other hand, flow values were recorded in the Marshall test as shown in Fig. 2b. It can be indicated that flow values increase rapidly as the asphalt contents increase. Based on the Iraqi specifications of roads and bridges SORB/R9 [20], the acceptable flow values should be within the range of (2 – 4 mm) for the base course. As a result, an average flow value of 3 mm could be achieved at asphalt content equal to 4.7%. The results in Fig. 2c depict a decrease in Marshall stiffness with the increase in the asphalt content.

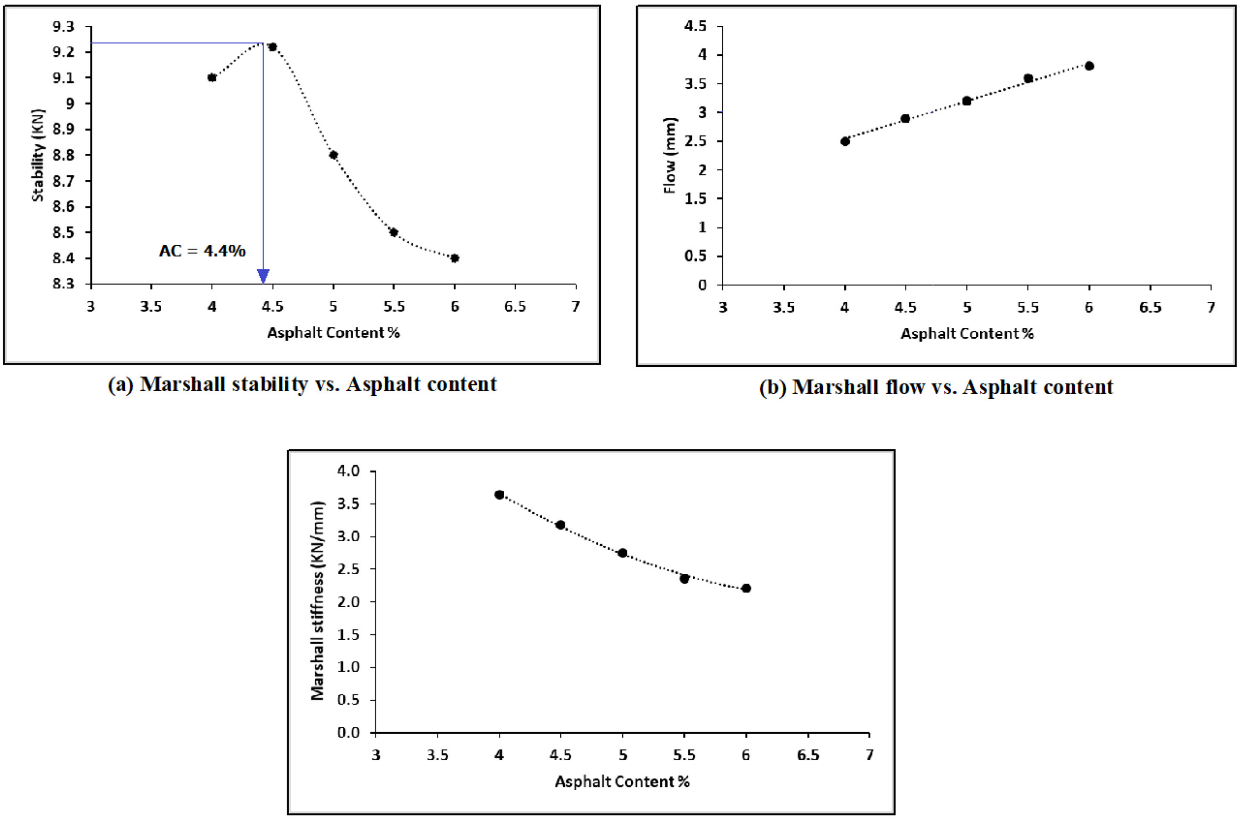

(a) Marshall stability vs. Asphalt content

(b) Marshall flow vs. Asphalt content

(c) Marshall stiffness vs. Asphalt content

Figure 2. Results of resistance to plastic flow (Marshall test)

Other results of asphalt contents in relation to bulk density, air voids, and voids in mineral aggregate (VMA) in percent can be shown in Fig. 3a, 3b, and 3c respectively. The asphalt content of 5.05% was achieved at a bulk density equal to 2.505 gm/cm^3. Then, a decrease in the magnitudes of bulk density was recorded as the asphalt contents increased as shown in Fig. 3a. Similarly, the percentages of air voids were determined and the results were illustrated in Fig. 3b. According to the Iraqi specifications of roads and bridges SORB/R9 [20], the acceptable limits of air voids are within the range of (3 – 6 %). As a result, the asphalt content of 4.75% could be achieved at air voids equal to 4.5%. Additionally, the VMA% were recorded between 13 and 16 for mixtures prepared with asphalt content less than 6% as shown in Fig. 3c. These results are accepted since the Iraqi SORB/R9 [20] recommends that the accepted VMA% should be 12% as a minimum.

Finally, the optimum asphalt content (OAC) can be determined by computing the average of means values of asphalt contents at maximum stability and maximum density as well as asphalt median of air voids ratio following previous works [31,32]. The OAC value was equal to 4.73%.

Resistance to moisture damage (Index of retained strength test). Other results in relation to moisture damage can be obtained by calculating the *IRS%* at obtained OAC value of 4.73%. According to the Iraqi specifications SORB/R9 [20], the accepted *IRS%* value should not be less than 70%. The values of S_1 and S_2 were equal to 2645 kg and 2430 kg, respectively. As a result, the accepted *IRS%* value was approximately equal to 92%.

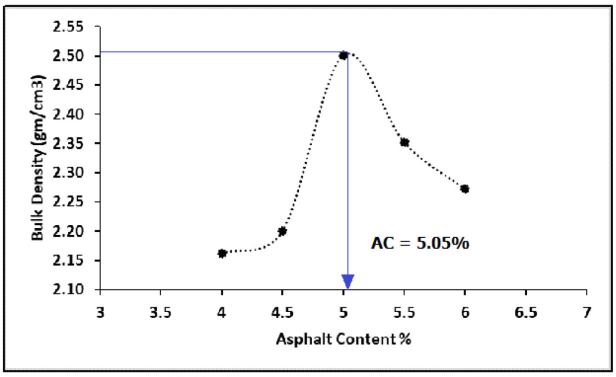

(a) Bulk density vs. Asphalt content

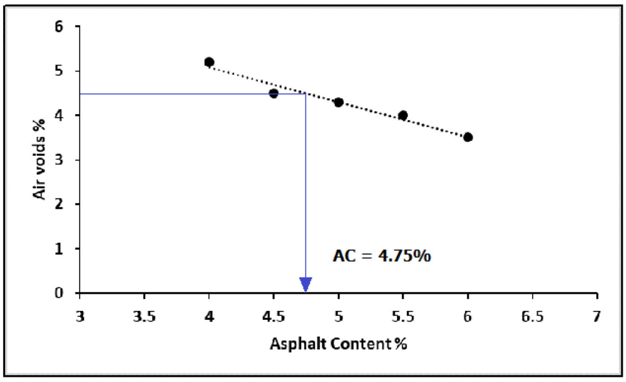

(b) Air voids% vs. Asphalt content

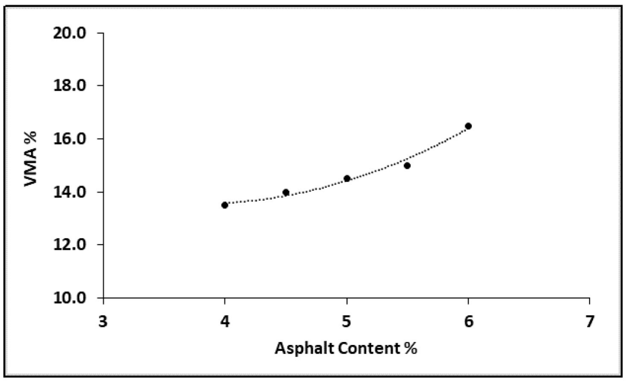

(c) VMA% vs. Asphalt content

Figure 3. Results of asphalt concrete mixture with regards to bulk density, air voids%, and VMA%

Summary

The methodology was defined in this study. The Iraqi specifications of roads and bridges SORB/R9 [20] were adopted in the current work for achieving mixed design requirements. Combined aggregate gradation was met the Iraqi SORB/R9 specification of the paved base course. Table 4 presents the results of tests that were conducted on asphalt concrete mixture prepared with 100% RCA. The results of Marshall and index of retained strength tests were obtained at optimum asphalt content equal to 4.73%. As a result, it can be suggested that the designed mixture was met all the requirements of SORB/R9 for paving base course at off-street parks and roads with low traffic, particularly at residential areas.

Table 4. Summary of the results of asphalt concrete mixture prepared with 100% RCA for base course

Test	Results of the current study	Iraqi SORB/R9 ranges of base course	Remarks
Marshall test			
OAC%	4.73%		
Bulk density at OAC%	2.34 gm/cm^3		
Marshall stability at OAC%	9.08 kN	Min 5 kN	Accepted
Marshall flow at OAC%	3.05 mm	2 – 4 mm	Accepted
Air voids at OAC%	4.6 %	3 – 6 %	Accepted
VMA% at OAC%	14.3%	Min 12%	Accepted
Immersion compression ratio test			
IRS%	92%	Min 70%	Accepted

Conclusions and Recommendations

This study aims to make an asphalt concrete mixture with 100% replacement of natural aggregate by RCA. Economically, these materials are lower cost and can be obtained from concrete waste. It is worth mentioning that the installation of waste recycling plants may affect positively reducing environmental pollutants particularly concrete wastes.

Furthermore, several recommendations can be drawn for future studies as follows:

1- These results are complete can be applied to prepare asphalt concrete mixture for the base course.
2- Using different proportions of RCA in the asphalt concrete mixtures for obtaining better results.
3- Using different aggregate gradations for other paved courses such as binder and surface courses.
4- Using different bitumen and filler types and contents to achieve the requirements of asphalt concrete mix design.

References

[1] P.J. Cosentino and H.H. Howell, Developing re-use applications and improving the economic benefits of Florida's waste materials. 2006, Florida Center for Solid and Hazardous Waste Management: USA.

[2] S.A. Frondistou and T. Itoh, Economic feasibility of concrete recycling. Journal of the Structural Division, 1977. 103(4): pp. 885-899.

[3] S.A. Chini, T.J. Sergenian and J. Marmaghani, Use of recycled aggregates for pavement. In: Materials for the new millennium. 2001: Washington, USA.

[4] S. Jayakody, C. Gallage, and A. Kumar, Assessment of recycled concrete aggregates for road base and sub-base. The 2nd International Conference on Geotechnique, Construction Materials and Environment. 2012: Kuala Lumpur, Malaysia.

[5] J.R. Jiménez, F. Agrela, J. Ayuso, and M. López, A comparative study of recycled aggregates from concrete and mixed debris as material for unbound road sub-base. Material Construction, 2011. 61(302): pp. 289-302.

[6] T.D. Kelly, The substitution of crushed cement concrete for construction aggregates. Geological Survey Circular 1177. 1998, USA.

[7] B. Prowell, G.E. Hurley and B. Frank, Warm-Mix Asphalt: Best Practices. Second edition. 2011, Lanham, MD, USA: National Asphalt Pavement Association (NAPA).

[8] S. Rakshvir and S.V. Barai, Studies on Recycled aggregates bases concrete. Waste Management Research, 2006. 24(3): pp. 225-233.

[9] S. Daquan, T. Yang, G. Sun, P. Qi, Y. Fan, and Z. Xingyi, Performance evaluation of asphalt mixtures containing recycled concrete aggregates. International Journal of Pavement Engineering, 2018. 19(5): pp. 422-428.

[10] Y. Hou, X. Ji, J. Li and X. Li, Adhesion between asphalt and recycled concrete aggregate and its impact on the properties of asphalt mixture. Journal of Materials, 2018. 11: pp. 25-28.

[11] C.H. Lee, J.C. Du and D.H. Shen, Evaluation of pre-coated recycled concrete aggregate for hot mix asphalt. Construction and Building Materials, 2012. 28: pp. 66-71.

[12] I. Pérez, J. Gallego, M. Toledano, and J. Taibo, Asphalt mixtures with construction and demolition debris. Proceedings of the Institution of Civil Engineers - Transport, 2010. 163(4): pp.1-9.

[13] Z.Y. Pan, G. Li, C.Y. Hong, H.L. Kuang, Y. Yu, F.X. Feng, D.M. Liu, and H. Du, Modified recycled concrete aggregates for asphalt mixture using microbial calcite precipitation. Journal of the Royal Society of Chemistry (RSC) Advances, 2015. 5(44): pp. 34854–34863.

[14] M.M. Rafi, A. Qadir and S.H. Siddiqui, Experimental testing of hot mix asphalt mixture made of recycled aggregates. Waste Management Research, 2011. 29(12): pp. 1316-1326.

[15] A.R. Pasandín and I. Pérez, Performance of hot-mix asphalt involving recycled concrete aggregates. International Journal of Pavement Engineering, 2020. 21(9): pp. 1044-1056.

[16] S. Bhusal, X. Li and H. Wen, Evaluation of Effects of Recycled Concrete Aggregate on Volumetrics of Hot-Mix Asphalt. 2011. 2205(1): pp. 36-39.

[17] A.R. Pasandín and I. Pérez, Mechanical properties of hot-mix asphalt made with recycled concrete aggregates coated with bitumen emulsion. Construction and Building Materials, 2014. 55: pp. 350–358.

[18] J. Qiu, D.Q.S. Tng and E.H. Yang, Surface treatment of recycled concrete aggregates through microbial carbonate precipitation. Construction and Building Materials, 2014. 57: pp. 144-150.

[19] Asphalt Institute, Mix design methods for asphalt concrete and other hot-mix types. MS-2. 1997.

[20] Ministry of Construction and Housing, General specification for roads and bridges (SORB/R9). 2003: Iraq.

[21] ASTM D5/D5M-20, Standard test method for penetration of bituminous materials, ASTM International, West Conshohocken, PA, 2021, www.astm.org.

[22] ASTM D88/D88M e1, Standard test method for saybolt viscosity, ASTM International, West Conshohocken, PA, 2021, www.astm.org.

[23] ASTM D113-17, Standard test method for ductility of asphalt materials, ASTM International, West Conshohocken, PA, 2021, www.astm.org.

[24] ASTM D36/D36M-14(2020), Standard test method for softening point of bitumen (Ring and Ball Apparatus), ASTM International, West Conshohocken, PA, 2021, www.astm.org.

[25] ASTM D70/D70M-21, Standard test method for specific gravity and density of semi-solid asphalt binder (Pycnometer Method), ASTM International, West Conshohocken, PA, 2021, www.astm.org.

[26] ASTM D92-18, Standard test method for flash and fire points by Cleveland open cup tester, ASTM International, West Conshohocken, PA, 2021, www.astm.org.

[27] ASTM C117-17, Standard test method for materials finer than 75-µm (No. 200) sieve in mineral aggregates by washing, ASTM International, West Conshohocken, PA, 2021, www.astm.org.

[28] ASTM D6926-20, Standard practice for preparation of asphalt mixture specimens using Marshall apparatus, ASTM International, West Conshohocken, PA, 2021, www.astm.org.

[29] ASTM D6927-15, Standard test method for Marshall stability and flow of asphalt mixtures, ASTM International, West Conshohocken, PA, 2021, www.astm.org.

[30] ASTM D1075-11, Standard test method for the effect of water on compressive strength of compacted bituminous mixtures, ASTM International, West Conshohocken, PA, 2021, www.astm.org.

[31] B.J. Al-Saeedi and H.A. Al-Jameel, Sustainable Performance of Iraqi Asphalt Base Course Using Recycled Glass as Aggregate Replacement. Journal of University of Babylon, 2018. 26(5): pp. 63-80.

[32] M. Arabani, Effect of glass cullet on the improvement of the dynamic behavior of asphalt concrete. Construction and Building Materials, 2011. 25(3): pp. 1181-1185.

Vol. (7), No. (2), (2019), 82-89
MUTHANNA JOURNAL OF ENGINEERING AND TECHNOLOGY (MJET)
مجلة المثنى للهندسة والتكنولوجيا
Journal homepage:www.muthjet.com
Print ISSN:2572-0317, Online ISSN:2572-0325

Efficiency Development of Light Weight High Strength Concrete by using Carbon Fibers.

Haider Araby Ibrahim[1,*], Mohammed Bally Mahdi[2], Basim Jabbar Abbas[3]
[1, 2, 3] Civil Engineering Department, Al-Muthanna University, Samawa, IRAQ

ARTICLE INFO

Received: 05/09/2019

Accepted: 06/11/2019

Keywords
Light weight high strength concrete, Carbon Fibers, Silica Fume, compressive strength

ABSTRACT
This study aims to progress brittleness of the high strength lightweight aggregate concrete (HSLWAC) by using Porcelinite stone as light weight aggregates and silica fume with water cement ratio 0.28 to give 41.34 MPa compressive strength at 28-days and reinforced with carbon fibers. Fifteen mixtures using in this work with three various lengths of (5mm, 10mm, and 20mm), five mixes for every length with volume fractions (0.25%, 0.5%, 1.0%, 1.5%, and 2%) of carbon fibers. The slump test, compression strength, flexural strength, splitting tensile strength, and modulus of elasticity were investigated to determine the mechanical properties of (HSLWAC). The density of reference (HSLWAC) that was get through the experimental work was (1835 Kg/m^3) at (28) days. The results shown that at general, the brittleness of (HSLWAC) improved with increased the content and length of carbon fibers, The optimum properties was for mix (L5) of 20mm length and 2% of carbon fibers of 45.44 MPa, 3.21MPa ,and 6.97MPa for compression strength, flexural strength, splitting tensile strength respectively.

*Corresponding author:
E-mail addresses: **arabyhaider@yahoo.com**

DOI: 10.18081/mjet/2019-7/82-89

Introduction

The use of high-strength Lightweight concrete (HSLWAC) can reduce the self-weight of structures and cross-sectional areas of structural elements. Both can increase the effective usable space for high-rise buildings and increase the span length for bridges [1]. The requirement for structural high strength lightweight aggregate concrete (HSLWAC) in many contemporary construction is increasing, owing to the benefit of higher strength/weight ratio, better capacity of tensile strain, minimum coefficient of thermal expansion because of the voids existing in the lightweight aggregates (L.W.A) and minimum density that is suitable for a decrease of load-bearing elements and the foundation size [2]. The lightweight high strength concrete has densities from 1000 to 2000 kg/m^3 and compressive strength more than 40 MPa [3]. Lightweight aggregates are normally available (volcanic cinders, pumice, diatomite, etc.) or unnaturally made (expanded shale, PFA, perlite, slate, etc.) [4].

(HSLWAC) is considered as a relatively brittle material as the concrete is strong under compression and weak under tension or flexure. Carbon fibers are inert, medically safe, chemically stable, low in density, and their strength-to-density ratio is one of the highest among all fiber types. Carbon fiber has a very high tensile strength (2110 to 2815 N/mm^2) and young's modulus. Patodi, and Rarhod, have concluded that, cement composites made with carbon fiber, as reinforcement will have very high modulus of elasticity and flexural strength [2].

Literature Review

There are many studies have dealt with improved (HSLWAC) characteristics:

Abdul kader Ismail A. et al. in (2013) [7]. Studied the mechanical properties of lightweight aggregate concrete (LWAC) using chopped carbon fibers 5mm length, 10μm diameter with different ratios of volume (0.5%, 1%, and 1.5%) results showed that the addition of carbon fiber increases the compressive strength is about 30%, splitting tensile strength about 58% and flexural strength about 35%.

Xiang Shu et al. in (2014) [6] carried out to investigate the effects of carbon fiber with different sizes on the mechanical properties of Portland cement mortar. The laboratory test results show that the hybrid fiber mix exhibited superior tensile performance to the microfiber mix.

Wasan Ismail Khalil, et al. in (2015) [7] studied some properties of high strength lightweight aggregate concrete (HSLWAC) reinforced with mono and hybrid fibers in different dimensions and types. High strength porcelinite lightweight aggregate concrete mix. The results shown that mono and hybrid fiber reinforced HSLWAC specimens show significant increase in splitting tensile strength and flexural strength in comparison with plain HSLWAC specimen.

Akar Abdulrazaqet al. in (2011) [8]. Studied the influence of high performance carbon fiber concrete using superplasticizer and condensed silica fume reinforced with different volume fractions (0%, 0.2%, 0.3%, 0.4% and 0.5%) of carbon fibers the results show that the addition of carbon fibers improves the mechanical properties of high performance concrete the addition of carbon fibers causes a slight increase in compressive strength and modulus of elasticity of high performance concrete when the fiber volume fraction increases, while the splitting tensile and flexural strengths shows a significant increase relative to the reference high performance concrete (without fiber). The percentage increase in splitting tensile and flexural strengths for high performance concrete with fiber volume fraction 0.5% at 28 days is about 45% and 46% respectively.

Materials

1. Cement

Type I, ordinary Portland cement used in this study from Al- Douh refectory. Test results shown the cement identified with Iraqi specifications No. 5/1984 [9] .The properties of cement shown in the table (1) and (2).

Table (1). Chemical properties of cement

Oxide Percentage	Cement	Limit of Iraqi Spec. No.5/1984
CaO	63.2	-
SiO2	18.9	-
Al2O3	3.8	-
Fe2O3	4.6	-
SO3	1.5	≤ 2.5
Mg O	1.7	5.0
L.O.I	1.9	4.0
L.S.F	0.9	0.66-1.02
I.R	0.4	≤ 1.5

Table (2). Physical properties of cement

Physical Properties	Test results	Limit of Iraqi Spec. No.5/1984
Initial setting time (vicat)	65 min.	≥ 45 min.
Final setting time (vicat)	170 min.	≤ 375
Compressive strength of mortar (MPa) 3-days	19.0	≥ 15
Compressive strength of mortar (MPa) 7-days	30.5	≥ 21
Specific gravity	3.1	-
Specific surface	3000	-

2. Aggregate.

2.1. Coarse Aggregate.

Porcelinite stone was used as coarse aggregate. The quarry of this stone is located in Rutba at the western desert in Anbar. It was received in medium lumps from the State Company of Geological Survey and Mining. The physical, chemical and mineral analysis tests were done by the State Company of Geological Survey and Mining (SCGSM). The stone was crushed by crushing machine. The maximum aggregate size was 12.5 mm. Porcelinite was graduated to the grading which was presented in table (3). Due to the porcelinite cellular structure, lightweight aggregate (LWA) absorbs more water than normal weight aggregate. In order to avoid the continuous absorption of porcelinite LWA which caused rapid slump loss, the aggregate was washed with water for sufficient time to attain saturation. Then , the water was dripped off and the aggregate spreads inside the laboratory for suitable time to bring the aggregate particles to saturated surface dry condition (SSD), which is recommended by ACI committee 211[9] respectively.

Table (3): Grading of Porcelinite Aggregate.

Sieve Size (mm)	Passing %	ASTM C330-04[16]
12.5	100	90-100
9.5	96	85-100
4.75	21	10-30
2.36	4	0-10
1.8	2	0-5

Table (4): Physical Properties of Fine Aggregate

Proprty	Results	Specification	Limit of Iraq Spec. No45/1984[17]
Bulk pecific gravity	2.55	ASTM C128-7[18]	
Absorption %	2.1	ASTM 128-97	
Dry loose unit weight (kg\m3)	1600	ASTM C29-97[14]	
Sulphate content SO3	0.09	I.O.S N 45-84	0.5(max)
Material finer than 0.075mm	0.7	BS-882-1965[19]	5.0(max)

2.2. Fine aggregate.

The grading of fine aggregate are listed in Table (4). A (4.75) mm maximum size of clean sand is used as fine aggregate. and compatible to the requirement of Iraqi specifications No. 45/1984 [10].

Table (5). Sieve analysis of fine aggregate.

Sieve size	Passing ratio (%)	Limit of ASTMC33-03
9.5mm	100.00	100
4.75mm	94.56	95-100
2.36mm	72.45	80-100
1.18mm	68.40	50-85
600µm	53.32	25-60
300µm	16.60	5-30
150µm	2.12	0-10

3. Superplasticizer.

Superplasticizer is high range water reducing additives, It meet the requirements of super plasticizer according to ASTM-C494 Type B, D and G [13].Table (6) shows the typical properties of superplasticizer. High range water reducing (HRWRA) added to decrease the water demand of the concrete, when Silica fume added and reducing w/c.

Table 6. Typical properties of superplasticizer

properties	Specifications
Specific gravity	1.2
Form	Liquid
PH	7-9

4. Silica Fume (SF)

Table (7) shown the properties of silica fume according to ASTM C-1240-05[14], which shown in Fig. (1-b), the silica fume added in a dry state to the cement and thoroughly mixed with it in order to provide a homogenous mixture. Silica fume have a very high water demand.

Table (7) shown the chemical and physical properties of silica fume.

Oxide composition	Oxide Content%	Physical Properties	ASTM C-1240 Limitations
SiO_2	91.4	-	≥ %85
L.O.I	0.53	-	≤ 6.0
SO_3	0.13	-	
MgO	1.03	-	-
Na2O	0.16	-	-
Percent retained on 45µm(No. 325) sieve ,max ,%	8	-	≤ 10
Specific gravity	-	2.21	-
Bulk density	-	310 kg/m^3	-
Specific Surface	-	20 m^2/gm.	≥ 15
form	-	Amorphous	-

5. Carbon Fiber (C.F.)

A High execution of carbon fiber used in this study shown in Fig. (1-a). Carbon fiber complied with requirements of ASTM C1116-02 [12].Table (8) indicated the characteristics of carbon fiber High performance high strength chopped carbon fiber brought form waste factory as filaments was used in this investigation. Table (8) indicates the mechanical properties of chopped carbon fiber used in this investigation.

Table (8): Physical and Technical Properties of carbon Fiber (C.F.)

Properties	Results
Filament Diameter, µm	8
Bulk Density (min.), g/L	427
Elongation, %	1.53
Tensile Strength, MPa	1635
Flexural Strength, MPa	260

(a)

(b)

Figure (1): (a) Carbon fibers (b) Silica fume.

Mix Proportions

The reference mixture is made by (ACI 211.2-02) [16], after several trial mixes were carried out in order to select the optimum dosage of (HRWRA) and silica fume. The (HRWRA) has been used to reduce the w/c ratio and maintain the same workability of the reference mix (100±5 mm slump according to ASTM C-143) which causes increase in the strength of LWAC. The selected HSLWAC has mix proportion of 1:1.35:1.87 (cement: sand: aggregate.) by weight with cement content 520 kg/m^3 and w/c ratio of 0.28, HRWRA 2.5 liter per 100 kg and 5% SF as replacement by weight of cement. The compressive strength and oven dry density of the selected mix are 62.3 N/mm^2 and 1955 kg/m^3 respectively at 28 day age. The carbon fiber is used in varying length 5 mm, 10 mm, and 20 mm with (0.25%, 0.5%, 1.0%, 1.5%, and 2%) in volume fraction. Table (8) shows the proportions of mixes of (HSLWAC) with coarse aggregate. for all mixtures the aggregates was used in saturated surface dry case (S.S.D.) Specific surface area of (S.F.) is greater than the cement, therefore the concrete performance is reduced fundamentally and more water is needed to fix it, because the concrete Performance should not be changed; the amount of superplasticizer is increased. [17].

Casting and Curing of (HSLWAC).

The samples cast in three layers by rodding 25 times with applying a vibration for (10) seconds. After mixing, the specimens disposed of the molds and maintained in the water until they will arrive the test age of (7) and (28) days when they are ready to do the experimental tests.

Concrete testing.

(HSLWAC) specimens prepared at general according to ASTM C192-02.[21].For each mix, six (150 mm) standard cubic steel molds used for casting specimens and for Compression strength in (7) and (28) days in agreement with ASTM C39-98 [22], the splitting tensile strength used two molds of (100X200) mm cylindrical concrete samples measured conformity to the ASTM C 496- 86[23], two (100X100X400mm) prisms for flexural strength at (28) day, correspond with ASTM(C293–02).[24].

Table 9: Mix Proportion for cubic meter of concrete.

Ingredients	Quantity (kg/m^3)
Cement content	520
Fine aggregate	700
Coarse aggregate	995
water	146
Superplasticizer	11.3
Silica fume	5

Table 10: Mix Designation for fiber content in volume fraction.

Fiber Volume friction (%)	Length of carbon fiber (mm)		
	5	10	20
0	CF0	CF0	CF0
0.25	M1	N1	L1
0.5	M2	N2	L2
1.0	M3	N3	L3
1.5	M4	N4	L4
2.0	M5	N5	L5

Results and Discussion

Workability (slump)

In this study, the quantity of water and SP were kept constant for all mixes in order to evaluate the effects of different CF fibers on the workability of OPC. Slump tests were carried out to determine the consistency of fresh concrete. The use of carbon fibers is well known to affect the workability and flowability of plain concrete intrinsically [26]. From Fig. 2, it can be seen that the slump value of fresh (HSLWAC) decreases due to an increase in CF fiber volume fraction. The addition of carbon fibres from 0.25% to 2% of volume fraction for length 5mm reduces the range of slump values by approximately 6.3%–36.8%. The results also indicate that, the carbon fibers of long length produced a lower slump, for length 10 mm the reduction in slump values was 9.5%-38.9% and length 25 mm the reduction in slump values was 15.8%-40%. Mehta and Montero [26] reported that a slump value for structural lightweight concrete in the range of 50–75 mm is comparable to an equivalent value of slump of 100–125 mm for normal concrete. This phenomenon might be attributed to the long length of fibres have higher effective surface area for the cement paste to wrap around due to the high fiber content and long of fibres, which in turn, increases the viscosity of the development of a fiber–matrix bond compared to shorter fibres. The bond increases the viscosity which restrains the mixture from segregation and flow. The fibres have the tendency to absorb admixture [27].

Table 11: Fresh and hardened properties of (HSLWAC) with carbon fibers

Length of Carbon Fibers (mm)	% of Carbon Fibers	Slump (mm)	Compressive Strength MPa 7-days	Compressive Strength MPa 28-days	Split Tensile Strength MPa	Flexural Strength MPa	Modulus of Elasticity MPa
5	0	95	35.14	41.34	2.12	3.74	27722
	0.25	89	35.43	41.68	2.33	4.54	27903
	0.5	81	35.83	42.15	2.48	4.88	28098
	1.0	73	36.19	42.58	2.69	5.25	29256
	1.5	66	36.75	43.23	3.01	5.89	31510
	2.0	60	36.91	43.42	3.15	6.01	32617
10	0	95	35.14	41.34	2.12	3.74	27722
	0.25	86	35.57	41.85	2.45	4.68	28120
	0.5	78	36.11	42.48	2.88	5.34	28311
	1.0	70	36.52	42.97	3.01	5.48	33709
	1.5	64	37.10	43.65	3.07	6.32	36952
	2.0	58	37.60	44.23	3.18	6.57	39400
15	0	95	35.14	41.34	2.12	3.74	27722
	0.25	80	35.90	42.23	2.56	4.95	28406
	0.5	72	36.70	43.18	2.78	5.74	33792
	1.0	65	37.58	44.21	3.02	5.89	36433
	1.5	59	38.15	44.88	3.12	6.65	39800
	2.0	57	38.62	45.44	3.21	6.97	40413

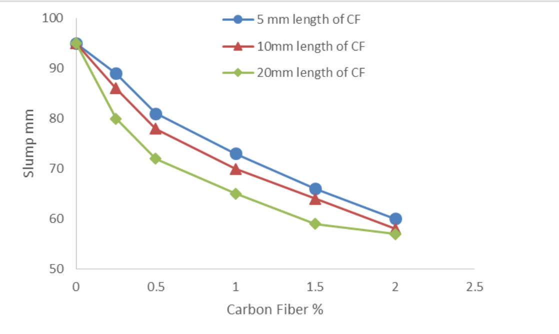

Figure (2) slump mm of all mixes with deferent length of carbon fibers.

Results of Compression strength.

As it is seen in table (11) presents the Compression strength test results and figure (3) at (7) and (28) day, it can be found that (HSLWAC) made with Carbon Fibers (C.F.) in addition silica fume had more Compression strength than control mix, the raise in the Compression strength at 28 days was more than their conformable Compression strength at (7) days due to the condensation of product of hydration process with silica fume about the Carbon fiber and loss the transition zone porous and further improves the mechanical properties of the concrete [29]. Figure 3 presents the variation of compressive strength with carbon fiber content, it is observed that, compressive strength increases with fiber length and fiber content. The increase in strength is more predominant for 20 mm length fibers. For the given fiber content, 20 mm length fibers show higher compressive strength compare to 5 mm and 10 mm length fibers. At 2% fiber content 20 mm length fiber shows 10% increase in compressive strength whereas the increase is by compressive strength whereas the increase is by 5.03% and 7% for 5 mm and 10 mm length of fibers respectively, compared with the strength of high strength concrete with 0% carbon fiber. This condition can be attributed to the improvement in the mechanical bond strength when the fibers both have the ability to delay the micro- crack formation and arrest their propagation afterward up to a certain extent [14, 15]. The maximum Compression strength of (HSLWAC) was (45.44) MPa at (28) days of age founded in the mix (L5) with 2% of carbon fibers.

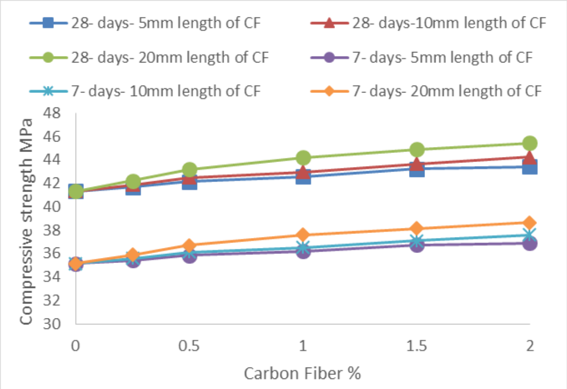

Figure (3) compressive strength with carbon fibers percentage at (7) and (28) days for different lengths.

Splitting Tensile Strength

The test results on split tensile strength of (HSLWAC) with carbon fibers is shown in Table 11 and plotted in Fig 4. It is observed from the Fig. 4, that the split tensile strength shows increase in strength with increasing fiber content relative to the plain specimens (without fiber). The percentage increase in splitting tensile strength for 5mm length HSLWAC mixes (M1, M2, M3, M4, and M5) containing of volume fraction 0.25%, 0.5 %, 1%, 1.5% and 2% carbon fiber is 10%, 17%, 26.9%, 41.5% and 48.6% respectively relative to the CF0 specimens. This is attributed to the mechanism of fibers in arresting crack progression and the improvement of bond between fibers and matrix due to the extra dense calcium silicate hydrate gel obtained from silica fume addition [18].

Also Fig. (4) indicate that the 20 mm length fibers show higher split tensile strength compare to 10 mm length fibers. The percentage increase in splitting tensile strength for HSLWAC mixes containing 20mm fiber type (L1, L2, L3, L4, and L5) with volume fraction 0.5%, 1% and 0.25% carbon fiber is 4.5%, 3.6%, 0.3%, 1.6% and 0.9% respectively relative to 10mm length fibers . This is attributed to the mechanism of fibers in arresting crack progression and the improvement of bond between fibers and matrix due to the extra dense calcium silicate hydrate gel obtained from silica fume addition [18].

Splitting failure characteristics of HSLWAC completely change with presents of fibers. Non fibrous concrete specimens suddenly failed in a brittle manner and separated into two parts; all samples of mono and hybrid fibrous HSLWAC consist of two parts still connected by fibers bridging the major crack. A reduction in crack width was observed in hybrid fibers HSLWAC which significantly contributed to the reduction in overall crack area.

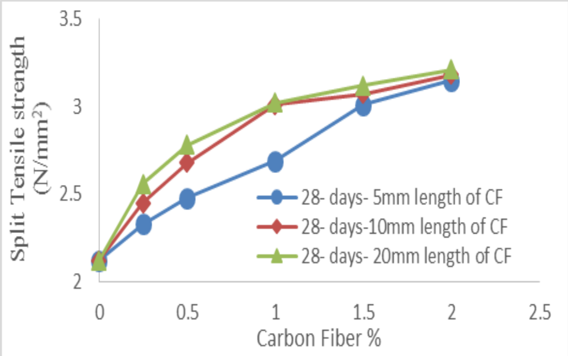

Figure. (4) Splitting tensile strength with carbon fibers percentage at (28) days with different lengths.

Flexural Strength

Flexural strength test results are given in Table (11) and plotted in Fig 5, show significant improvement in flexural strength with the addition of carbon fibers. The increase in flexural strength is more sensitive with fiber content compared to compressive and split tensile strength, for a given fiber length. Maximum increase of 86.4% in flexural strength is observed at mix (M5) content for 5 mm length fiber compared to a flexural strength of high strength concrete with 0% fibers.

The comparison between flexural strength values for HSLWAC specimens of 20 mm length mixes (L1, L2, L3, L4, and L5) and 10mm length mix specimens (N1, N2, N3, N4, and N5) shows that the percentage of increase in flexural strength is 6.88%, 5.8%, 11.7%, 7.5%, 5.2% and 6.1% respectively. This is because carbon fibers are strong and stiff and they can blunt and arrest microcracks before they coalesce into macro cracks leading to fracture [23].Plain HSLWAC exhibited brittle failure under flexural with the specimen being separated into two pieces. Fibrous high strength lightweight aggregate concrete mix with carbon fiber content 0.25% shows the same behavior. This is due to the lower elastic modulus of the carbon fiber.

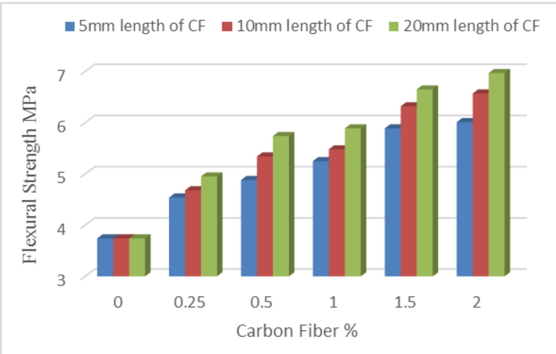

Figure. (5) Flexural strength with carbon fibers percentage for different lengths.

Modulus of elasticity

Test results for Modulus of elasticity indicate that in table (11) and figure (6). The addition of carbon fibers show branching raise in the elasticity. Like to strength properties the modulus of elasticity also shows increased values at higher fiber content. For example at 5 mm length the modulus of elasticity shows increase with increasing fiber content relative to the plain specimens (without fiber). The percentage increase in modulus of elasticity HSLWAC mixes (M1, M2, M3, M4, and M5) containing of volume fraction form 0.25% to 2% carbon fiber is in the range 0.7% - 17.7% respectively relative to the (CF0) reference mix. Also the increasing length of carbon fibers shown raises the modulus of elasticity as in the other strength factors.

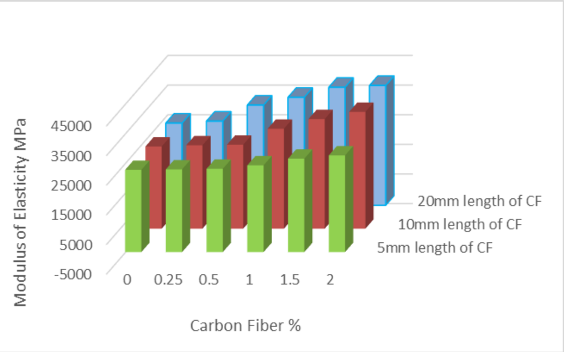

Figure (6). Modulus of elasticity for all mixes.

CONCLUSIONS

The control (HSLWAC) has a density of (1835) kg/m^3, and the voids content was reducing with increasing the percentage of silica fume, the lowest density of (1746.72) kg/m^3 was from the mix (PC5) at 28-days. It permeability coefficient (K) and voids content was (0.324) cm/s, and (30.21%) respectively.

(1) Carbon fibres reduce the slump value of concrete. The reduction in slump value is within the range of 11%–64% for different length of carbon fibres. However.

(2) The compressive strength of (HSLWAC) increases with an increase in carbon fibres content. Plain (HSLWAC) concrete has a 28-day compressive strength of 41.34 MPa, and this value increases to 43.42 MPa when the concrete is reinforced with 2% volume fraction for mix (M5) of 5 mm length carbon fibers, also the compressive strength of (HSLWAC) increases with longer the length of carbon fibres to 10mm and 20mm were 45.44 MPa and 44.23MPa for mixes (N5) and (L5) of 2% volume fraction.

(3) The excess the content of carbon fibers in HSLWAC with 5mm length significantly improves the splitting tensile strength of mix (M5) reinforced specimens was 48.6% relative to the reference specimens. HSLWAC specimens show significant increase in splitting tensile strength with increasing content. The percentage increase in splitting tensile strength for HSLWAC mixes containing 20mm fiber type (L1, L2, L3, L4, and L5) with volume fraction 0.5%, 1% and 0.25% carbon fiber is 4.5%, 3.6%, 0.3%, 1.6% and 0.9% respectively relative to 10mm length fibers.

(4) The effect of incorporating of carbon fibres in improving the flexural strength with increased content of carbon fibers is more pronounced compared to its effect on splitting tensile strength. The higher percentage increase in flexural strength for (L5) mix was 6.97 MPa compared with reference concrete mix (CF0).

(5) For Modulus of elasticity indicate that the addition of carbon fibers show marginal increase in the elasticity. Similar to strength properties the modulus of elasticity also shows increased values at higher fiber length and fiber content.

References

1. Kılıç, A., Atiş, C.D., Yaşar, E. and Özcan, F., 2003. High-strength lightweight concrete made with scoria aggregate containing mineral admixtures. Cement and Concrete Research, 33(10), pp.1595-1599.
2. Chia, K.S. and Zhang, M.H., 2002. Water permeability and chloride penetrability of high-strength lightweight aggregate concrete. Cement and Concrete Research, 32(4), pp.639-645.
3. Committee, A.C.I., 2009. 213.(nd). Guide for Structural Lightweight-Aggregate Concrete (ACI 213R-03). ACI Manual of Concrete Practice, pp.1-20.
4. Domagała, L., 2015. The effect of lightweight aggregate water absorption on the reduction of water-cement ratio in fresh concrete. Procedia Engineering, 108, pp.206-213.
5. Abdul kader Ismail A. L., 2013. The effect of lightweight aggregate water absorption on the reduction of water-cement ratio in fresh concrete. Procedia Engineering, 108, pp.206-213.
6 Yang, X., Wei, J., Nanni, A. and Dharani, L.R., 2004. Shape effect on the performance of carbon fiber reinforced polymer wraps. Journal of Composites for Construction, 8(5), pp.444-451.

7. Khalil, W.I. and Mozan, S.A.A.J., 2015. Some Properties of Hybrid Fibers High Strength Lightweight Aggregate Concrete. Engineering and Technology Journal, 33(4 Part (A) Engineering), pp.815-829.
8. Khalil, W.I. and Abdulrazaq, A., 2011. Mechanical Properties of High Performance Carbon Fiber Concrete. Engineering and Technology Journal, 29(5), pp.906-924.
9. Iraqi specification No. 5 (1984); “specification for Portland Cement”.

10. ASTM C 330-04. (2004). Standard Specification for Lightweight Aggregates for Structural Concrete.

11. ASTM, C., 2001. 128. Standard test method for specific gravity and absorption.
12. ASTM Specf.C33-01. (2001). Standard Specification for Aggregates, Annual Book of ASTM Standards, PP1-8.
13. ASTM-C494 -02 “Standard Specification for Chemical Admixtures for Concrete” Annual Book of ASTM Standards, 2002.
14. ASTM C1240-05“Standard Specification for Use of Silica Fume as a Mineral Admixture in Hydraulic-Cement Concrete, Mortar, and Grout” Vol.04.0.2,pp.1-7
15. ASTM C1116-02 “Standard Specification for Fiber-Reinforced Concrete and Shotcrete” Annual Book of ASTM Standards, 2002
16. ACI Committee report 211.2-98. (1998). Standard Practice for Selecting Proportions for Structural Lightweight Concrete. American Concrete Institute, Farmington Hills. MI, United States.
17. ASTM, C., 1996. 143. Standard test method for slump of hydraulic cement concrete, ASTM International, West Conshohocken, PA, USA, 4.
18. Rachel J.D. “chemical and physical effects of silica fume on the mechanical behavior of concrete” ACI materials journal, Nov.-Dec. 1989, P.P. 609-613

19. ASTM C192-02” Standard Practic for Making Curing Concrete Test Specimens in the Laboratory “Annual Book of ASTM Standards, Vol 04.02.
20. ASTM (39) -98). “Standard test method for Compression strength of cylindrical concrete specimens.” Annual Book of ASTM Standards, Vol. 04.02

21. ASTM C 496- 86 “Standard Test Method for Splitting Tensile Strength of Cylindrical Concrete Specimens” Annual Book of ASTM Standards,Vol.04-02,1989,pp.259-262.

22.Standard, A.S.T.M., 2010. C469/C469M,(2010). Standard test method for static modulus of elasticity and Piosson’s ratio of concrete in compression.

23. ASTMC293 – 02 “Standard Test Method for Flexural Strength of Concrete (Using Simple Beam with Center-Point Loading)” Annual Book of ASTM Standards, Vol.04-02

24. Shehata M. “Optimizing the strength and permeability of (HSLWAC)”. Ryerson University, Department of Civil Engineering; 2010.

25. Montero, M.A. and Mehta, M., 1983. Pain in the anterior abdominal wall. Treatment by selective destruction of the nerve by heat. Revista espanola de anestesiologia y reanimacion, 30(1), p.13.
26. M. Mazloom A.A. Ramezanianpour, J.J. Brooks “Effect of silica fume on mechanical properties of high-strength concrete” Cement & Concrete Composites 26 (2004) 347–357.
27. .Elsaid, A.; Dawood, M.; Seracino, R.; and Bobko, C. (2011). Mechanical properties of kenaf fibre reinforced concrete, Construction and Building.Materias, 25(4), 1991-2001.
28. Mohamed R. A. S. “Effect of carbons fibers on the mechanical properties of normal concrete” Journal of Engineering Sciences, Assiut University, Vol. 34, No. 4, pp. 1049-1059, July 2006.
29. Mohit Dwivedi,Shobhit Mishra,Vishal Singh 2014 “Effect of Polypropylene Fibres on Flexural Strength of M30 Grade Concrete” IOSR Journal of Mechanical and Civil Engineering e-ISSN: 2278-1684,p-ISSN: 2320-334X, Volume 11, Issue 4 Ver. II ,PP 93-97.
30. Jing Yang, Guoliang Jiang2003. “Experimental study on properties of pervious concrete pavement materials” Cement and Concrete Research 33 p.p 381–386.

PAPER • OPEN ACCESS

Mechanical Properties of Lightweight Aggregate Moderate Strength Concrete reinforcement with Hybrid Fibers

To cite this article: Haider Araby Ibrahim *et al* 2019 *IOP Conf. Ser.: Mater. Sci. Eng.* **584** 012048

IOP Conf. Series: Materials Science and Engineering **584** (2019) 012048 doi:10.1088/1757-899X/584/1/012048

Mechanical Properties of Lightweight Aggregate Moderate Strength Concrete reinforcement with Hybrid Fibers

Haider Araby Ibrahim [1,*], Mohammed Bally Mahdi [2], Basim Jabbar Abbas [3]

[1, 2, 3] Civil Engineering Department, Al-Muthanna University, Samawa, Iraq.
*Corresponding Author: email: arabyhaider@yahoo.com

Abstract. This study aims to detect the mechanical properties of lightweight aggregate moderate strength concrete (LWAMSC) reinforced with single and hybrid fibers in various types and sizes. Moderate strength pumice lightweight aggregate concrete mix with compressive strength 40 MPa at 28 day age with silica fume and superplastizier was used. The fibers used include macro hooked steel fiber with aspect ratio 80, steel fiber with aspect ratio 60, and polypropylene fiber (P.P.F). Two groups of (LWAMSC) mixes were made with reference concrete mix (without fibers). The first group of mixes were substituted three (LWAMSC) mixes with different single fiber including, concrete mix reinforced with Polypropylene (P.P.F) about 0.75 % volume fraction (P1), concrete mix reinforced with macro hooked steel fiber type SF1 with volume fraction 0.75% mix (M1) and concrete mix reinforced with macro hooked steel fiber type SF1 volume fraction 1.5% mix (M2). The second group of fiber reinforcement (0.75% steel fiber type (SF1) + 0.75% steel fiber (SF2) mix (H1), (1% steel fiber (FS1)+ 0. 5% steel fiber type (SF2) mix (H2)),and finaly (1% steel fiber type (SF1)+0.5% PPF mix (H3)). Dry density, strengths of compressive, splitting tensile, and flexural of (LWAMSC) were examined. generally single and hybrid reinforcement fiber of (LWAMSC) show important increase at flexural strength and splitting tensile strength in comparison with reference concrete.The results also show that, the optimum added proportion of fiber steel type (SF1) was (1.0%) and with (0.5%) steel fiber type (SF2) that portion raised the strengths of compressive, flexural, and splitting tensile around (4.34%), (52.93%), and (297%) respectively comparison with control mixture.

Keywords: moderate-strength concretes, lightweight aggregates; dry density, hybrid fibers.

1. Introduction

In a new moderate rise building, the size of columns and the wide of the span between beams concrete structures were increased, it is needed lightweight moderate strength for low stiffness concrete. A diminished concrete density for a similar strength level allows a sparing in dead load for basic foundations, but increase the strength of light weight concrete lead to moderate brittle behavior [1].

Lightweight aggregate moderate strength concrete (LWAMSC) is structural lightweight concrete utilize at concrete building structure with a 28-day compressive strength of (40 MPa) or greater, and has a density less than 1500 kg/m^3 [2], high brittleness low tensile/compressive strength ratio, low flexural strength, larger shrinkage. Therefore, steel fiber is needed for enhanced the mechanical properties of lightweight moderate strength mixture for increasing the tensile/compressive ratio, toughness, and resistance against deformation.[3],[4].To keep on the workability of concrete, a moderate-range water-reducing admixture (superplasticizer) was used within mixing operations with water-cement ratio lower than 0.4 Pumice is a porous, volcanic rock. It is light grey in colour , cheap lightweight aggregates used as lightweight coarse aggregates.The especial application of this type of concrete in the area of ocean engineering structures, long-span bridges and moderate buildings, etc [5].

2. Literature review

Although little knowledge for mechanical properties (LWAMSC) with hybrid fibers, some authors have got adequate results in this field , Jianming Gao, et al. in (1997) [6], found the effect of fiber volume and aspect ratio on the mechanical behaviour is extremely prominent, but strength of compressive is little improved and varied from 70.2 to 85.4 MPa.The ratio of tensile /compressive strength is improved. Strength of flexural varied from 4.94 to 8.7MPa.

While O. Kayali, et al. in (2003) [7] studied the effect of polypropylene and steel fibers on lightweight moderate strength aggregate concrete with Sintered fly ash were used as lightweight aggregates, polypropylene fiber with 0.561% at concrete volume, lead to a 90% addition to the tensile strength and a 20% to the rupture modulus and 1.7% by volume of steel fibers addition at the indirect strength of tensile about 118% and the rupture modulus by about 80%.

In 2011, N.A. Libre et al. [8] observed the increase in mechanical properties and energy absorption capacity when the addition of steel fibers. Polypropylene fibers have a minor effect in mechanical properties of hardened concrete made with both steel and polypropylene fibers. The steel fibers volume fraction at 0.5% ,1% but the PP fibers various 0.2% ,and 0.4%.Furthermore, H.K. Ahmed, et al. in (2017)[9] studied the influence of three types of polypropylene fibers with different volume fraction (Vf) on compressive strength, flexural strength, splitting tensile strength, and static modulus of elasticity. Results show significantly increased in all types of strength with all types of polypropylene fibers and compressive strength it was improved at Vf =0.25% and decrease at Vf =0.75%.

3.Materials and methodology

3.1. Cement

For experimental work, the ordinary Portland cement was used from Al- Douh refectory. Tables 1 and 2 show that the cement test results according to the ASTM standers C150-02 [10].

Table 1. Chemical analysis of cement

Oxides	percentage	Limit of ASTM Specf.C150-02a/2002
CaO	63.2	-
SiO2	18.9	-
Al2O3	3.8	-
Fe2O3	4.6	-
SO3	1.5	≤ 2.3
MgO	1.7	≤ 6.0
L.O.I	1.9	≤ 3.0
L.S.F	0.9	-
I.R.	0.4	≤ 0.75
C3A	2.32	≤ 5.0

Table 2. Physical properties of cement

Physical properties	Test results	Limit of ASTM Specf.C150-02a/2002
Initial setting time (vicat)	65 min.	45min.(Min.)
Final setting time (vicat)	170 min.	375 min. (Max.)
Compressive strength of mortar (MPa) 3-days	19.0	15 (Min.)
Compressive strength of mortar (MPa)7-days	30.5	21 (Min.)

IOP Conf. Series: Materials Science and Engineering **584** (2019) 012048 doi:10.1088/1757-899X/584/1/012048

3.2. Aggregate

3.2.1. Fine aggregate

Natural river sand was used as a fine aggregate which is passing through the sieve aggregate of 4.75 mm. Table 3 shows the gradation of the aggregate which is compatible to the required specifications of ASTM C33-01[11].

Table 3. Sieve analysis of fine aggregate

Sieve size	Passing ratio (%)	Limit of ASTMC33-01
9.5mm	100.00	100
4.75mm	94.56	95-100
2.36mm	72.45	80-100
1.18mm	68.40	50-85
600µm	53.32	25-60
300µm	16.60	5-30
150µm	2.12	0-10

3.2.2. Pumice lightweight coarse aggregate

Pumice was used to make preparations for the (LWAMSC) mixtures. The quarry of this stone is found in the north of Iraq in AL- Sulaymania governorate. Pumice stone has a dark colour, moderate permeability, and low density, porous form of vitrified volcanic rock and moderate silicon oxide (SiO2) concrete. Crushed Pumice stone was used as a coarse lightweight aggregate of nominal size (12.5 - 4.75) mm in this work as shown in Figure 1. Pumice pieces were broken manually and graded as per the requirement of ASTM C 330-04 [12]. Table 4 and 5 illustrate the physical properties and the grading for pumice, and the Figure 2 shows the graph of the grading of pumice aggregates.

Figure 1. Pumice pieces

Table 4. Physical properties of lightweight coarse aggregate (pumice)

Tests, ASTM C 127	Test Results	Limits
Loose bulk density (kg/m3)	569	880 (max)
Oven dry bulk specific gravity	1.88	
Absorption % (24 Hours)	2.51	
specific gravity	2.53	

Table 5. Pumice grading of coarse lightweight aggregate

Sieve size (mm)	Percent Passing	Limit required by ASTMStandardC330-04
12.5	100	100
9.5	97	80-100
4.75	12	5-40
2.36	2	0-20
1.18	0	0-10

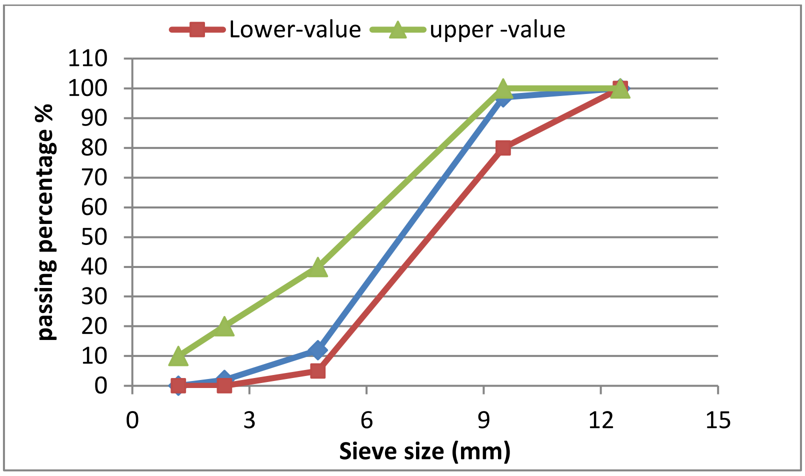

Figure 2. Sieve analysis of Pumice grading of coarse lightweight aggregate.

3.3. High range water reducing admixture (Superplasticizer)

High range water reducing admixture (HRWRA) superplasticizer is a chemical compound used to reduce the amount of water with the same workability for producing moderate strength concrete, according to ASTM-C494 Type G [13]. Because of the fibers addition reducing the workability of mixtures[5]. So (HRWRA) must be used . Table 6 shows the typical properties of superplasticizer.

Table 6. Typical properties of superplasticizer

properties	Specifications
Specific gravity	1.2
Form	Liquid
PH	7-9

3.4. Fibers

Table 7 shows the physical and technical properties of fibers used in this work. Two types of macro hooked steel fibers (SF1and SF2) with an aspect ratio of 80, and 60 and Polypropylene fiber (PPF) with aspect ratio 677 complied with requirements of ASTM C1116-02[14]. Figure 3 shows the two types of fibers that used in this work.

Table 7. Properties of fibers

Property	**Steel Fiber, SF1**	**Steel Fiber, SF2**	**polypropylene Fibers (P.P.F)**
Density (Kg/m3)	7880	7880	7900
Tensile strength (MPa)	1100	1100	360
Diameter (mm)	0.5	0.5	0.018
Length (mm)	40	30	12
Geometry	hooked	hooked	Fibrillated
Aspect ratio	80	60	677

(a) Standard hooked-end steel fibers (b) Polypropylene fibers**.**

Figure 3. Types of fibers

3.5. Silica fume

Silica fume utilized in this work was purchased from Sika Company. The chemical composition and physical requirements of the purchased silica fume satisfied the requirements of ASTM C 1240-06 - 06[15].

3.6. Mix Proportions

The volumetric method ACI 211.2 [2] was used for mix design with proportions as 1: 1.33: 0.89 (cement: sand: aggregate) by weight.The reference lightweight aggregate moderate strength concrete mix to give at 28-day age a compressive strength (42 MPa), after many tries, used the mixes with cement content 490 Kg/m3, silica fume 53kg/m3, water-cement ratio 0.31 and slump (80 mm) for good workability was used (HRWRA) 1.2 liter per 100 kg of cement without fiber (0F) as shows in table (8).The high absorption of pumice aggregates directly effects on the quality of the LW concrete. In order to solve this problem, the pre-soaking method was used for pumice aggregates to control the high absorption of pumice aggregates for a fixed time.Generally, 24 hours the time was needed to achieve the 80% of the water absorption [16].Two groups of concrete were made, the first group of mixes were substituted three (LWAMSC) with different single fiber including, concrete mix reinforced with Polypropylene (P.P.F) about 0.75 % volume fraction (P1), concrete mix reinforced with macro hooked steel fiber type SF1 with volume fraction 0.75% mix (M1) and concrete mix reinforced with macro hooked steel fiber type SF1 volume fraction 1.5% mix (M2). In the second group, three (LWAMSC) with hybrid fiber including concrete mix reinforced with a combination of (SF1) steel fiber 0.75% volume fraction + (SF2) steel fiber 0.75% volume fraction (H1). Concrete mix reinforced with a combination of macro (SF1) steel fiber with 1.0 % volume fraction +(SF2) steel fiber and 0. 5% volume fraction (H2). Finally, the concrete mix contains a combination of (SF1) macro steel fiber 1.0% volume fraction + micro PPF with 0.5% volume fraction (H3).

Table 8. Mix Proportions of (LWAMSC)

Mix Design	Steel Fiber % of vol. (SF1)	Steel Fiber % of vol. (SF2)	(P.P) Fiber % of vol.	Pumice coarse aggregates (Kg/m3)	Fine aggregates (Kg/m3)	Cement content (Kg/m^3)	W/C	Silica fume (Kg/m^3)
Ref.- (RF)	0.0	0.0	0.0	435	650	490	0.31	53
0.75%PPF- (P1)	0.0	0.0	0.75	435	650	490	0.31	53
0.75%SF1- (M1)	0.75	0.0	0.0	435	650	490	0.31	53
1.5%SF1- (M2)	1.5	0.0	0.0	435	650	490	0.31	53
0.75%SF1- 0.75%SF2- (H1)	0.75	0.75	0.0	435	650	490	0.31	53
1%SF1- 0.5%SF2- H2)	1.0	0.5	0.0	435	650	490	0.31	53
1%SF1-0.5%PPF- (H3)	1.0	0.0	0.5	435	650	490	0.31	53

3.7. Casting and curing of (LWAMSC)

To produce of lightweight aggregate moderate strength with fiber reinforced concrete, pumice as coarse aggregates and fine aggregates were mixed at the beginning with dry case for one minute. Then, cement and silica fume were added to the mix. Amid the blending activity, the fibers were added and all the materials were mixed for 2 minutes together with the continuous addition of fibers. Hard and continuous mixing was made for the avoidance of fibers to be clumped. Finally, to get a specific mixture containing water,(HRWR) was slowly added to the mixture during the mixing for 3 minutes.

After filling up the moulds, the concrete samples were to rduce the entrapped voids using a vibrating table for a period of 8 to 12 seconds. The samples were maintained in the laboratory for 24 hours,and then stored in the water of a constant 20±2 °C for 7 and 28 days, up to a time the day of the testing.

3.8. Concrete testing

According to ASTM C192-88 [17],the concrete resistance of compression of (LWAMSC) samples were examined during 7 and 28 days of treatment period. For strength of compression at (7) and (28) days in conformance to requirements for ASTM C39-98 [18], utilize six standard steel cubic moulds (150×150×150) mm for casting the samples, while for the strength of splitting tensile emploied two cylindrical moulds of (100×200) mm and the concrete was evaluated according to ASTM C 496-90 [19]. Finally, according to ASTM(C78–98) [20], two prisms of (100×100×400) mm were used for the strength of flexural (Modulus of Rupture) for (28) days.

3.9. Air Dry Density

Air dry density test was performed in accordance with ASTM C567-85[21] by using (100×200) mm cylindrical specimens. The specimens left in moulds for 1 day inside a moisture cabinet, then they were stripped from the moulds and wrapped securely with a polythene bag for 6 days. After that, they were removed from the bag and immersed in water for 1 day. On the second day saturated surface dry and suspended-immersed weight were taken. The specimens were left in the laboratory for 21 days, then the dried specimens were weighted at the 28-day. The air dry density was calculated by using the following equation:-

$$Air\ dry\ density\ (kg/\mathbf{m^3}) = \frac{(A \times 997)}{(B\text{-}C)} \tag{1}$$

where :
A = weight of concrete cylinder, as dried (kg).
B = saturated surface-dry weight of cylinder (kg).
C = suspended-immersed weight of cylinder (kg).

4. Resultant and Discussion

4.1. Bulk density

The hardened concrete densities which were tested at 28-day are shown in Table 9 and Figure 4. The results of the bulk density of the (P.P.F) fibers did not have a significant effect on the concrete density. While, the density of concrete is dirctly influenced at fibers of steel, but the mean density of concrete that not contain steel fibers was 1760 kg/m^3, the average density of hybrid fibers concretes of H1,H2, H3 were 1862, 1856, and 1843 kg/m^3 .This is clearly due to the moderate specific gravity of steel fibers, the density of (LWAMSC) shows the increment of 1.5% steel fiber greater the concrete density at about 116 kg/m^3. The influence fibers steel on growing the concrete density samples very important in the case of lightweight concrete in which the reduction of the density is very significance.

Table 9. Compresive of compression results of (LWAMSC) samples at 7 and 28 days

Mix Design	Average Bulk density (kg/m^3)	Comp. strength 7 days MPa	Comp. strength 28-day MPa
Ref.- (RF)	1768	32.75	41.45
0.75%PPF- (P1)	1769	33.12	42.12
0.75%SF1- (M1)	1840	34.45	44.35
1.5%SF1- (M2)	1860	30.11	37.64
0.75%SF1- 0.75%SF2- (H1)	1862	30.89	38.76
1.0%SF1- 0.5%SF2- (H2)	1856	34.52	43.25
1.0%SF1-0.5%PPF- (H3)	1843	34.35	43.05

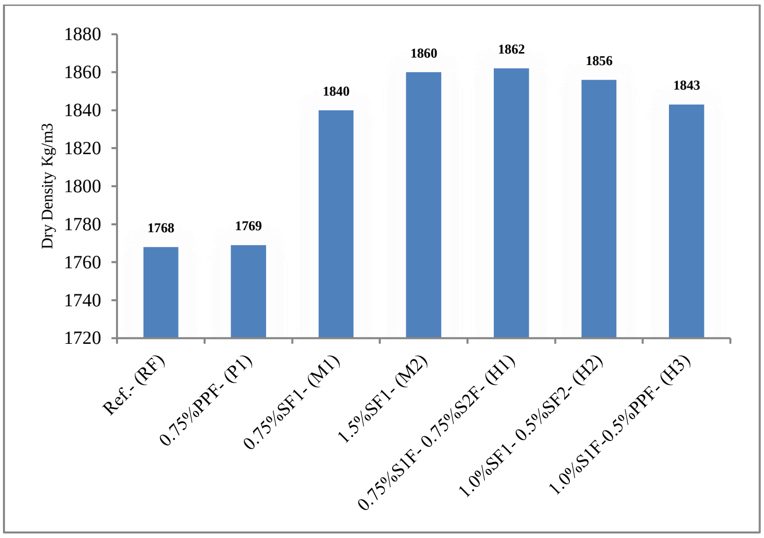

Figure 4. Dry density test resultants of (LWAMSC) at 28-day

4.2. Compressive Strength

Table 9 and Figure 5 explain the increment of the compressive strength results of all (LWAMSC) at 7-day and 28-day within the age. It was noted that the compressive strength of polypropylene fiber type (P1) with volume fraction of 0.75% was slightly better than the refrence concrete (RF) in about 1.13% at 7days and 1.6% at 28-days respectively. Concrete mixes containing single fiber, steel fiber of M1 is showed the higher compressive strength about 5.19%, and 6.97% for 7 and 28 days respectively in comparison with refrence concrete. This is due to the small amount of fibers enhanced the cement paste for micro crack phases and improved the crack strength.

It has been noticed that the addition of fibers in concrete mix of (M2) come to be very hard at 1.5% of steel fiber volume fraction and mixture can not completely compacted, thus the compressive strength of concrete become smaller than to the refrence concrete.The partly exchange to steel fibers type (M2) of 1.5% steel fiber type (SF1) with hybrid fiber (H1, H2, and H3) of low volume fraction of steel fiber type SF2 (0.75% and 0.5%), polypropylene fibers (0.5%) shown that increasing in the compressive strength by about 2.97%, 14.9%, %, and 20.21% respectively at 28-day . This is because of the hybrid fibers with varying types and sizes would suggest different put down conditions. Moreover, this social position can be ascribed to the becoming better in the mechanical strength of bond as the fibers both have the capacity gaudily the microcrack arrangement and to detain their diffusion afterwards up to a certain scale[22].

(LWAMSC) Hybrid fibers mixes with 1.0% of steel fiber type SF1 and 0.5% fraction of volume of (P.P.F) show the moderately advancing in compressive strength. This is because, in comparison with longer and moderate specific gravity fibers, shorter and low specific gravity are more efficient in delaying cracks owing to the moderate specific contact surface of nonmetallic fibers [23].

The using of two types of macro steel fibers in (LWAMSC) with volume fraction 0.75% for each (mix H1), shows decreasing in compressive strength in comparison with reference mix (mix RF).This is due to the pores and honeycombs which can be formed during placing of moderate volume fraction of steel fibers as a result of not completed consolidation [24].

IOP Conf. Series: Materials Science and Engineering **584** (2019) 012048 doi:10.1088/1757-899X/584/1/012048

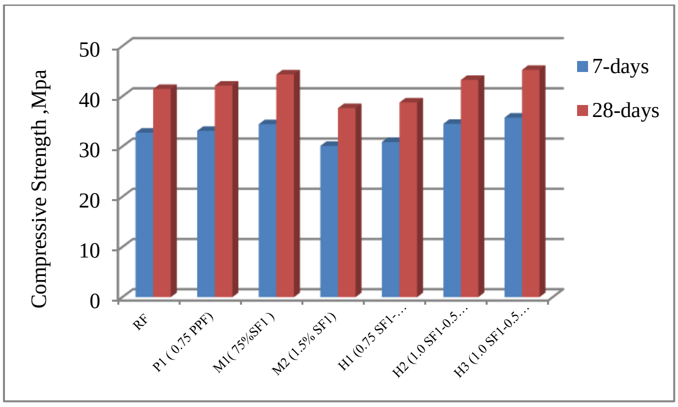

Fig. 5. Compressive Strength test of (LWAMSC) results at 7-day and 28-day

4.3. Splitting Tensile Strength

Table 10 and Figure 6 list the effects of fibers in (LWAMSC) appreciably, increasing the splitting tensile strength for alone type and hybrid fibers concrete mixtures compared to the reference concrete. The amount of increase in splitting tensile strength for (LWAMSC) mixes containing single steel fiber type (M1) with volume fraction 0.75%, and 0.75% polypropylene fiber (P1) is 295.8%, and 221.6% successively comparison to the refrence concrete. This is ascribed to the mechanism of fibers in detention cracking progression and the improvement of the bond between fibers and matrix due to the extra dense calcium silicate hydrate gel obtained from silica fume addition [25].

The comparison between splitting tensile strength values of (LWAMSC) mix having one steel fiber type (M2) with a volume fraction of 1.5% and the hybrid fiber mixes H1, H2, and H3 shows that the increase ratio in strength of splitting tensile of hybrid fiber (LWAMSC) is about 6.85%, 20.25%, and 7.47%, respectively.

Similar to the case of compressive strength, steel-polypropylene fibers mix (H3) shows the moderateest splitting tensile strength relative to all fibrous (LWAMSC) mixes (with mono or hybrid fiber). This is because of the cooperation of hybrid fibers, small fibers may bridge the microcracks more qualification, because they are not thick and their amount in mixture is much paramount than tof the great thick fibers, for the same fiber quantity. As the microcracks grown and join upto very large macrocracks, the long hooked-end fibers become more and more active in crack bridging. In this way, the strength of tensile and ductility can be improved. Long fibers can therefore provide a stable post peak response, but short fibers will be less active because they are being more pulled out, therfore the width of crack increasing [26].

4.4.Flexural Strength

The flexural resistance test proceeds for all (LWAMSC) combined are coincident in Table 10 and Figure 7. The conclusion show that the incorporation of fibers increment the flexural strength in single and multi-fibers heterogeneous suitable to mix together. The percentages of increased in parameter of breach for single steel fibre (LWAMSC) at fragment 0.75%, 1.5% of M1, and M2 are 52.37%, 29.52% and 60.64% for 0.75% of polypropylene fibers (P1) compared with reference concrete. The purpose for this improvement in parameter of fracture is that after table bully, the fibers will move the cargo that the concretion uniform until great by interfacial fetters between them. The principle for this increase in modulus of rupture is that after cement paste cracking, the fibers is carried the load that the concrete without changing up to cracking by means of bond of interfacial between the fibers and the matrix. Therefore, the fibers resist the dissemination of cracks and do not fail without warning, which source an increase in load carrying ability [27].

The comparison between strength of flexural values for (LWAMSC) samples containing 1.5% of steel fiber type (M2) and hybrid fiber samples H1, H2, and H3 shows that the increase ratio of strength of flexural for hybrid fiber (LWAMSC) samples is 20.9%, 35.61%, and 12.02% respectively. It can be observed that (LWAMSC) samples containing a merge of steel and polypropylene fibers (mix H3) show the lowest percentage increase in modulus of rupture relative to mono steel fiber mix (M1). This is because of the lower strength of (P.P.F) tensile and also the not strong bonding between cement matrix and(P.P.F) [28].

Table 10. Results of tensile of splitting and flexural strengths tests for (LWAMSC) mixtures

Mix Design	Splitting tensile resistance 28 day MPa	Flexural strength 28 day MPa
Ref.- (RF)	0.97	3.76
0.75%PPF- (P1)	3.12	3.87
0.75%SF1- (M1)	3.84	5.53
1.5%SF1- (M2)	3.21	4.24
0.75%S1F- 0.75%S2F- (H1)	3.43	5.12
1.0%SF1- 0.5%SF2- (H2)	3.86	5.75
1.0%S1F-0.5%PPF- (H3)	3.45	4.75

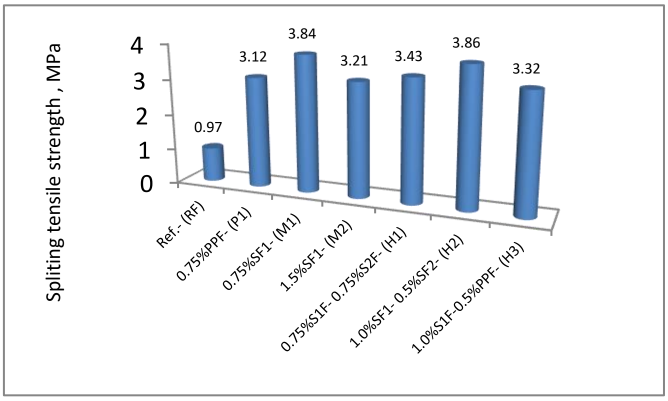

Figure 6. Strength of splitting tensile for overall (LWAMSC) mixtures of 28-day

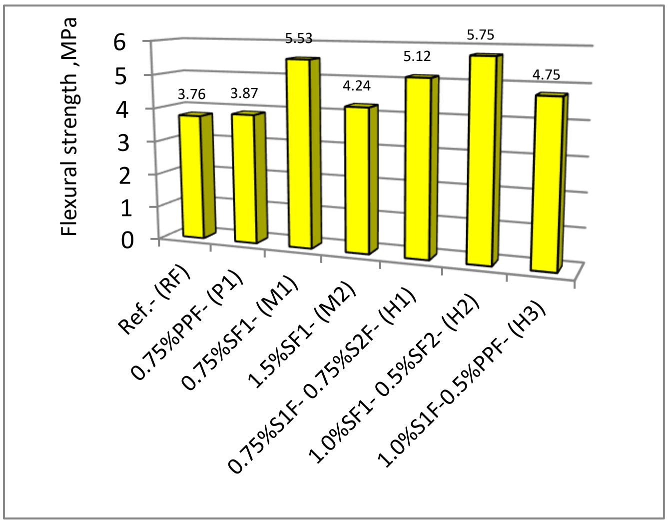

Figure 7. Strength of flexural and ratio of single and hybrid fibers

5. Conclusion

- The addition of steel fibers to (LWAMSC) increases its oven dry density of all mixes. Hybrid (LWAMSC) mixe containing a combination of steel fibers 0.75% steel fiber type (SF1) + 0.5% polypropylene fiber show densities less than that containing 1.5% of mono steel fiber type (SF1).
- The use of 0.75% volume fraction of macro steel fiber type (SF1) and polypropylene fibers increases the cube compressive strength at 28 day by about 5.19%, and 6.97% relative to the refrence concrete, and the partial replacement of macro steel fibers type SF1 with 0.75% of SF2 (H1), 0.5% SF2 (H2), and 0.5% polypropylene fiber (H3) increases the compressive strength at 28 day by about 2.9%,14.9%, and 20.21% compared to the 1.5% SF1- (M2)
- The inclusion of fibers in (LWAMSC) significantly improves the splitting tensile strength for both single and hybrid fiber reinforced samplesrelative to the reference concrete. Hybrid fiber reinforced (LWAMSC) samples show significant increase in splitting tensile strength. The percentage of increase in splitting tensile strength for (LWAMSC) specimens prepared from H1, H2, and H3 mixes is about 6.85%, 20.25%, and 7.47%, respectively attribute to the control mixture.
- The incorporation of fibers increases the flexural strength in single and hybrid fiber concrete compare to the reference concrete. The increase ratio of flexural strength for hybrid (LWAMSC) supplied of mixtures H1, H2, and H3 is 20.9%, 35.61%, and 12.02% respectively relative to the reference concrete.
- The resultant indicated that, the most efficient state addition proportion of hybrid fiber was 1.0% of (SF1) with 0.5% of (SF2) this ratio raised the strengths of compressive, flexural, and split tensile for 4.34%, 52.93%, and 297% successively, comparing to reference concrete.

References

[1] Ries J P, Boyle M J, Bremner T W, Burg R G, Crocker D A, Dodl C L, Robinson G M, Ramme B W, Mccall W C, Mor A A, Rowe S K, Sheetz S R, Snow P G, Speck J F and Vaysburd A M 2010 Guide for Structural Lightweight-Aggregate Concrete Reported by ACI Committee 213 1–38

[2] Prestera J R, Dixon D E and Crocker D A 1990 Standard practice for selecting proportions for structural lightweight concrete (ACI 211.2) *ACI Materials Journal* 87 638–51

[3] Campione G 2005 Mechanical properties of steel fibre reinforced lightweight concrete with pumice stone or expanded clay aggregates *Materials and Structures* 34 201–10

[4] Korolev E V and Inozemtcev A S 2013 Preparation and Research of the High-Strength Lightweight Concrete Based on Hollow Microspheres *Advanced Materials Research* 746 285–8

[5] Libre N A, Shekarchi M, Mahoutian M and Soroushian P 2011 Mechanical properties of hybrid fiber reinforced lightweight aggregate concrete made with natural pumice *Construction and Building Materials* 25 2458–64

[6] Gao J, Sun W and Morino K 1997 Mechanical properties of steel fiber-reinforced, high-strength, lightweight concrete *Cement and Concrete Composites* 19 307–13

[7] Kayali O, Haque M N and Zhu B 2003 Some characteristics of high strength fiber reinforced lightweight aggregate concrete *Cement and Concrete Composites* 25 207–13

[8] Iqbal S, Ali A, Holschemacher K and Bier T A 2015 Mechanical properties of steel fiber reinforced high strength lightweight self-compacting concrete (SHLSCC) *Construction and Building Materials* 98 325–33

[9] Aslam M, Shafigh P, Alizadeh Nomeli M and Zamin Jumaat M 2017 Manufacturing of high-strength lightweight aggregate concrete using blended coarse lightweight aggregates *Journal of Building Engineering* 13 53–62

[10] Yap S P, Chen P Z C, Goh Y, Ibrahim H A, Mo K H and Yuen C W 2018 Characterization of pervious concrete with blended natural aggregate and recycled concrete aggregates *Journal of Cleaner Production* 181 155–65

[11] Shaikh F U A 2016 Mechanical and durability properties of fly ash geopolymer concrete

containing recycled coarse aggregates *International Journal of Sustainable Built Environment* 5 277–87

[12] Test C C, Mortar H, Concrete C, Specimens C C, Concrete L, Freezing R and Concrete S L 2010 Standard Specification for Lightweight Aggregates for Structural Concrete 1 i 1–4

[13] Gorgots V D 2006 About drawdown drilling parameters design procedure at primary formation exposing by a horizontal wellbore *Neftyanoe Khozyaistvo - Oil Industry* 120–1

[14] Gold R 1999 Standard Specification for 95 1–4

[15] PCA 2018 Chemical Admixtures 1–21

[16] Kamal M M, Safan M A, Etman Z A and Kasem B M 2013 Mechanical properties of self-compacted fiber concrete mixes *HBRC Journal* 10 25–34

[17] Test C C, Aggregate C, Aggregate F, Content A, Rooms M and Concrete P 2002 2.2 Astm C192 *Management* 04 1–8

[18] ASTM:C39/C39M-15a 2012 Standard test method for compressive strength of cylindrical concrete specimens *ASTM International* 04 1–7

[19] ASTM C496-96 1996 Standard Test Method for Splitting Tensile Strength of Cylindrical Concrete Specimens *ASTM International, West Conshohocken, PA* 04 1–4

[20] Speci- C C T, Cores T D and Speci- C C T Astm C78 1–3

[21] Smith D R, Lia J M and Ap L 2012 Potential Application of ASTM C 1701 for Evaluating Surface Infiltration of Permeable Interlocking Concrete Pavements *10th International Conference on Concrete Block Paving Shanghai* 1–8

[22] Mozan S A A 2015 Some Properties of Hybrid Fibers High Strength Lightweight Aggregate Concrete 33 815–29

[23] Pereira E B, Fischer G and Barros J A O 2012 Effect of hybrid fiber reinforcement on the cracking process in fiber reinforced cementitious composites *Cement and Concrete Composites* 34 1114–23

[24] Allan M L and Kukacka L E 1995 Strength and durability of polypropylene fibre reinforced grouts *Cement and Concrete Research* 25 511–21

[25] Dawood E T and Ramli M 2011 Contribution of hybrid fibers on the hybrid fibers on the properties of high strength concrete having high workability *Procedia Engineering* 14 814–20

[26] Jitchaiyaphum K, Sinsiri T and Chindaprasirt P 2011 Cellular lightweight concrete containing pozzolan materials *Procedia Engineering* 14 1157–64

[27] Al-Swaidani A M, Aliyan S D and Adarnaly N 2016 Mechanical strength development of mortars containing volcanic scoria-based binders with different fineness *Engineering Science and Technology, an International Journal* 19 970–9

[28] Yasar E, Atis C D, Kilic A and Gulsen H 2003 Strength properties of lightweight concrete made with basaltic pumice and fly ash *Materials Letters* 57 2267–70.

International Information and Engineering Technology Association
Advancing the World of Information and Engineering

Mathematical Modelling of Engineering Problems
Vol. 8, No. 2, April, 2021, pp. 230-236
Journal homepage: http://iieta.org/journals/mmep

Modelling Trip Distribution Using the Gravity Model and Fratar's Method

Ishraq Hameed Naser[1], Mohammed Bally Mahdi[2*], Fatin Hadi Meqtoof[3], Hiba Akrm Etih[1]

[1] College of Engineering, Al-Iraqia University, Baghdad 10001, Iraq
[2] College of Engineering, Al-Muthanna University, Samawah 66001, Iraq
[3] College of Education of Girls, Thi Qar University, Thi Qar 64001, Iraq

Corresponding Author Email: engmohbaly@mu.edu.iq

https://doi.org/10.18280/mmep.080209

Received: 12 August 2020
Accepted: 23 December 2020

Keywords:
trip distribution, gravity model, Fratar's method, trip origin, trip destination

ABSTRACT

Trip Distribution is a difficult and significant model in the urban transportation planning process. This paper creates and assesses a satisfactory model of the trip distribution stage for the Nasiriyah city by using two models, Gravity and Fratar methods. A large sample was used for developing the model. The research methodology depends on discussing the theoretical fundamentals of the various methods for estimating the trips distribution and examining the suitability of these fundamentals for the conditions of the selected study area. Two different models had been used, namely; Frater and Gravity model. These models were calibrated using real data. The study tests the accuracy of the models, including overall statistical assessments of the predicted movements. Finally, the study recommended to use Fratar Method. These results had been confirmed to the literature that, if the area is a homogenous growth, the best model is the growth factor (Fratar's method) and if the area is experiencing rapid changes. The gravity model will produce satisfactory results because it takes into account the competition in different land uses.

1. INTRODUCTION

Because of substantial growth in recent years, and continued future growth, the City of Al-Nasiriyah is confronted with various difficulties of arranging and dealing with its development system and transport framework especially inside the central business district (CBD). The city has development plans for the future, these plans will create major transport demands that will affect the current transport infrastructures and systems, also the transport demands will affect the current transport frameworks, especially the street organize inside the downtown area. Hence, the point of this examination is building up a transport model for the Nasiriyah region.

The transport model will help the city in setting up the future of transport request and test the effect of land use development, significant turns of events and street organize alternatives. The model of the investigation territory involves the urban zone is a trip distribution. It is a model of movement between zones - trips or links. Trip distribution models are designed to generate the best possible forecasts of destination choices based on traffic generation and attraction information for each travel area and genetic travel cost between each pair of zone [1-4].

The trip distribution model helps to control the changing in land uses. For instance, if a shopping centre is being arranged, so can make adjusted for the current trip generation model to fit the designed site (e.g., adding 500 retail occupations to the zone in which the shopping centre will exist). At that point, the model of trip generation is re-run with the new anticipated information, where the outing distribution model is applied to the anticipated beginnings and goals information. The outcome would be a model of likely outings to the new shopping center. The principle of trip distribution forecasting represents by estimating the relations or linkages for trip attractions among traffic zones [5].

For depicting the distribution of trips between zones, the literature depends on a matrix as a form. The matrix is a table that consists of two-dimension. The cells within the table represent the volumes of traffic that affected of generation zone to attraction zone and denoted by (Ti- j). (Ti- j) a symbol represents the trips that generate at zone i and ended at zone j. O-D network is comprised of lines and sections that speak to the root and goal zones individually. In this way, the O-D grid is required for the directional traffic task [6]. Three significant steps in an O-D matrix table, firstly, the traffic volume, secondly, the O-D matrix, and finally, the total trip of production and attraction. Those are represented essential datum of transportation systems planning and operations [7].

A mixture of purposes depends on a datum in the O-D matrix such as new road designs and existing road improvements (widening or adding more lanes) due to rising transportation demand services and facilities. It is additionally basic in examining the effects of the execution of traffic activity situations to current traffic circumstance, social, and natural divisions. The situations may include the course change, street enclosure because of street works or maintenances, the emergence of crises because of cataclysmic event, for example, seismic tremor, a tsunami wave, forest fire and significant flood. The traffic administrators can predict the circumstances prone to happen and henceforth inform the street clients with enough time preceding the changes. Hence, O-D networks are the fundamental wellspring of data for some reasons and should be readied rigorously [6]. Throughout the years, modellers have utilized a few unique definitions of trip distribution. The first was the Fratar or Growth model. This technique was presented by Fratar (1955). This structure extrapolated a base year trip table to the future dependent on development however doesn't consider the changing in spatial availability because of expanded gracefully or changes in movement designs and congestion [1]. In any case, the Fratar method is used routinely for anticipating through excursions in an urban zone and now and then in any event, for external - internal trips [8].

The following model created was the gravity model. The gravity model is entropy expansion model is generally utilized for trip conveyance examination [9], and the mediating openings model. Assessment of a few model structures in the 1960s inferred that "the gravity model and interceding opportunity model demonstrated equivalent unwavering quality and utility in reproducing the 1948 and 1955 trip distribution for Washington, D.C." [6].

2. METHODOLOGY

The basic of adoption a model for trips distribution is taken into consideration reaching for a reasonable approximation to the observed trip "(Matches between trips that are modelled and observed) with a note, there are no special statistics for calculating observed distribution". While for predicted distribution, a simple model was used to approximate the actual empirical distribution.

To achieve this, the following detailed objectives have been set:

(1) Gathering important information depending on the form had been implemented in the case study of Nasiriyah city.
(2) Estimating trip production for each zone by adopting the average trip rate (trips/inhabitant/day) for the entire city by using a category analysis method. However, the trip attracted to each zone was essentially estimated through building trip attraction model using simple linear regression, which was adopted as an essential parameter.
(3) Develop an improved trip distribution model that can investigate its validity.
(4) The calculation for developing model done at zone number 1 then duplicated for all zones.
(5) Make a comparison between the observed and modelled distribution to see whether the model creates a sensible guess.

2.1 Nassiriyah strategic transport model

Nasiriyah city is the urban area, it is a homogenous growth and doesn't experience rapid changes in land uses. The number of population for the city of Nasiriyah was 523236 person depending on Insights registration results for 2017 [10]. The absolute number of household in Nasiriyah city is evaluated to be about 58013 households. The selected study area is distinct. Whereas the boundary of the study area represented by the imaginary line, is termed as the 'external cordon'. The area that largely determines the travel pattern within the external cordon line is subdivided into zones. These zones are variety in order to promote data collection for transport planning processes. The sub-division into zones further helps to connect the sources and destinations of travel geographically. Zones within the study area are referred to as internal zones while those outside the study area are referred to as external zones [11]. In this study, 22 zones are the total number of Traffic Analysis Zones (TAZ). Figure 1 provides descriptions of these zones.

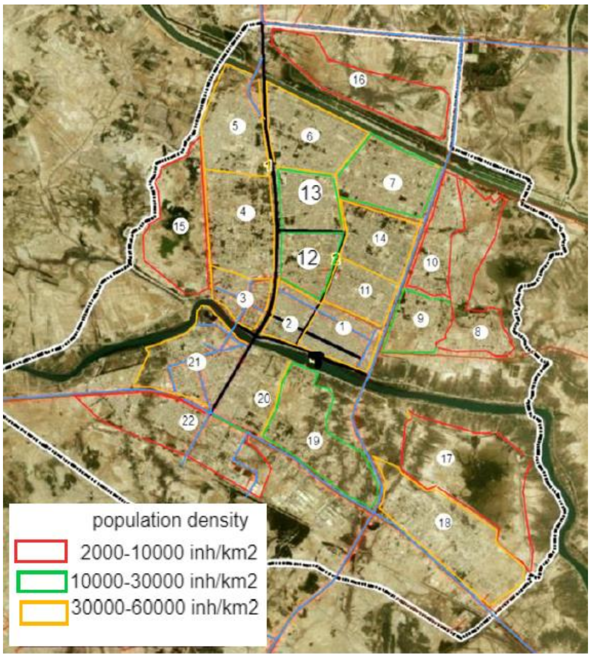

Figure 1. Nasiriyah city zones

3. MODEL DEVELOPMENT

Onset, two trip distribution matrices should be recognized. The first is observed distribution. This is the real number of outings that are observed for every starting point zone and every destination zone. The observed distribution is determined by essentially specifying the number of trips of every attraction cause. This is once in a while called a trips connection (or trips pair). The second is generally called the modeled distribution. In this case is used for approximately analytical distribution. Trips originating in each origin zone are situated in destination areas, usually based on being directly proportional to attractions and inversely proportional to costs (or impedance).

Furthermore, two model have been used in metropolitan region to achieve the best result for an acceptable assessment. First, is the Gravity model. This model gets its name from the way that it is adroitly founded on Newton's Law of attractive energy, which express that power of fascination between two bodies is straightforwardly relative to the result of the majority of the two bodies and conversely corresponding to the square of the separation between them. Eq. (1) is utilized for the estimation of the Gravity model [4, 11]. The other model is a Fratar's method [9, 12] used Eq. (2).

$$Tij = \alpha\ Oi\ Dj\ f(dij) \quad (1)$$

where, Tij is trips produced in Zone i and attracted to zone j, Oi, Dj is the total trip ends produced at i and attracted at j, $f(dij)$ *is* the generalized function of distance between any pair of zones i and j and α is the proportionality factor " Unique form of this travel distance function" that will be used throughout this paper is given as follows:

$$f(dij)= C/ti\text{-}j^n$$

where:

C: Calibration factor for the friction factor, i = origin zone, j = destination zone, n = number of zone i = origin zone j = destination zone n = number of zone.

For the second model can be represented in the following functional form

$$Ti-j = Li-j \times \frac{Pi}{pi} \times \frac{Aj}{aj} \times \frac{\sum_{j=1}^{n} ti-j}{\sum_{j=1}^{n} \frac{Aj}{aj} \times ti-j} \quad (2)$$

where, Ti-j is the summation of future trip production between i and j, ti-j is the current trip production, Pi is the summation of trip production prediction, pi is the current trip production from zone I, Aj is the summation of future trip attraction to zone j and aj is the current trip attraction to zone j.

3.1 The input of model

Develop a model of distribution needs many estimations. Firstly, estimate trip generation by Households. Secondly calculate the parameters which required in the model building for trip distribution stage by Gravity model such as (Ki, Lj, Impedance function, m and x). As well as estimation the summation of future trips production and attraction Fratar's method. Generally, the data source for all estimation above consists of details of the person travels survey conducted by home interview of Nasiriyah city for the year 2018. The statistical accepted sample size was the minimum sample size needed for conducting the household survey is [10]:

Sample Size = (1/70) * 58013 = 1214 households.

3.2 Calculating the variables of the model

Trip Generation by Households (H.H): The trips generated by households are classified as Home-Based (HB) and Non-Home-Based (NHB). Home-based trips have one end, either origin or destination, located at the home zone of the trip maker. If both ends of a trip are located in zones where the trip maker does not live, it is considered as a non-home-based trip [13]. For modelling, the study adopted the HB trips which had been categorized as four purposes which are: Home Based Work (HBW), Home Based education (HBE), Home Based Shopping (HBSH) and Home Based Other (HBO), which gave a satisfying data can adopt at model development. The Non-Home Based (NHB) had been excluded because the number of forms of their that obtained from Home Interview Survey (HIS) was too few and it cannot represent the individual movement. Thus, "Category Analysis" [9, 14] had been used to obtain trip rate by splitting the household at each traffic zone for categories according to the average person per household. Two curves had been developed. One, reveals the relation between the rate of household size and proportion of population. While, the other, reveals the relation between the rate of trips /trip purpose and household size as shown in Figure 2 and Figure 3 respectively. The rate of the household is extracted from dropping the value of H.H size for zone on a curves in Figure 2 to obtain the rate of H.H/ H.H size as illustrated in Figure 4

Sequentially, Figure 3 shows the relationship between the rate of trips/trip destination and the size of the household; the analysis will extrapolate the average trip rate according to trip purpose as Figure 5.

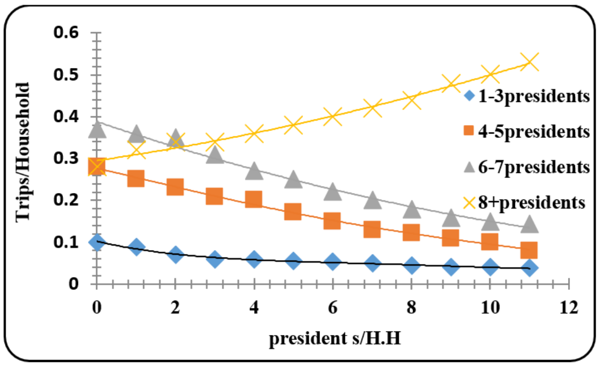

Figure 2. Relation between the rate of household size and proportion of a person

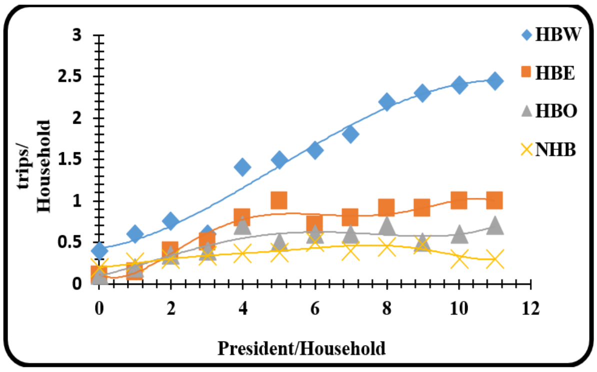

Figure 3. Relation between the rate of trips /trip purpose and household size

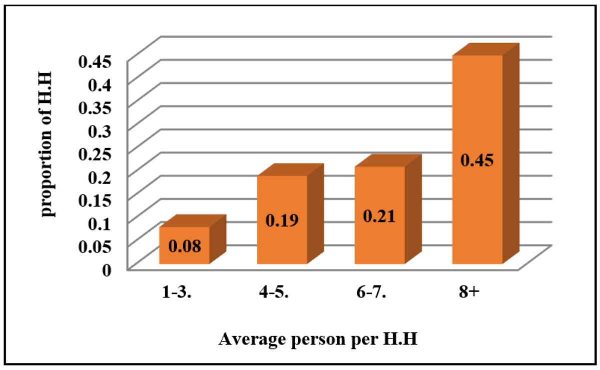

Figure 4. Rate of H.H/ H.H size

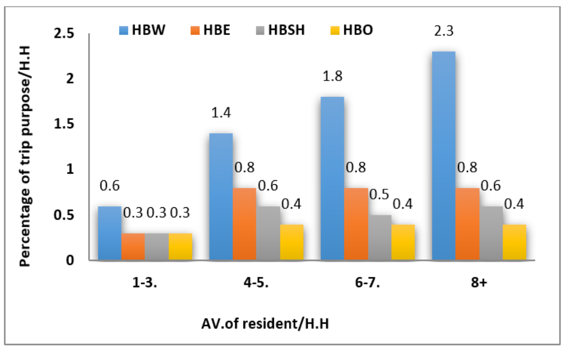

Figure 5. Average trip rate according to trip purpose

The trip production in any zone depending on H.H and average trip rate. For estimation rate of household trip production, it's multiplying the average household trip rate according to the purpose for each household size by its percentage in Figure 3 then have been multiply by the total number of the household at each zone. Thus bellow the estimating of trip production for zone No.1.

Average H.B.W rate=0.6×0.08+1.4×0.19+1.8×0.21+2.3×0.45=1.7

Since the No. of (HBW) trip for zone 1 = 1.7× (No. of H.H for zone 1 = 948[10])=1.7×948 = 1612 trip

The same procedure has been applied for estimating all trips purpose for all city as shown in Table 1.

Table 1. Trips Production by purpose at all zones for the base year

	Zone No.																						
Trip purpose	**1**	**2**	**3**	**4**	**5**	**6**	**7**	**8**	**9**	**10**	**11**	**12**	**13**	**14**	**15**	**16**	**17**	**18**	**19**	**20**	**21**	**22**	**sum**
HBW	**1612**	**3752**	**3457**	**23823**	**34149**	**42037**	**86150**	**89378**	**95029**	**56050**	**47127**	**56061**	**93166**	**62281**	**19819**	**34196**	**48144**	**25199**	**75071**	**21143**	**33417**	**3752**	**95295**
HBE	**796**	**1581**	**576**	**513**	**759**	**1311**	**1632**	**1929**	**1470**	**1638**	**1242**	**1272**	**1389**	**1377**	**729**	**735**	**957**	**1125**	**237**	**939**	**858**	**951**	**23574**
HBSH	**588**	**273**	**237**	**576**	**474**	**744**	**519**	**552**	**1629**	**399**	**264**	**381**	**438**	**723**	**453**	**309**	**681**	**624**	**267**	**312**	**537**	**291**	**10884**
HBO	**408**	**243**	**237**	**279**	**309**	**603**	**261**	**231**	**327**	**156**	**186**	**318**	**513**	**399**	**252**	**189**	**339**	**534**	**135**	**309**	**321**	**291**	**6528**
SUM	**3404**	**3039**	**1479**	**2139**	**2373**	**3546**	**3711**	**4596**	**5439**	**3120**	**2643**	**3180**	**3654**	**3585**	**2514**	**2370**	**3120**	**3288**	**1029**	**2403**	**2679**	**2643**	**63735**

Table 2. Rate of trip attraction/purpose

Trip purpose	**HBW**	**HBED**	**HBO**	**NHB**	**SUM**
Rate / total trips	42%	37.2%	14.8%	6%	100%

Table 3. Trip Attraction for 2020

Trip Attraction	**Zone No**																						
	1	**2**	**3**	**4**	**5**	**6**	**7**	**8**	**9**	**10**	**11**	**12**	**13**	**14**	**15**	**16**	**17**	**18**	**19**	**20**	**21**	**22**	**Sum**
Attraction	19412	8398	7046	3758	21479	5396	2359	2454	2930	1066	822	5396	4205	3513	11019	1846	1263	716	2096	2321	2995	4459	114949
HBW 42%	8153	3527	2959	1578	9021	2266	991	1031	1231	448	345	2266	1766	1475	4628	775	530	300	880	975	1258	1873	8153
HBED 37.2%	7221	3124	2621	1398	7990	2007	878	913	1090	397	306	2007	1564	1307	4099	687	470	266	780	863	1114	1659	42761
HBSH 14.8%	2873	1243	1043	556	3179	799	349	363	434	158	122	799	622	520	1631	273	187	106	310	344	443	660	17012
HBO 6%	1165	504	423	225	1289	324	142	147	176	64	49	324	252	211	661	111	76	43	126	139	180	268	6897

Otherwise, trip attraction, it is a typical practice to utilize total models as linear regression conditions [15] for trip attractions. The dependent variable for these total models is trip attraction. While, the independent variables and according to Figure 5, the trip work had been got the largest use, therefor the study adopted just the employment variable for the building attraction model which represent zonal total values. But it is recommended to expand the model attraction by adopting other variables (e.g. educational and recreation) for reaching more accuracy outcomes. Thus, the study reached for relation at Eq. (3) below:

$$Aj = 1.689Ej + 586 \tag{3}$$

where, Aj is the trip attraction for zone j and Ej is the zonal employment j.

The correlation coefficient of the model achieved 80%, and the rate of trip per No. of trips purpose it's going to excreted results as shown in Table 2.

The rate above at Table 2 will be duplicated for all zones to obtain the trip attraction within the city for the base year. Table 3 reveals the estimation of a trip attraction of Nassiriyah city for the base year of 2020.

The number of the trips generated between all of the zones of origin i and all of the zones of destination j should be equal to the total end of trip generated in the zone of origin for any destination zone, similar declarations can be mad. These are recognized as the constraints on flow conservation are given as follows:

$$\sum_{j=1}^{n} T\mathrm{ij} = Oi \tag{4}$$

$$\sum_{i=1}^{n} T\mathrm{ij} = Dj \tag{5}$$

Based on Eq. (1) will be obtained:

$$\sum_{j=1}^{n} (\mathrm{Ki\ Lj\ .Oi.Dj\ f(dij)}) = Oi \tag{6}$$

$$\sum_{i=1}^{n} (\mathrm{Ki\ Lj\ .Oi.Dj\ f(dij)}) = Dj \tag{7}$$

By arranging the equations above obtained the following equations:

$$Lj\ Dj \sum_{j=1}^{n} (\mathrm{Ki\ .Oi\ f(dij)}) = Dj \tag{8}$$

$$Ki\ Oi \sum_{j=1}^{n} (\mathrm{Lj\ .Dj\ f(dij)}) = Oi \tag{9}$$

Finally, the study is reaching to two equations as bellow:

$$\mathrm{Ki} = \frac{1}{\sum_{j=1}^{n} (\mathrm{Lj\ .Dj\ f(dij)})} \tag{10}$$

$$\mathrm{Lj} = \frac{1}{\sum_{i=1}^{n} (\mathrm{Ki.\ Oi\ f(dij)})} \tag{11}$$

Another step, the impedance function takes different formulas of functions [13], so for investigate the study very important step is calculating Impedance function. As the literature, the impedance function takes different formulas of functions [13], so for investigate the study distance had been using the following Equation as an impedance function. The impedance function takes different formulas of functions [13], so for investigate the study distance had been using the following Equation as an impedance function.

$$f(dij) = (di - j)^m \times e^{-x \cdot dij} \quad (12)$$

where:

di-j = distance between zone i and j, x, m = constant

The matrix of distance had been estimated depending on a plan of the Nassiriyah city on scale (1: 100000). At this stage, program used to distribute the trips on zones inside and at outside of the city, upon on Gravity Model and for calculating all variables which show in steps (a, b and c). While the constant (x, m) found by two stages, one supposes limit values for (m, x) as illustrate in bellow formula:

$$f(di - j) = di - j^{1.6} \times e^{-0.78\, di-j} \quad (13)$$

By substituting the value of (d) from the distance matrix to find the constant (Ki, Lj) so suppose K1=1 and using Eq. (11) will obtain a value of the parameter of Lj. Then entering this value in Equation 10 for reaches to a new value of Ki. Thus, the iterative process continues until the values of Ki Thus, the iterative process continues until the values of Ki, Lj converge of the next iterative process, thus obtaining the values of (Ki, Lj), at last going to calculate trip distribution matrix (Ti-j) and compare it with the observed trip matrix for a base year that's lead to estimate the ratio of error as follows:

$$\mathrm{R.Error} = \Sigma i \Sigma j \frac{\mathrm{Ti-j.T\hat{}\,i-j}}{\mathrm{Ti-j}} \quad (14)$$

where, $\mathrm{T\hat{}\,i-j}$ is the calculating value and $\mathrm{Ti-j}$ is the observed value.

At comparative the ratio of error in the formula above with the opposite values that lead to determining the need to change the constant value (m, x) at impedance function. The value of m and x at range (1.8-2.5) and (0.5-0.75) respectively, these steps represent the second stage in the correction. The dependability of model investigation at estimates the constant value in the model as (Ki, Lj, m, x) according to permitted data for the base year. When comparing with observation value, can select the model for future prediction.

At Stage 2, The study used Fratar's method for distributing the trips. It is one of Growth factored methods, the advantage of this method, its take all growth factors for different areas at distribution trips. The study used the Eq. (2) as mention earlier in section 3. The model involved many periods to reach for a matrix, which the different at its been convergence in value of trips that attracted to all zones at the base year with the value of trip attraction at the target year. The growth factor has been determining as greater than 1 and less than 1.2.

The outcomes of trip distribution models are usually calibrated by contrast between O-D trips observed verses O-D trips modelled so, the findings indicate that in most volume groups up to 4000 trips with the gravity model, the Fratar system forecasts compare best with the O-D assignments as illustrated in Figure 6.

Figure 6 shows a linear relationship. It is showing the slopes and R2 for each model. Thus, it shows that Frater's method was accurate for the base year of the study area according to the value of the coefficient of determination was 0.977, it is representing a high value to explain the strength between the observed and modelled trips. While the Gravity model among the zones did not give accurate results here the coefficient of determination was 0.2012.

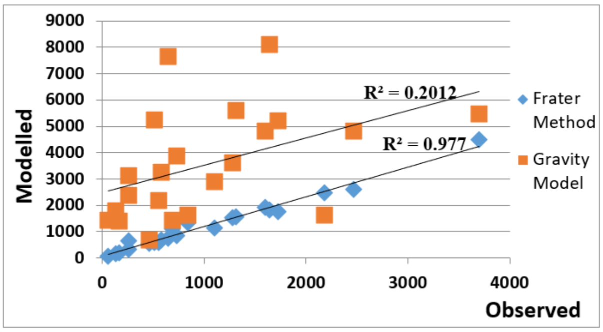

Figure 6. Calibration of models

4. STATSTICAL ANALYSIS FOR EVALUATION TRIP DISTRBUTION MODELS

As mention in section 3. The outcomes of trip distribution models are usually calculated by the contrast between modelled O-D trips and observed ones. More precisely, this paper will analyze the effects of the calibrated models using three parameters, as follows [16]:

1- The root means square error percentage (RMSE percentage), a metric for the average of individual O-D pairs, can be determined as follows:

$$\%\mathrm{RMSE} = \frac{\mathrm{RMSE}}{\mathrm{t-}} \times 100 \quad (15)$$

where, $\mathrm{RMSE} = \sqrt{\frac{\Sigma_{ij}\, tij - Tij}{X}}$, $\mathrm{t-} \; = \frac{\Sigma_{ij}(tij)}{X}$, tij is observed trips between zone i and zone j, Tij is estimated trips between zone i and zone j and X is number of observed non-zero O-D pairs.

2- Percentage of mean absolute change per trip (%MADPT) that can be calculated as follow:

$$\%\mathrm{MADPT} = \frac{\sum_{ij} |tij + Tij|}{\sum_{ij} tij} \times 100 \quad (16)$$

3- Mean absolute change per cell (MADPC) that can be calculated as follows:

$$\%MADPC = \frac{\sum_{ij} |tij + Tij|}{n} \times 100 \quad (17)$$

So, the three parameters above gave the result as a Table 4 bellow:

Table 4. Statically result of Fratar and Gravity mode

Model	Parameters		
	RMSE%	**MADPT %**	**MADPC%**
Gravity	276	69	155
Fratar	161	24	70

Table 5. Modelled trip matrix for the base year 2020

Zone No		Destination																					
		1	2	3	4	5	6	7	8	9	10	11	12	13	14	15	16	17	18	19	20	21	22	sum
	1	846	134	134	150	22	20	76	57	547	113	143	466	39	20	47	18	33	320	655	31	326	480	4607
	2	688	90	90	69	26	14	31	59	300	37	128	111	141	25	95	46	31	276	446	46	220	479	3458
	3	1275	86	86	64	31	21	33	72	235	43	131	96	24	29	44	417	59	131	589	224	1506	443	5638
	4	1600	131	131	74	55	39	34	56	1015	46	300	70	17	17	39	85	77	280	2248	2900	667	1004	10814
	5	1729	128	128	173	29	24	31	46	317	33	187	224	9	11	20	207	20	373	726	243	1357	261	6200
	6	1636	85	85	147	24	13	38	96	781	57	122	113	16	9	27	278	43	1470	1338	72	131	410	7077
	7	2185	87	87	70	21	16	29	57	967	68	56	345	22	27	33	100	1431	78	1140	52	85	672	7610
	8	261	86	86	44	26	9	20	17	130	122	60	134	21	20	20	497	564	68	740	40	39	98	3101
	9	559	56	56	52	31	11	25	29	503	65	68	91	31	74	1654	143	59	113	744	20	329	512	5160
	10	261	38	38	29	16	13	16	17	134	115	24	72	43	711	56	60	18	44	540	26	55	122	2405
Origin	11	131	64	64	48	26	11	18	35	116	116	29	121	367	43	30	135	26	59	261	24	40	74	1773
	12	1307	147	147	117	12	17	27	59	837	141	81	1654	16	17	46	102	27	108	880	60	173	421	6306
	13	649	116	116	85	27	22	34	53	1129	86	419	134	13	29	99	143	38	450	774	261	306	742	5656
	14	3697	89	89	60	47	11	22	35	663	246	43	341	21	30	57	134	44	74	726	56	74	930	7474
	15	2468	113	113	37	22	21	42	59	2731	122	73	61	9	8	31	46	20	146	531	30	555	551	7829
	16	728	83	83	89	29	17	64	982	190	99	42	55	21	35	29	69	47	186	551	16	254	215	3873
	17	576	40	40	26	25	29	507	46	134	147	103	100	14	24	30	74	31	42	711	46	172	325	3261
	18	169	26	26	31	39	447	21	24	118	60	24	57	7	7	27	42	24	37	76	20	94	76	1420
	19	456	43	43	57	2341	26	40	43	313	137	68	86	11	13	18	59	21	56	442	47	115	245	4661
	20	55	17	17	885	14	13	13	30	94	27	24	42	8	7	4	5	8	56	57	39	21	39	1451
	21	516	2152	2152	46	56	26	70	61	453	363	98	276	11	16	35	65	29	85	563	5	55	170	4044
	22	1097	113	113	37	57	33	43	60	450	161	61	204	22	26	29	99	42	221	840	42	245	332	3463
sum		228623894389423602947822120419621213023732252482285211662440279426614642155476787 326 8545107282																						

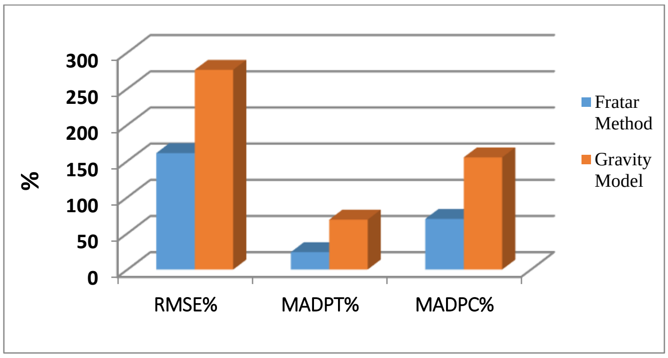

Figure 7. Statical result for Fratar and Gravity model

Table 4 shows the values for the various model formulations of the above-mentioned error measures. The graphical presentation of these outcomes is shown in Figure 7. It can be noticed that the best trip distribution model is the Fratar, based on Table 4 and Figure 7. With a significant relative variance, the Fratar Approach showed the lowest values of the three error steps. The percent RMSE of gravity forms improved by Fratar by about 39 percent with respect to the percent MADPT value, the improvement was about 61 compared to the gravity model.

Accordingly, a trip distribution matrix was built based on the results of the Fratar method, as shown in Table 5.

5. RESULTS AND DISCUSSION

(1) First of all, the process of data collection and survey conducting for each zone needs a long time and cost with large stresses. Hence it must be planned before starting, as well as it's required an institution work. Data that obtained wasn't an accuracy but, it gave acceptable information.

(2) To outline the main point of modelling trip distribution, it is depending on building trip generation model which represent a firstly studying that had been conducted in all Nasiriyah city take on the household characteristics. The model of attraction that used in modelling had been represented by the relationship between the number of trips and number of employees (Ej) at the same zone represented by Eq. (3). The model is a simplified the purpose of study, as well as it gives a good result. But recommend to inter other variables for this equation such as educational and recreation. The model attraction can use for redistribution of employment on the zones of the city for secure balance between zones to reduce traffic volume on the Central Business District network (CBD).

(3) For the modelling trip distribution, Model of Fratar proved its possibility of using it in forecasting for Al Nasiriyah city, because this method is successfully used for a homogenous growth areas. As well as in updating the data of the survey of the origin and destination of trips that collected recently, although this method does not care for rapid growth patterns. The Fratar's method has been used, it gave satisfactory results.

(4) Gravity model did not investigate a real result because Nassiriyah city is a medium-sized so as the city is not experiencing rapid changes, as well as the distances between its sectors, do not constitute an obstacle for any trip.

(5) For the gravity model, the best calibrated friction factor functions are as follows:

$$f(di-j) = di-j^{1.6} \times e^{-0.78\, di-j}$$

(6) The developing Matrix of trip distribution can be adopted for enhancing transportation network.

Finally, the study recommended:

(1) Adopt future academic studies interested with trip distribution according to its purpose take into the model split and traffic assignment to suggest the alternative for a quote strategy of the transportation system.

(2) The issue of outing conveyance is non-direct nature therefore the study recommends to use Neural Networks (NN) is appropriate for tending to the non-direct issues.

REFERENCES

[1] Goel, S., Singh, J.B., Sinha, A.K. (2012). Trip distribution model for Delhi urban area using genetic algorithm. International Journal of Computer Engineering Science (IJCES), 2(3): 1-8.

[2] de Grange, L., Fernández, E., de Cea, J. (2010). A consolidated model of trip distribution. Transportation Research Part E: Logistics and Transportation Review, 46(1): 61-75. https://doi.org/10.1016/j.tre.2009.06.001

[3] Rasouli, M. (2014). Trip distribution modelling using neural network. Doctoral dissertation, Curtin University.

[4] Mathew, T.V., Rao, K.K. (2006). Introduction to Transportation Engineering. Civil Engineering–Transportation Engineering. IIT Bombay, NPTEL ONLINE.

[5] Salter, R.J. (1996). Highway Traffic Analysis and Design. Macmillan International Higher Education.

[6] Yaldi, G., Taylor, M.A., Yue, W.L. (2011). Forecasting origin-destination matrices by using neural network approach: A comparison of testing performance between back propagation, variable learning rate and Levenberg-Marquardt algorithms. In Australasian Transport Research Forum.

[7] Herijanto, W., Thorpe, N. (2005). Developing the singly constrained gravity model for application in developing countries. Journal of the Eastern Asia Society for Transportation Studies, 6: 1708-1723. https://doi.org/10.11175/easts.6.1708

[8] Abdel-Aal, M.M.M. (2014). Calibrating a trip distribution gravity model stratified by the trip purposes for the city of Alexandria. Alexandria Engineering Journal, 53(3): 677-689. https://doi.org/10.1016/j.aej.2014.04.006

[9] Chatterjee, A., Venigalla, M.M. (2004). Travel demand forecasting for urban transportation planning. Handbook of Transportation Engineering. ISBN: 978-0071391221.

[10] Population Statistics Directorate - City of Nassiriyah - Central Statistical Organization-household for Neighborhoods Housing for the city of Nassiriyah, 2017.

[11] de Dios Ortúzar, J., Willumsen, L.G. (2011). Modelling Transport. John Wiley & Sons.

[12] de Dios Ortúzar, J., Willumsen, L.G. (1996). Modeling Transport, Second edition. John Wiley & Sons Ltd., England.

[13] Kadiyali, L.R., Lal, N.B. (2011). Traffic Engineering and Transport Planning. Khanna Publishers, 9th Reprint.

[14] Garber, N.J., Hoel, L.A. (2014). Traffic and Highway Engineering. Cengage Learning.

[15] Papacostas, C.S., Prevedouros, P.D. (1993). Transportation Engineering and Planning. 3rd ed, Prentice, Hall of India, Private Limited.

[16] Transportation Planning Center (TRANSPLAN). (1999). Study of calibration the strategic national transportation models. Transport Planning Authority, Ministry of Transportation, Egypt.

OPEN ACCESS Freely available online

International Journal of Advancements in Technology

Research

Performance Evaluation of Fiber and Silica fume on Pervious Concrete Pavements Containing Waste Recycled Concrete Aggregate

Haider A Ibrahim*, Mohammed B Mahdi, Basim J Abbas

Civil Engineering Department, Al-Muthanna University, Samawa, Iraq

ABSTRACT

Pervious concrete as a paving material rehabilitate on a new interest due to its efficiency to permit water to drainage over itself to flow groundwater and reducing storm water runoff. The employment of Recycled Coarse Aggregates (RCA) from site of construction and destruction wastes to product green concrete as a sustainable solve with varied environmental interests. Three different series (A, B, and C) of pervious concrete were used in this work, every series consisting of four mixtures, The (series A) mixtures with RCA replacement were 25%, 50%, 75% and 100% by weight of Natural Coarse Aggregate (NA), and (series B) mixtures using the same replacement ratios of RCA in addition of (silica fume SF) of 2.5%, 5%, 10%, and 12% by weight of cement to strengthen the cement past of pervious concrete. Finally, the (series C) mixtures were included the similar ratios of RCA and SF in addition to glass fibers of volume fraction 0.05%, 0.1%, 0.15%, and 0.2%. The properties of RCA pervious concrete investigated from density, hydraulic conductivity coefficient, porosity, and strength indices were compressive, flexural, and splitting tensile strengths. The test results shows that the use of RCA slightly affect hydraulic conductivity and nugatory effect on compressive, tensile, and flexural strengths where the use of silica fume and glass fibres more strong effect on the hydraulic conductivity and positive effect on pervious concrete flexural, splitting tensile strengths.

Keywords: Pervious concrete pavements; Recycled concrete aggregates; Silica fume; Glass fibers; Hydraulic conductivity

INTRODUCTION

Each year for several reasons amounts of site and demolition wastes created the removal of these wastes is a hard environmental and public problem. Therefore, construction recycling and wastes of demolition for use as aggregates to manufacture new concrete can minimize the trouble of storage of waste and keep natural aggregate needed of resources [1]. Most classic Pavements surfaces prevent water from go to the subsoil under them. These impervious surfaces excess runoff, leads to flooding, pervious concrete pavement is the only means to gain environmental utilities. By blockade rainwater and permitting it to flow into the ground, also is tactical in reloading groundwater, reducing storm water runoff and considered a special type of porous concrete. Porous concrete can be classified into two types: one in which the voids is present in the aggregate component of the mixture RCA, and one in which porosity is introduced in the no aggregate component of the mixture previous concrete [2]. Pervious concrete also indicated to as absorbent concrete or permeable concrete is an unusual concrete has linked pores ranging in size from 2 to 8 mm and void contents from 18% to 35%. The cement paste envelope layer of pervious concrete is very thin. Thus, the strength of pervious concrete depends primarily on the strength of thin binder paste that its compressive strength is relatively low ranging from 2.8 to 28.0 MPa. Pervious concrete owns a bulk unit weight in extent between 1600 kg/m^3 and 2000 kg/m^3, and flexural strength generally ranges between about 1 MPa and 3.8 MPa [3]. It is different from normal concrete in a way that it includes very less or no amount of fine aggregate with comparatively rise porosity and

Correspondence to: Haider A Ibrahim, Civil Engineering Department, Al-Muthanna University, Samawa, Iraq, E-mail: arabyhaider@yahoo.com

Received date: August 19, 2019; **Accepted date:** September 3, 2019**; Published date:** September 18, 2019

Citation: Haider A Ibrahim, Mohammed B Mahdi, Basim J Abbas (2019) Performance Evaluation of Fiber and Silica fume on Pervious Concrete Pavements Containing Waste Recycled Concrete Aggregate. Int J Adv Technol 10:230. doi: 10.24105/0976-4860.10.230

high water permeability. Pervious concrete is used for a number of civil engineering and architectural applications such as in park areas, areas with light traffic, pedestrian walkways and tennis courts [4]. The interconnected voids of pervious concrete allow water to pass through and thus it can be used to reduce storm water runoff rate and in other employments like water purification, acoustic sucking the pervious concrete pavement be able to intake the vehicle noise, which to become quiet and comfortable environment. In rainy days, the pervious concrete pavement has no plash on the surface and does not luminosity at night. This improves the rest and safety of drivers [5]. As hydraulic structures but head for to reduce compressive strength too much less than normal concrete due to its high porosity and lack of fine aggregates, several studies have been carried out on mechanical properties of pervious concrete using Recycled Concrete Aggregate (RCA) by 0, 10, 20, 30, 50, and 100% were changed with coarse natural aggregates, results indicate that up to 50% substitution of course aggregate can be used in pervious concrete without compromising strength and hydraulic conductivity significantly . Mechanical properties of pervious concrete decreases and permeability increases with the increase in percentage of recycled aggregates [7]. The changes in mix composition with fiber, w/c ratio of 0.33, and supplementary cementitious additives like silica fume ash can easily are used in order to increase the mechanical properties of pervious concrete [8].

Rizvi et al. [9] studied the effects of different percentages of RCA content on void ratio, compressive strength, and permeability in pervious concrete. Increasing RCA content led to a decrease in compressive strength, an increase in permeability, and an increase in void ratio. Decreases in compressive strength were attributed to RCA being weaker than conventional 36 aggregates. Increases in permeability and void ratio were due to RCA being more angular than the virgin aggregate. This study showed pervious concrete with 15% RCA had compressive strength, permeability, and void content similar to that of the control mix. The authors recommended further research should be conducted to determine the effects of using different sources of RCA in pervious concrete.

MATERIALS

Portland cement type 1 conforming to ASTM C 150 [10]. Superplasticizer (SP) Type F [11] is used because of low water-cementitious ratios specified for pervious concrete. Recycled Concrete Aggregate (RCA) was the material used in this work according to ACI 555-01[12] was collected from a demolition site. The appearances are shown in Figure 1. RCA was crushed and sieved to obtain 4.75-9.50 mm particles for use as recycled coarse aggregates. Natural limestone Aggregate (NA), and RCA meets requirements specified by ASTM C33 [13]. Their properties are shown in Table 1. The low density, high water absorption and high Los Angeles abrasion loss of the recycled aggregate were due to the high porosity of adhered cement mortar on the recycled aggregate as indicated by previous researchers [14]. Silica Fume (SF) with 93.3% SiO^2 content, 25000 m^2/kg surface area, and 2.2 specific gravity was used in this study to boost pervious concrete properties, the chemical analysis of SF is shown in Table 1. Glass fiber with 2.63 (gr/cm^3) Specific gravity, 12 mm length and 0.1 mm diameter used as added material to concrete.

Table 1: The physical properties of NA and RCA.

Properties	NA	RCA	Specification
Dry- density (Kg/m^3)	1435	1350	ASTM C29 [15]
Fineness of modulus	5.88	5.98	ASTM 136 [16]
Specific gravity	2.69	2.57	ASTMC127 [17]
Absorption (%)	0.45	4.57	ASTM C127 [18]
Abrasion loss Angeles (%)	28.3	44.2	ASTM C127 [19]

Table 2: The chemical composition of Portland cement and silica fume.

Material	Chemical composition					
	SiO_2	Al_2O_3	CaO	MgO	Fe_2O_3	SO_3
Cement	22.6	5.6	62.7	1.7	4.3	2.5
Silica fumes	93.3	0.73	0.85	1.21	0.49	1.02

Figure 1: RCA and Glass fibers.

METHODOLOGY AND MIX PROPORTION

Hydraulic conductivity and porosity

The significant key characteristics of pervious concrete are its hydraulic conductivity. It was measured using the constant head method in accordance to ASTM D-2434-68 [19]. Figure 2 shows the device used to define the pervious concrete permeation used to inspect the permeation of cylindrical samples of (100 × 200) mm. To keep from the leakage of water between model and test device, the cylindrical sample was covered with a rubber tube and tightened by circular clamps. Water was permitted into the specimen to obtain a steady-state flow. The hydraulic conductivity of pervious concrete was computed by using Eq. (1)

Hydraulic Conductivity Coefficient, (cm/s), k=Ql/Hat (1)

Where Q is quantity of water (mm^3), L is length of pervious concrete specimen (150 mm), H is water head (200 mm), A is the cross-sectional area of sample, and, t is time taken for the water head to flow through the specimen (s).

ASTM C1754 [20], was followed to calculate the density and the porosity of pervious concrete, porosity of pervious concrete; It is a ratio of the volume of voids, to all volume of cement paste and aggregate cylinders, (method A) at 28 days of age was used, by taking the difference in weights of an oven-dried (100 mm × 200 mm) cylindrical specimens, the test was performed at three samples for each mix design.

Figure 2: Constructed a device for a hydraulic conductivity test.

Concrete testing

Pervious concrete samples set in general, according to ASTM C192-02 [21]. For each mix, three (150 mm) standard cubic steel molds used for casting specimens and for Compression strength in (28) days in agreement with ASTM C39-98 [22], the splitting tensile strength used three molds of (100 200) mm cylindrical concrete samples measured conformity to the ASTM C 496M-04 two (100 × 100 × 400 mm) prisms for flexural strength at (28) day, correspond with ASTM C78-02 [23,24]. Moreover, in order to calculate the hydraulic conductivity coefficient and porosity, three (100 × 200) mm cylindrical specimens casts. The samples cast in three layers by Rodding 25 times by applying a vibration for (10) seconds. After mixing, the specimens disposed of the molds and maintained in the water until they will arrive the test age of (28) days when they are ready to do the experimental tests.

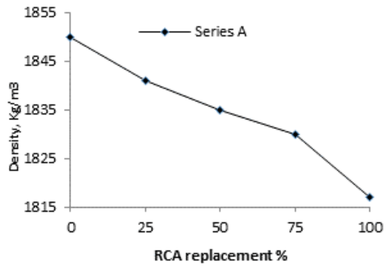

Figure 3: Density for series A.

Table 3: Mix proportions for all mixes.

Mix Design	Cement Content Kg/m^3	Water (Kg/m^3)	Coarse (Kgm^3)	Aggregates	Glass Fiber%	Silica Fume%	S.P.% of Cement
			NA	RCA			
NC-0	370	98	1400	0	0	0	0
Series A							
RC25%-(R1)	370	98	1050	350	0	0	1.83
RC50%-(R2)	370	98	700	700	0	0	2.34
RC75%-(R3)	370	98	350	1050	0	0	2.6
RC100% -(R4)	370	98	0	1400	0	0	2.9
Series B							
RC25%-S 2.5%-(RS1)	360.75	98	1050	350	0	2.5	2.76
RC50%-S 5%-(RS2)	351.5	98	700	700	0	5	3.14
RC75%-S10%-(RS3)	333	98	350	1050	0	10	3.37
RC100%-S12%-(RS4)	325.6	98	0	1400	0	12	3.52
Series C							

RC25-GL0.5%- S 2.5% (RGS1)	360.75	98	1050	350	0.5	2.5	3.32
RC50-GL0.1%-S 5% (RGS2)	351.5	98	700	700	0.1	5	3.65
RC75-GL0.15%-S10%- (RGS3)	333	98	350	1050	0.15	10	3.85
RC100 -GL0.2%-S12% (RGS4)	325.6	98	0	1400	0.2	12	4.23

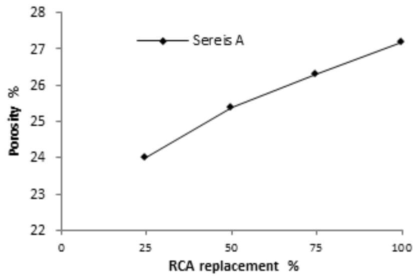

Figure 4: Porosity for series A.

Mix proportions

The pervious concrete proportioning mixture with RCA is different compared to normal concrete. The density of RCA is usually lower and higher more absorbent of water compared to natural aggregate due to the cement paste has a high attraction to water [24]. This absorption capacity of the cement paste is one of the most significant differences in properties and which distinguishes RCA from natural aggregate, execution of concrete with RCA depends on the water-cement (w/c) ratio of the genuine concrete and the w/c ratio of the recently created concrete, it's designed to allow the discharge of water through its surface. The first stride in proportion the mixture is to define the aggregate void ratio, correspondence with ASTM C29 [14], the aggregate specific gravity. The void content of aggregate that will be used in a previous concrete mixture variable and depend on the grading. The reference mixture is made by ACI 211.3-02 [25], and the target void content range of the pervious concrete mixture should be specified The control pervious concrete (NC) consisted of (370 kg) of Portland cement, 98 kg of water, and (1450 kg) of NA for 1 m^3 of concrete with three series A, B, and C, each series consist of four mixes.

In series A the NA was replaced with RCA at the levels of 0%, 25%, 50%, 75%, and100% by weight of coarse aggregate for (R1, R2, R3, and R4), but series B the silica fume replacement with cement at (2.5%, 5%, 10%, and 12%) for the same percentages of the RCA were replaced with NA. Series C was containing glass fibers at (0.5%, 0.1%, 0.15%, and 0.2%) with the same present of RCA and silica fume, Table 3 gives the summary of pervious concrete mix proportions, for all mixtures the aggregates were used in saturated surface dry casings S.S.D. Specific surface area of S.F is greater than the cement, therefore the concrete performance is reduced fundamentally and more water is needed to fix it, because the concrete Performance should not be changed; the amount of superplasticizer is increased.

RESULTS AND DISCUSSION

Effect of RCA replacement level (series A)

Density and porosity: The effect of employing recycled concrete aggregate as a coarse aggregate replacement on density is declared in Figure 3, it is obvious that the use of recycled concrete aggregate slightly decreases density in general, the use of recycled concrete aggregate decreases the density of pervious concrete. This manner may be due to the higher voids ratio of recycled aggregate. For example, in (series A), the reduction in hardened density of pervious concrete at 100% recycled aggregate replacement level is 1.8% compared with that of control mix. From the test results, the reduction in concrete density as a result of the increasing of recycled concrete aggregate is 0.5%, 0.8%, 1.1% for 25%, 50%, 75% recycled concrete aggregate replacement level, respectively. The density values of pervious concrete correspond with the submitted values by ACI 522 [3], which summed up in Table 4.

Figure 4 shows the effectiveness of recycled aggregate replacement level on porosity. From this figure, the utilizing of RCA increases the porosity which demonstrates the reduction in pervious concrete density like the results of using recycled aggregate concrete. The increase in concrete porosity ratio for (R1, R2, R3, and R4) mixtures are 4.3%, 10.4%, 14.3%, and 18.3 for 25%, 50%, 75%, and 100% replacement level compared with that of control mix. The increase of porosity because of the lower workability of pervious concrete with RCA due to more angular shape of recycled aggregate compared with that of natural aggregate [5]. The results of porosity agree with those suggested by ACI 522R [3].

Hydraulic conductivity: Figure 5 debates the effect of RCA replacement grades on pervious concrete. From the test results, the rising of recycled aggregate content increases hydraulic conductivity the slightly increase percentage in pervious concrete water permeability made with (series A) is 0.5%, 9.1%, 10.9%, and 13.6% for 25%, 50%, 75%, and 100% recycled concrete aggregate replacement levels, respectively. In addition, it is renowned that the achieved values of

Hydraulic Conductivity are remaining in the ideal ranges given in Table 4.

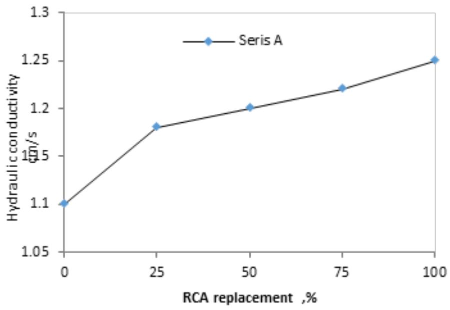

Figure 5: Hydraulic conductivity coefficient for series A with RCA replacement.

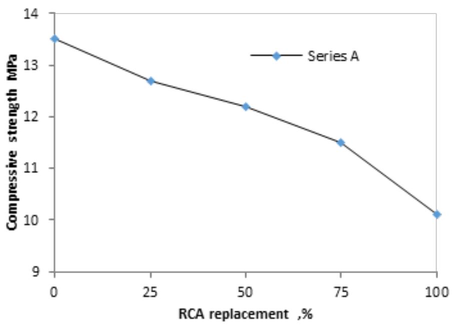

Figure 6: Compression strength with RCA replacement percent for series A at (28) day.

Compressive strength: The effect of RCA replacement levels on pervious concrete compressive strength is illustrative in Figure 6; it is obvious that the use of RCA has an important effect on compressive strength where the excess of RCA content reduces the resulting concrete compressive strength. This inefficient influence may be due to the higher porosity in concrete with RCA and due to the poor bonding between RCA and cement paste [26]. In addition, the bad transition zone properties between recycled aggregate and cement paste may cause this negative effect [27]. The reduction in 28 days concrete compressive strength is 6%, 10%, 14.8% and 25% for 25%, 50%, 75% and 100% recycled aggregate levels, respectively compared with that of control mix. Finally, it is important to mention that although the using of recycled aggregate adversely affected the compressive strength of pervious concrete the achieved results stay fulfil the proposed typical ranges by ACI 522 [3].

Flexural and splitting tensile strength: Figure 7 shows the effect of RCA replacement levels on pervious concrete flexural strength. From this Figure, the increase of replacement levels of the recycled aggregate reduces the pervious concrete flexural strength. The range of decrease in flexural strength as the results of using recycled aggregate from 25% to 100% replacement levels is 10.8% to 41%, respectively. This behavior is the same for splitting tensile strength as shown in Figure 7 and Table 4. The negative effect of using recycled aggregate may be assigned to the bad properties of transition zone in case of RCA. The transition zone greatly affects the concrete tensile strength [28].

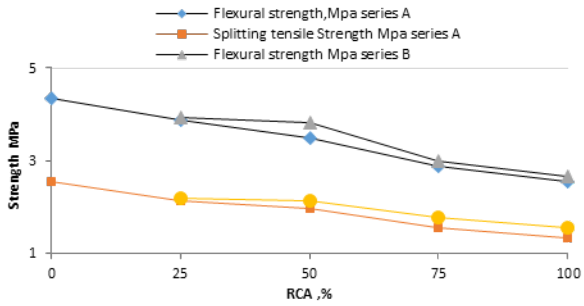

Figure 7: Flexural and splitting tensile strengths with RCA replacement percent for series A and B at (28) day.

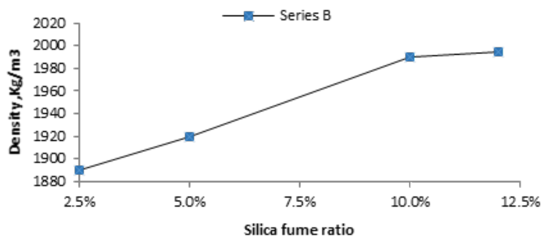

Figure 8: Porosity for series B with silica fume ratios.

Addition of silica Fume to RCA pervious concrete (Series B)

Density and porosity of pervious concrete: In Table 4, it can be seen that by incorporating SF with the same replacement level of RCA, for series A, and B, the increase of silica fume content to series B mixes increase density of pervious concrete as shown in Figure 8. As an example, the increase in pervious concrete density is 2.7%, 4.6%, 8.7%, and 9.7% for 2.5%, 5%, 10% and 12% silica fume content, respectively in comparison between series A and B mixes. The influence of using silica fume on porosity of pervious concrete is shown in Figure 9. From this figure, the increase in silica fume levels decreases the resulting voids ratios. From the test results, the decrease in hardened pervious concrete voids ratio in the range from 11.3% to 23.5% from 2.5% to 12% silica fume. This behavior may be due to the filling effect of silica fume in addition to the good ability of compaction in the presence of very fine silica fume [29].

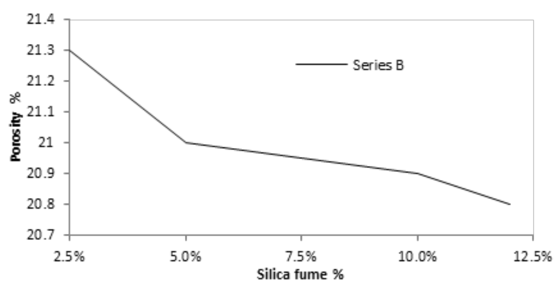

Figure 9: Porosity for series B with silica fume ratios.

Table 4: Results of all mixtures.

Mix Design	Bulk density Kg/m^3	Hydraulic Conductivity cm/s	Porosity (%)	Comp. Strength 28-day	Flexural Strength 28-day	Tensile Strength 28-day
				MPa	MPa	MPa
NC-0	1850	1.1	23	13.5	4.34	2.56
Series A						
RC25%-(R1)	1841	1.18	24	12.7	3.87	2.12
RC50%-(R2)	1835	1.2	25.4	12.2	3.5	1.98
RC75%-(R3)	1830	1.22	26.3	11.5	2.87	1.54
RC100%-(R4)	1817	1.25	27.2	10.1	2.56	1.33
Series B						
RC25%-S 2.5%-(RS1)	1890	1.12	21.3	14.87	3.93	2.18
RC50%-S 5%-(RS2)	1920	1.08	21	16.21	3.43	2.14
RC75%-S10%-(RS3)	1990	0.97	20.9	17.35	2.98	1.78
RC100%-S12%-(RS4)	1995	0.95	20.8	17.51	2.66	1.54
Series C						
RC25-GL0.5%- S 2.5% (RGS1)	1887	0.9	21	14.99	4.76	3.32
RC50-GL0.1%-S 5% (RGS2)	1916	0.89	21.9	14.32	7.54	4.23
RC75-GL0.15%-S10%-RGS3)	1986	0.88	22.8	13.61	8.54	5.43
RC100 -GL0.2%-S12% (RGS4)	1990	0.82	24	9.54	8.56	4.98

Hydraulic conductivity coefficient: The silica fumes influence of series B on Hydraulic Conductivity is shown in Figure 10. From the test results for concrete with the same replacement of recycled aggregate, the increase of the silica fume decreases pervious concrete hydraulic conductivity coefficient.

These results may be due to the improving of pervious concrete density as the result of adding silica fume. The decrease in pervious concrete porosity is 5.1%, 10%, 20.5%, and 19.2% for RS1, RS2, RS3, and RS4 mixtures of 2.5%, 5%, 10% and 12% silica fume, respectively compared with series A.

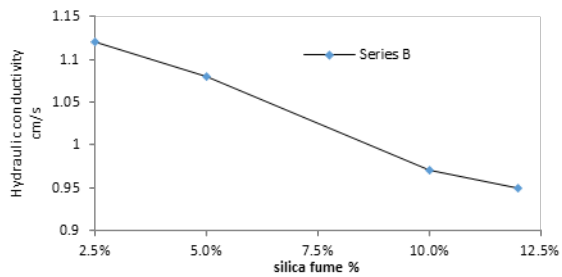

Figure 10: Hydraulic conductivity coefficient for series B with SF ratios.

Compressive strength of pervious concrete: From this Figures 11 and 12, it can be found by comparing the series A and B the influence of silica fume on pervious concrete compressive strength, the use of silica fume enhances pervious concrete compressive strength. This increase on 28 days compressive strength for pervious concrete with the Similar RCA replacement ratios and is 17.1%, 32.9%, 50.9% and 73.4% for 2.5%, 5%, 10%, and 12% silica fume, respectively. This enhancement may be attributed to the improvement of cement matrix because of filling effect and Pozzolanic reaction of silica fume [30].

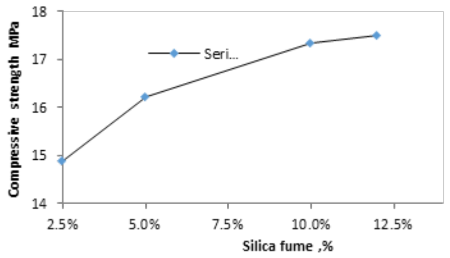

Figure 11: Compression strength with SF ratios for Series B at (28) day.

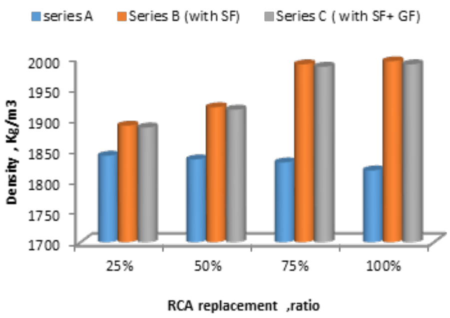

Figure 12: Density for all series with RCA replacement ratio.

Flexural and splitting tensile strength: Figure 7 shows the influence of silica fume on 28 days pervious concrete flexural and splitting tensile strength. From this figure, it is clear that the silica fume slightly improves pervious concrete flexural and splitting tensile strength. This improvement may be attributed to the enhancement of the cement matrix and transition zone because of using very fine silica fume [31]. For example for series B with recycled aggregate and silica fume, the increase in pervious concrete 28 days splitting tensile strength is 2.8%, 8.1%, 15.6%, and 15.7% for 2.5%, 5%, 10% and 12% silica fume compared with series A. This increase in splitting tensile strength enhances the tensile strength of pervious concrete mix with 100% recycled aggregate to the accepted limits given in Table 4.

Effect of glass fiber on the properties of RCA pervious concrete (series C)

Hardened density and Porosity: The experimental results of series C are shown in Figure 7. From the test results, the increase of glass fiber volume fraction decreases hardened pervious concrete density in the presence of silica fume compared to results of series B without glass fibers. These reductions are 0.1%, 0.21%, 0.2%, and 0.25% for hardened density of pervious concrete with 0.05%, 0.1%,0.15, and 0.2% glass fiber volume fraction, respectively compared with results of series C, these decreases in density of pervious concrete with glass fibers may be due to the lower density of glass fibers and the increase of voids ratio due to the presence of fiber [32].

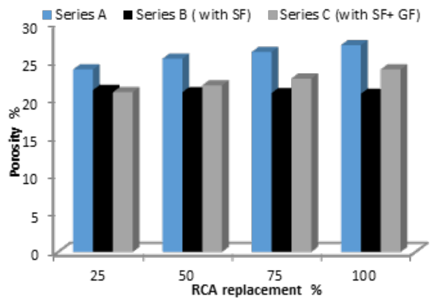

Figure 13: Porosity for all series with RCA.

The values of hardened density of pervious concrete match with the proposed values by ACI 522 [3]. The results of using glass fibers are presented in Figure 13 for the porosity of pervious concrete with SF at series C, it is clear that the increase of glass fibers levels slightly increases the resulting voids ratios. This is attributed to the absence of cohesion and bad dispersion of fibers [33]. From the test results, the increase in hardened pervious concrete porosity is 9% and 5.3% for 0.1% and 0.2% glass fiber volume fraction, respectively compared with series B. This slight increase in porosity decreases the density of pervious concrete with glass fibers.

Hydraulic conductivity coefficient: The influence of glass fibers volume fraction on Hydraulic Conductivity is given in Figure 9 and Figure 14. From the test results and in comperation between results of series B and C, the increase of glass fiber volume fraction increases pervious concrete hydraulic conductivity coefficient. These results may be due to the increase of the voids ratio of pervious concrete with the presence of glass fibers [34]. The increase in pervious concrete permeability is 2% and 8.7% for 0.1% and 0.2% glass fiber volume fraction, respectively compared with the control mix.

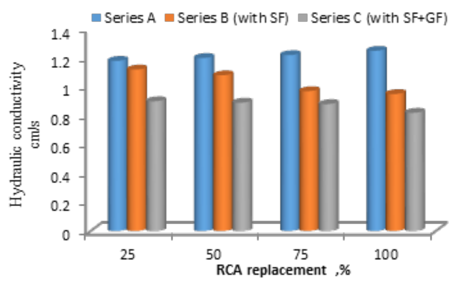

Figure 14: Hydraulic conductivity coefficient for all series with RCA.

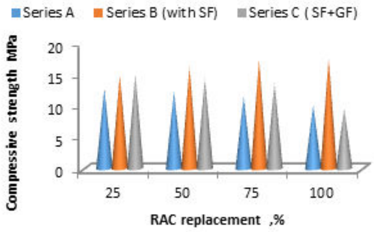

Figure 15: Compressive strength for all replacement ratios series with RCA.

Compressive strength: The influence of glass fibers at series C on compressive strength of pervious concrete is explained in Figure 10. From the figure 15, the use of glass fiber slightly decreases pervious concrete compressive strength the reduction in pervious concrete 28 days compressive strength is 1.6% and 3.2% for 1.5% and 3% glass fibers content . This behavior may be due to the lower modulus of elasticity of glass fibers [4].

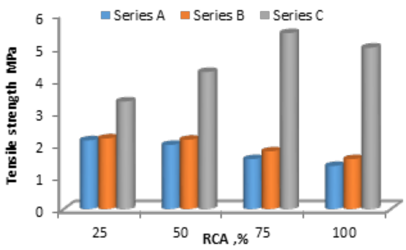

Figure 16: Tensile strength for all series with RCA.

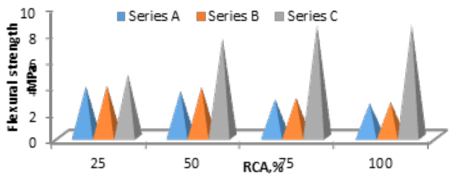

Figure 17: Flexural strength for all series with RCA.

Flexural and splitting tensile strength: Figures 11 explains the influence of glass fibers volume fraction on 28 days pervious concrete flexural and splitting tensile strength, it is clear that the glass fibers has improvement effect on pervious concrete flexural and splitting tensile strengths where the increase of glass fiber volume fraction enhances pervious concrete flexural and splitting tensile strength [Figure 16 and Figure 17]. For example, the increase in pervious concrete 28 days splitting tensile strength is 12.8% and 34.5% for 0.1% and 0.2% glass fiber volume fraction. The positive effect of glass fibers on pervious concrete tensile strength may be due to the bridging mechanism of glass fibers which arresting the failure propagation [35].

CONCLUSION

- The use of recycled concrete aggregate and glass fibers slightly affect the permeability indices where the use of silica fume yield more ingenuous effect on the hydraulic conductivity indices
- Utilizing recycled concrete aggregate has a significant negative effect on compressive strength but the achieved results are still in the proposed typical ranges by ACI 522R
- Tensile strength test results of pervious concrete indicate that the use of recycled aggregate has a significant negative effect where the use of 25% and 100% recycled aggregate generally produces splitting tensile strengths less that the recommended.
- Addition of silica fume significantly promotes strength indices of pervious concrete where it is recommended to use 5% silica fume in case of using recycled aggregate in pervious concrete production
- The use of glass fiber slightly decreases pervious concrete compressive strength, and has a positive effect on pervious concrete flexural, splitting tensile strength percentage. This improvement enhances the tensile strength of pervious concrete mix with 25% to 100% recycled aggregate to achieve the accepted limits

REFERENCES

1. Zaetang Y, Sata V, Wongsa A, Chindaprasirt P. Properties of pervious concrete containing recycled concrete block aggregate and recycled concrete aggregate. Constr Build Mater. 2016;111:15-21.
2. Silva RV, Brito J de, Dhir RK. Properties and composition of recycled aggregates from construction. Constr Build Mater. 2014;65:201-217.
3. American Concrete Institute (ACI) Committee 522. Pervious Concrete. ACI Committee Report, ACI 522R-06. 2006.
4. Wang H, Li H, Liang X, Xie N, Dai Z. Investigation on the mechanical properties and environmental impacts of pervious concrete containing fly ash based on the cement-aggregate ratio. Constr Build Mater. 2019;202:387-395.
5. Yang J, Jiang G. Experimental study on properties of pervious concrete pavement materials. Cement Concrete Res. 2003;33(3): 381-386.
6. Montes F, Haselbach L. Measuring hydraulic conductivity in pervious concrete. Environ Eng Sci. 2006;23(6):960-969.
7. El-Hassan H, Kianmehr P, Zouaoui S. Properties of pervious concrete incorporating recycled concrete aggregates and slag. Constr Build Mater. 2019;212:164-175.
8. Rizvi R, Tighe S, Henderson V. Evaluating the use of recycled concrete aggregate in pervious concrete pavement. J Trans Res Board. 2010;2164(1),132-140. s
9. ASTM International. Standard specification for portland cement, ASTM C150-12. 2012.

10. ASTM International. Standard specification for chemical admixtures for concrete, ASTM C494M-04. 2004.
11. American Concrete Institute (ACI) Committee 555. Removal and reuse of hardened concrete. ACI Committee Report. ACI 555R-01. 2001.
12. ASTM International. Standard specification for concrete aggregates, ASTM C33-03. 2003.
13. Rehder B, Banh K, Neithalath N. Fracture behavior of pervious concretes: The effects of pore structure and fibers. Eng Fract Mech. 2014;118:1-16.
14. ASTM International. Standard test method for bulk density (Unit Weight) and voids in aggregate, ASTM C29M-07. 2007.
15. ASTM International. Standard test method for sieve analysis of fine and coarse aggregates, ASTM C136-01. 2001.
16. ASTM International. Standard test method for density, relative density (specific gravity), and absorption of coarse aggregate, ASTM C 127-01. 2001.
17. ASTM International. Standard test method for resistance to degradation of small-size coarse aggregate by abrasion and impact in the Los Angeles machine, ASTM C 131-03.2003.
18. ASTM International. Standard test method for permeability of granular soils (constant head), ASTM D 2434-92. 1992.
19. ASTM International. Standard test method for density and void content of hardened pervious concrete, ASTM C1754/C1754M-12. 2012.
20. ASTM International. Standard practice for making and curing concrete test specimens in the laboratory, ASTMC192-02. 2016.
21. ASTM International. Standard test method for compressive strength of cylindrical concrete specimens, ASTM C39/C39M-03. 2003.
22. ASTM International. Standard test method for splitting tensile strength of cylindrical concrete specimens, ASTM C 496M-04.2004.
23. ASTM International. Standard test method for flexural strength of concrete (Using simple beam with third-point loading, ASTM C78-02. 2002.
24. Aliabdo AA, Abd Elmoaty AEM, Fawzy AM. Experimental investigation on permeability indices and strength of modified pervious concrete with recycled concrete aggregate. Constr Build Mater. 2018;193:105–127.
25. American Concrete Institute (ACI) committee 211.3 Guide for selecting proportions for no-slump concrete. ACI standard practice, ACI 211.3R-02.2002.
26. Huang B, Wu H, Shu X, Burdette EG. Laboratory evaluation of permeability and strength of polymer-modified pervious concrete. Constr Build Mater. 2010;24(5):818-823.
27. Bernardo MP, Cunanan PJS, Lopez JLC, Rarugal EJR., Sarukunaselan K. Qualitative investigation of the application of pervious concrete as pavement for storm water runoff management using hydrologic modelling system (HEC-HMS). J Telecommun Electron Comput Eng. 2018;10:63-66.
28. Hun S, Joo D, Sung G, Taek K. Tensile behavior of ultra high performance hybrid fiber reinforced concrete. Cement Concrete Comp. 2012;34(2):172-184.
29. Reddy JKC, Babu PSSA. Significance of silica fume on the mechanical properties of recycled aggregate concrete. Int J Sci Res. 2016;5:2319-7064.
30. Yap SP, Chen PZC, Goh Y, Ibrahim HA, Mo KH, Yuen CW. Characterization of pervious concrete with blended natural aggregate and recycled concrete aggregates. J Clean Prod. 2018;181:155-165.
31. Raghwani JR, Shah D, Bhavsar JK. Performance assessment of pervious concrete by using silica fume. J Civil Eng Environ Technol. 2016;4(3):269-273.
32. Bhogayata AC, Arora NK. Workability, strength, and durability of concrete containing recycled plastic fibers and styrene-butadiene rubber latex. Constr Build Mater. 2018;180:382-395.
33. Kapoor K, Ahmad T, Afzal G. Experimental study on infiltration properties of pervious concrete. Sustainable Engineering. 2019.
34. Pourbaba M, Asefi E, Sadaghian H, Mirmiran A. Effect of age on the compressive strength of ultra-high-performance fiber-reinforced concrete. Constr Build Mater. 2018;175:402-410.
35. Cui X, Zhang J, Huang D, Liu Z, Hou F, Cui S, et al. Experimental study on the relationship between permeability and strength of pervious concrete. J Mater Civil Eng. 2017;29(11):212-217.

sustainability

MDPI

Article

Simulation-Based Analysis of the Effect of Significant Traffic Parameters on Lane Changing for Driving Logic "Cautious" on a Freeway

Danish Farooq * and Janos Juhasz

Department of Transport Technology and Economics, Budapest University of Technology and Economics, Stoczek u. 2, H-1111 Budapest, Hungary; janos.juhasz@mail.bme.hu

* Correspondence: farooq.danish@mail.bme.hu

Received: 1 August 2019; Accepted: 24 October 2019; Published: 28 October 2019

check for updates

Abstract: Lane changing of traffic flow is a complicated and significant behavior for traffic safety on the road. Frequent lane changing can cause serious traffic safety issues, particularly on a two-lane road section of a freeway. This study aimed to analyze the effect of significant traffic parameters for traffic safety on lane change frequency using the studied calibrated values for driving logic "conscious" in VISSIM. Video-recorded traffic data were utilized to calibrate the model under specified traffic conditions, and the relationship between observed variables were estimated using simulation plots. The results revealed that changes in average desired speed and traffic volume had a positive relationship with lane change frequency. In addition, lane change frequency was observed to be higher when the speed distribution was set large. 3D surface plots were also developed to show the integrated effect of specified traffic parameters on lane change frequency. Results showed that high average desired speed and large desired speed distribution coupled with high traffic volume increased the lane change frequency tremendously. The study also attempted to develop a regression model to quantify the effect of the observed parameters on lane change frequency. The regression model results showed that desired speed distribution had the highest effect on lane change frequency compared to other traffic parameters. The findings of the current study highlight the most significant traffic parameters that influence the lane change frequency.

Keywords: lane change frequency; traffic parameters; cautious; VISSIM; 3D surface plots; regression model; traffic safety

1. Introduction

The Global Status Report on Road Safety stated that the number of annual road traffic deaths has reached 1.35 million [1]. Although 90% of these deaths are centered in low- and middle-income countries, traffic accidents in WHO's European Region cause at least 120,000 deaths and injure 2.4 million people each year [2]. European roads have been stated as the safest in the world, with a 19% reduction in road fatalities over the last six years. While attaining the strategic target of halving the number of road deaths between 2010 and 2020, which is still an acute challenge, it is worth aiming to save every single life [3]. The Road Safety Action Program (2014–2016) was incorporated into the Hungarian Transport Strategy, which also sets targets to decrease the number of road fatalities by 50% between 2010 and 2020 [4]. However, according to the Hungarian Central Statistical Office data, there were 625 road fatalities in 2017, a 2.9% rise compared to 2016 [5]. The situation analysis of the Road Safety Action Program declares that most of the accidents are caused by human-related factors, and tackling them is therefore the most dynamic objective of road safety initiatives [4]. Some previous studies have estimated human factors to be the sole or primary causal factor in approximately 90% of road traffic accidents [6–9].

Frequent lane-changing behavior has an adverse effect on traffic efficiency under advanced traffic demand [10]. Li et al. [11] examined the aggressive lane-changing behavior of fast vehicles and the consequences of different lane-changing behavior with the proposed symmetric two-lane cellular automaton. The act of changing lanes was observed as one of the most common causes of accidents in the United states. Also, according to official statistics, at least 33% of all road crashes occur when vehicles change lanes or veer off the road [12].

Previous studies have shown accidents to be "multicausal" events as they are considered to be a failure of the complex interactions between driver behavior, traffic, vehicle design, road geometry, and environmental conditions [13,14]. Another research [15] found that crash occurrence had a substantial correlation with the average speed, the standard deviation of speed at the upstream loop detector station, the variance in the average speed at the upstream and downstream loop detector stations, and traffic volume. Therefore, it is difficult to detect a single causal factor that can be held responsible for an accident occurrence [16].

A recent research [17] showed that, despite the influence of various factors, speed variance is particularly worth noting as it has been frequently reported as a critical risk factor in estimating crash risk on expressways. Some studies have found both speed and speed variance to be significant factors for predicting crash frequency [18,19]. Elvik [20] reviewed 13 studies that assessed the effects of speed variance on crash rates based on loop detector data. Although almost all of these studies observed that a large variance in speed increased the risk of crashes, numerical estimations of the effect varied significantly. It is also possible that variations in speed between following vehicles on a road as well as between the lanes of a roadway affects accident risk [21–23]. However, the finding [24] that effects of speed changes tend to be higher on rural roads and motorways than on roads in built-up areas roads suggests that the initial speed is a significant factor. This was confirmed in a re-analysis of the data [25] that presented that the effect of a specified relative change in speed on the number and severity of crashes is greater when the initial speed is higher.

Two mathematical models—the power model and the exponential model—describe the relationship between the mean speed of traffic and road safety, defined as the number of fatalities and the number of injury accidents, with high accuracy [26]. One limitation of both the power model and the exponential model is that they only consider changes in average speed and therefore disregard possible changes in the shape of the speed distribution [27]. However, speed dispersion is recommended to proactively measure road safety because it presents a consistent assessment of microscopic potential risks [28]. Moreover, the effects of speed and speed variations seem to be related to other traffic variables, such as traffic flow [29,30].

Other than speed, traffic volume is one of the most studied factors in crash rate predictions [31,32]. Traffic volume, speed, and density are the three main parameters used for the characterization of traffic conditions [33]. Traffic conditions with high volume and high speed variation within the same lane represent conditions with lower levels of service and therefore unstable flow. These conditions can create higher crash risk because of the limited space between vehicles [13,30].

Microscopic simulation models are finding increased application in the evaluation of safety performance and crash prediction. Before these models can be applied, they must be calibrated based on real-world traffic conditions. The main purpose of calibration is to ensure that parameter inputs in the simulation model produce the best estimates of safety performance. Previous studies have focused on the accuracy and reproducibility of simulated output but not the ability of the performance measure to reflect actual crashes. However, with an accurate estimate of the crash potential index (CPI) from a simulation, it would be possible to compare simulated safety performance with observed crashes [34]. The process of developing a microsimulation model starts with an existing condition model and then transitions into the development of various scenarios representing future-year alternatives [35]. Microscopic traffic simulation-based safety analysis provides fast, safe, and cost-effective means of evaluating traffic safety compared to field implementation and testing [36–38]. Some previous studies have utilized video data to obtain important information to calibrate several traffic safety parameters [34,39]. The effectiveness of a calibration process as well as the preceding considerations can be best evaluated by performing "controlled" experiments in which all the model inputs are known [40].

The VISSIM model can be applied to examine various traffic scenarios for varying roadway and traffic conditions. A microsimulation model, VISSIM is suitable for simulating and studying heterogeneous traffic flow in expressways to a satisfactory extent [41]. The VISSIM model is used to generate traffic flow for a wide range, from lower to higher levels, and to investigate the number of lane changes in multilane highways [39].

The lane-changing phenomenon is considered as an act of driving maneuver that moves a vehicle from one lane to another when both lanes have the same direction of travel [42]. The actual lane-changing logic in VISSIM is utilized to choose if it is possible to change to the desired neighbor lane or not. The desired lane is an effect of the lane selection process for any free or mandatory lane changes based on gap acceptance. A free lane change considers a lane change of a vehicle to obtain speed advantages or more space [43]. Some previous studies have focused on the relationship between speed variations and crash rates or crash risk [19,31,44–47], while other studies have examined the number of lane changes under different traffic flow parameters to analyze the capacity of multilane roads [39,48–50]. However, these studies lacked research specifically regarding the identification and quantification of significant traffic parameters that affect lane changing using real data by considering lane changing as one of the essential subjects of sustainable traffic safety.

This study aimed to estimate the effect of significant traffic parameters for traffic safety on lane changing using VISSIM for a two-lane road section of a freeway. We utilized calibrated model data for driving logic "conscious" to estimate the relationship between specified traffic parameters and lane change frequency. Furthermore, 3D surface plots were developed to analyze the integrated effect of observed variables on lane change frequency. We also attempted to develop a regression expression to quantify the effect of observed traffic parameters on lane change frequency. The study recommends that there should be more focus on traffic parameters that significantly influence lane changing in order to enhance traffic safety.

The paper is organized as follows. The need for analyzing the effect of significant traffic safety parameters on lane changing has already been described in this section. The method used, including video data collection and presentation of simulation parameters, is detailed in Section 2. Analysis of the effect of traffic parameters on lane change frequency as well as 3D surface plots and regression model results are presented in Section 3, Section 4 provides the conclusions and discusses future works.

2. Materials and Methods

2.1. Video Data Analysis

Video data analysis was performed using CarCam to collect real traffic data on a two-lane road section near Budapest. The road was approximately 5 km long (M1 motorway, Hungary) in one direction of travel. Video data collection was performed for 4 hours from 7 a.m. to 9 a.m. and 3 p.m. to 5 p.m. on a typical weekday under clear weather conditions. The collected video data were then extracted with the help of semiautomated data extraction software to get the mean speed of cars and traffic volume at each 5 min interval. First, the results of video data analysis were utilized to measure the mean speed by measuring the time taken by a vehicle to cross the longitudinal section of 30 m using a software program. The plot results showed that most of the vehicles were travelling at varying speeds with dispersion between 100 and 140 km/h, as shown in Figure 1. Second, the results of video data analysis were utilized to measure the traffic volume on a specified road section for the stated period. The plot results showed that traffic volume varied significantly in different time intervals. However, it helped to obtain information about the minimum (960 veh/hr) and maximum (2280 veh/hr) traffic counts for simulation analysis purposes, as shown in Figure 2.

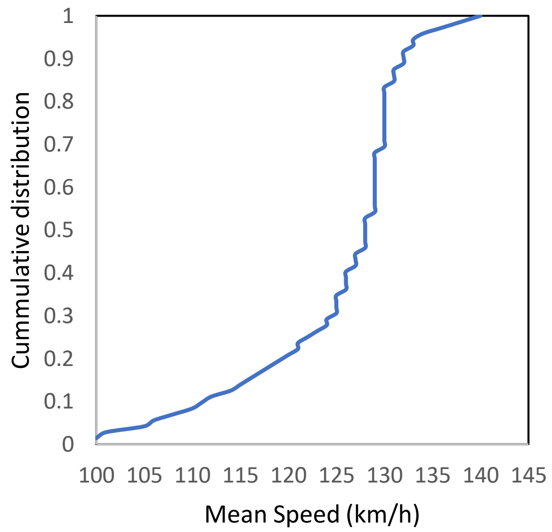

Figure 1. Real speed data.

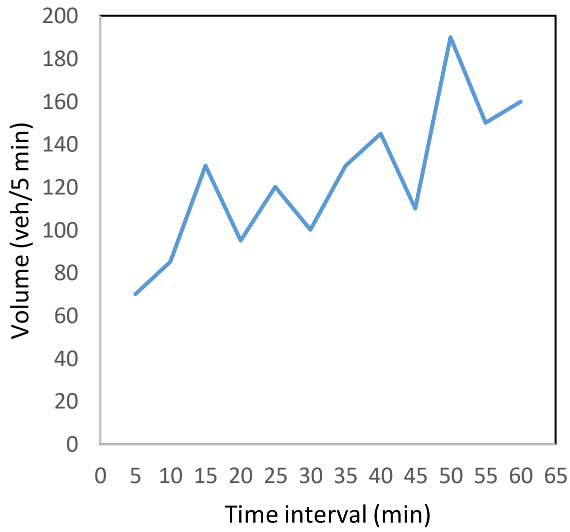

Figure 2. Real traffic volume data.

2.2. VISSIM Simulation

We wanted to utilize a microscopic simulation method to analyze the lane change frequency of cars on a two-lane road section of a freeway, that is, one direction of a road section under various specified traffic conditions. We chose the VISSIM software as a simulation tool for analysis of the effect of different traffic parameters on lane changing due to its powerful multimodel modeling capabilities. PTV VISSIM was first developed in 1992 by PTV Planung Transport Verkehr AGin Karlsruhe, Germany, based on the continuous effort of Wiedemann regarding car-following behavior [39]. VISSIM is the most advanced and commonly used microscopic traffic simulation software [51]. VISSIM is a behavior-based and time-step simulation model program. The software has three basic mechanisms: traffic flow models, traffic control models, and a data analysis package. It can be useful to analyze different transportation problems, such as freeway operations, dynamic traffic assignments, the interaction of different transportation modes, signal prioritization and optimization, traffic management strategies, pedestrian flows, etc. [52]. A previous study also concluded that the VISSIM simulation environment is well suited for freeway studies involving complex interactions with few and well-reasoned modifications to reproduce driver behavior parameters [53].

For the development of the base model, a 5 km road network with straight and twisty links was used to efficiently utilize the available PTV licensed software (VISSIM 11) space. The width of the road section was set at 7 m, with each lane being 3.5 m wide. The road networks in VISSIM can be designed either as lane-oriented or space-oriented, i.e., vehicles can change anywhere in the road without lane restrictions. Any number of vehicle types can be designed and overtaking of vehicles can be allowed on both the sides [54]. On a two-lane road link, we employed only cars as a "vehicle type" in the VISSIM model and used the right-side rule, which allows overtaking of vehicles in the left lane. It must be noted that there is a permanent overtaking ban for vehicles over 3.5 tons on certain two-lane sections of the Hungarian motorway network [55]. The simulation data was extracted for 3600 s, and the option "lane changes evaluation active" was selected to record lane change data. Lane change frequency was evaluated as the number of lane changes per hour (n/h). The important information about simulation parameters is tabulated in Table 1.

Table 1. Simulation parameters.

Simulation Parameters	
Number of lanes	2
Lane change frequency	n/h (number of lane changes per hour)
Length of road section	5 km
Simulation period	3600 s
Vehicle type	Cars
Road type	Freeway
Simulation model	Wiedemann 99 model

We applied the Wiedemann 99 model, which is suitable for freeways with no merging areas, to observe the effect of significant traffic parameters on lane changing for driving logic "cautious". The Wiedemann 99 car-following model was developed in 1999 to offer greater control of the car-following characteristics for freeway modeling in VISSIM. The Wiedemann 99 model consists of 10 calibration parameters, all labeled with a "CC" prefix [39,56]. The car-following logic controls the way a vehicle interacts with other vehicles at four modes of driving: free-driving, approaching a vehicle, following a vehicle, and braking. Similarly, the lane-changing logic controls the way a vehicle interacts with others during the processes of lane selection, merging to traffic, and diverging from traffic [57]. We considered calibrated values of the car-following model as suggested by a recent study for driving logic "cautious" [58]. Most European drivers have been observed as "cautious" about driving characteristics, which can affect the driving style and road safety, as analyzed in previous studies [59,60]. Table 2 provides a description with the default and calibrated values for each of the "CC" parameters associated with the Wiedemann 99 model.

In VISSIM, the lane-changing behavior is controlled by a set of factors for local calibration of VISSIM models. Accordingly, VISSIM lane-changing behavior is characterized by maximum and accepted deceleration rates for the merging (own) and trailing vehicle. Driver aggressiveness can be controlled by modifying the maximum and accepted deceleration rates as well as the reduction rate of the deceleration value as the vehicle approaches its merge point [35]. We further considered the calibrated values of lane change as suggested by a recent study for driving logic "cautious", as shown in Table 3.

Based on the above measures, we considered the following:

(1) Effect of average desired speed on lane change frequency;
(2) Effect of desired speed distribution on lane change frequency;
(3) Effect of traffic volume on lane change frequency.

We first considered simulating the effect of average desired speed variation on lane change frequency. Previous studies have noticed that changes in speed affects serious crashes substantially more than less serious crashes, with most data related to rural roads and motorways [13,61]. In the past 20 years, nearly all countries have either increased or decreased their speed limits on the motorway network. In addition, the speed limits in Hungary outside built-up areas were increased from 120 to 130 km/h on motorways and from 100 to 110 km/h on motor roads (semimotorways) in 2001 [24]. Based on observed video speed data, the average speed in this study varied from 110 to 130 km/h with a wider range (110, 115, 120, 125, and 130 km/h) to measure their effect on lane changing for road safety. In London, the noncompliance level (the level of noncompliance with the speed limit) ranges from 4% to 73%, while the noncompliance level ranges from 2% to 82% outside London [17]. The speed range for each simulated average speed was given as an input in the model, as shown in Figure 3.

Table 2. Wiedemann 99 model parameters [58].

VISSIM Code	Description	Default Values	Calibrated Values (Cautious)
CC0	Standstill distance: Desired distance between lead and following vehicle at v = 0 mph	1.5 m	1.5 m
CC1	Headway Time: Desired time in seconds between lead and following vehicle	0.90 s	1.5 s
CC2	Following variation: Additional distance over safety distance that a vehicle requires	4 m	0 m
CC3	Threshold for entering "following" state: Time in seconds before a vehicle starts to decelerate to reach safety distance (negative)	−8 s	−10 s
CC4	Negative "following" threshold: Specifies variation in speed between lead and following vehicle	−0.35	−0.1
CC5	Positive "following" threshold: Specifies variation in speed between lead and following vehicle	0.35	0.1
CC6	Speed dependency of oscillation: Influence of distance on speed oscillation	11.44	0
CC7	Oscillation acceleration: Acceleration during the oscillation process	0.25 m/s^2	0.1 m/s^2
CC8	Standstill acceleration: Desired acceleration starting from standstill	3.5 m/s^2	3.5 m/s^2
CC9	Acceleration at 80 mph: Desired acceleration at 80 mph	1.5 m/s^2	1.5 m/s^2

Table 3. Lane change parameters [58].

Parameters	Default Values		Calibrated Values (Cautious)	
	Own	Trailing Vehicle	Own	Trailing Vehicle
Maximum deceleration	−4	−3	−3.5	−2.5
−1 m/s^2 per distance	100	100	80	80
Accepted deceleration	−1	−1	−1	−1

We further simulated the effect of desired speed distribution on lane change frequency for a freeway by maintaining the average speed at 130 km/h. The distribution function of desired speeds is a particularly important parameter as it has an impact on lane change frequency. VISSIM provides the opportunity to distribute the percentage of speed values over smaller to larger limits. In VISSIM, the desired speed is a significant parameter that has a great influence on travelling speeds, which is explained as a distribution rather than a fixed value [62]. The speed distribution represents the proportion of vehicles driving at or below certain speeds. It is also likely to use the speed distribution to specify how the speed of all vehicles varies [27]. A previous study stated that high-risk drivers exceed the speed limit by at least 25 km/h, so the "desired speed distribution" of the vehicles that represent speeding drivers was set as 120–150 km/h [63]. We considered real speed data (Figure 1) to analyze the effect of different speed distributions on lane changing for road safety. The largest speed distribution was set between 100 and 140 km/h with higher speed variations of traffic flow, and some other speed distributions were also set to comprehensively analyze the effect of speed distribution on lane changing. Accordingly, the smallest speed distribution was set between 120 and 140 km/h with lower speed variations of traffic flow. The maximum and minimum values of the speeds and the dispersion between these values were defined for an average speed of 130 km/h (freeway) in the model, as shown in Figure 4.

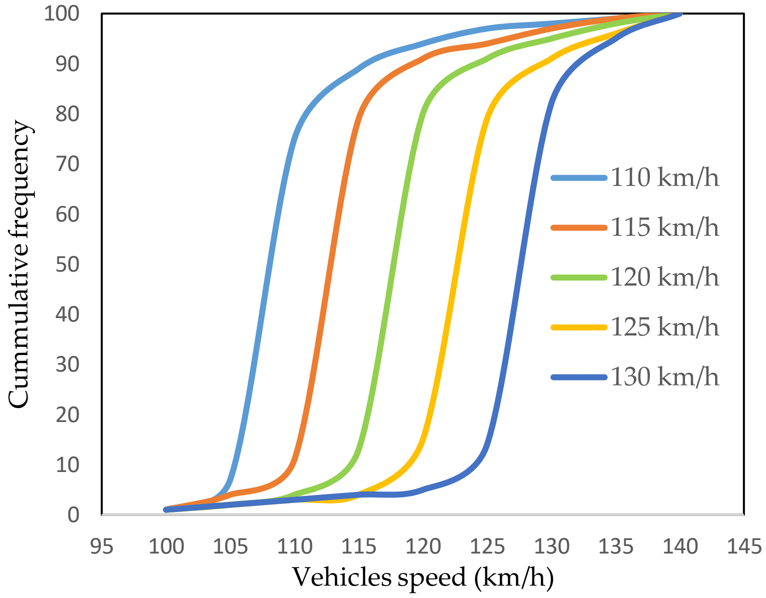

Figure 3. Speed range for nominated average speeds.

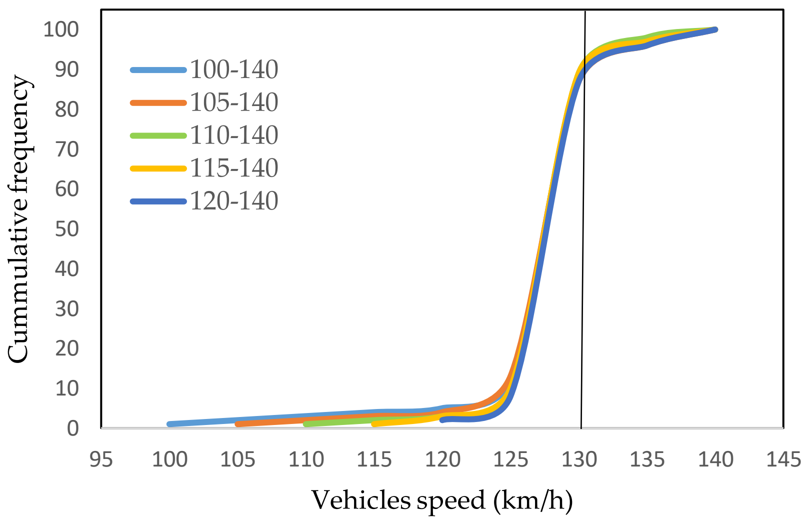

Figure 4. Speed distribution profile for a freeway (130 km/h).

The VISSIM simulation was also used to measure the effect of designated traffic volume on lane change frequency. Traffic volume was set for each simulation, which defined the number of vehicles in a specific period for the two-lane road section of the freeway. A previous study noticed that traffic volume is one of the most influential parameters to model driving behavior [52]. Lane change behavior of vehicles characterizes macroscopic traffic flow behavior and significantly affects operational characteristics on the highway [39]. Another study observed the effect of hourly traffic volume on crash incident rate, with the lowest rate being when traffic flowed at a rate of 1000–1500 vehicles/h, while crash rates increased when traffic increased to a level of 3000 vehicles/h [64]. We measured the effect of traffic volume on lane changing by considering real traffic data (Figure 2). For VISSIM simulation, the traffic volume of cars varied from 1000 to 3000 vehicles per hour with an interval of 500 vehicles per hour, which is approximate to real observed traffic data.

3. Results

Modeling of lane changing for road safety was done by changing the values of the model parameters from the default setting to driving logic "conscious" with basic field input data, such as desired speed and traffic volume (veh/hr) as per field observation. We analyzed the effect of various traffic parameters on lane change frequency based on VISSIM simulation data. Simulations were run based on specified traffic data to measure lane change frequency, and the results are tabulated in Table 4. Simulations were run three times for each traffic scenario, and the average value was used to validate the output results, such as the number of lane changes. This is similar to a previous study, which performed the generation of different parameter combinations with three replicates for each case study [65]. Lane change frequency was measured as the number of lane changes per hour (n/h). It is important to specify that we considered a traffic volume of 2500 vehicles per hour to measure the effect of average desired speed and desired speed distribution on lane change frequency. The analysis was initiated by measuring the effect of average desired speed variance on lane change frequency. Results showed that lane change frequency increased with the increase in average desired speed. After that, we analyzed the effect of speed distribution on lane change frequency for the freeway. Results showed high lane change frequency for larger speed variation between predefined speed limits. Large variations in speed between vehicles on a two-lane road can give rise to conflicts, which in turn can lead to lane changing risk. Moreover, we investigated the effect of traffic volume on lane change frequency for the freeway. Traffic volume input was varied from low to higher levels, and simulation runs were performed for one hour. The simulation considered the speed limit of cars as 130 km/h (freeway). Results showed that lane change frequency increased with the increase in traffic volume.

Table 4. Effect of traffic parameters on lane change frequency.

Average Speed (km/h)	Lane Change Frequency (n/h)	Speed Distribution	Lane Change Frequency (n/h)	Traffic Volume (veh/h)	Lane Change Frequency (n/h)
110	728	120–140	340	1000	382
115	1347	115–140	684	1500	826
120	1434	110–140	872	2000	1386
125	1674	105–140	1347	2500	1808
130	1808	100–140	1628	3000	2228

Considering the above simulation results, we analyzed the relationship between designated traffic parameters and lane change frequency. Polynomial curves (second degree) were found to better fit the relationship between observed traffic parameters (average desired speed, desired speed distribution, traffic volume) and lane change frequency. Furthermore, the equation of each curve was placed in plots to represent the relationship between a dependent variable (lane change frequency) and the independent variable. The R-squared (R^2) value was also calculated, which can be defined as the percentage of variation in the response variable that is explained by the model. The higher the R^2 value, the better the model fits the data.

3.1. *Effect of Average Desired Speed on Lane Change Frequency*

Lane change frequency was measured for each simulation, with the average desired speed varying from 110 to 130 km/h with an interval of 5 km/h. Each observed average speed was simulated under a specified speed range (Figure 3). The relationship between average desired speed (km/h) and lane change frequency (n/h) is plotted in Figure 5. It can be seen that there was a positive relationship between the two variables, with lane change frequency increasing with the increase in average desired speed of cars. The results can be explained by the fact that high-speed conditions can cause frequent overtaking maneuvers [66]. A previous study showed that, after the implementation of higher speed limit, the number of injury crashes, as compared to the control, rose significantly on 130 km/h roads but not on 110 km/h roads [62].

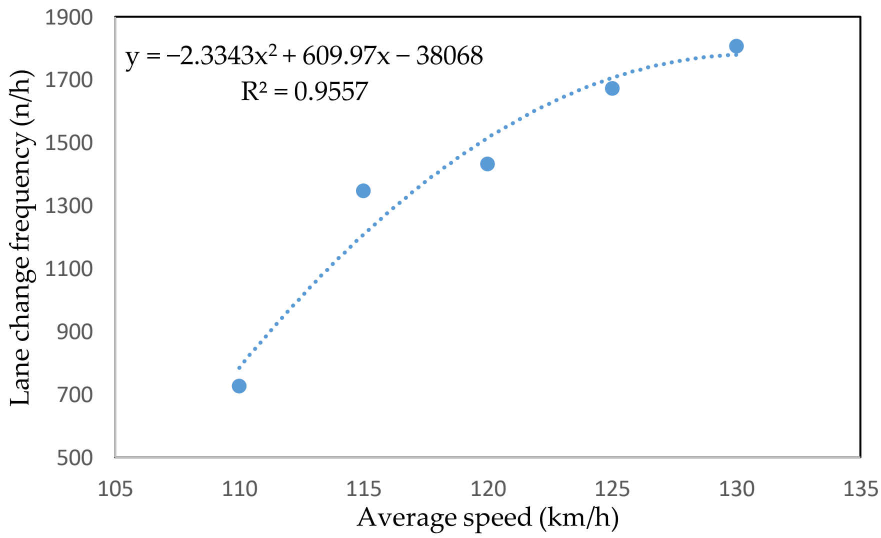

Figure 5. Effect of average speed variation on lane change frequency.

3.2. *Effect of Desired Speed Distribution on Lane Change Frequency*

The effect of speed distribution on lane change frequency was analyzed, and the results are plotted in Figure 6. All speed distribution data were set by maintaining an average speed at 130 km/h (freeway) (Figure 4). A previous study on displacement of speed distribution showed larger displacements for higher speeds [67]. The plot results showed higher lane change frequency for large speed dispersion and lower lane change frequency for small speed dispersion between predefined limits. In other words, when speed distribution was high, the examined vehicles tended to change lanes frequently due to the difference in speeds between vehicles. Some previous studies have found speed variations to be positively related to crashes [44,45,47,68].

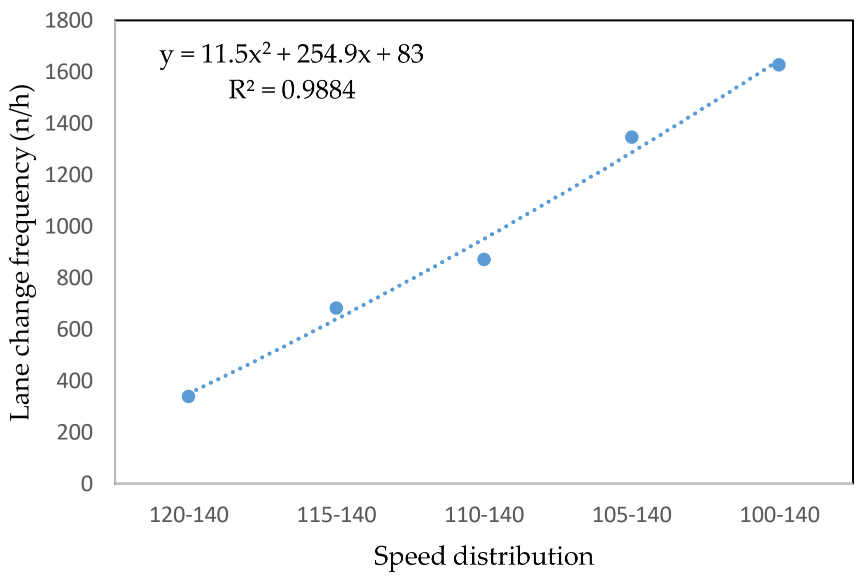

Figure 6. Effect of desired speed distribution on lane change frequency.

3.3. *Effect of Traffic Volume on Lane Change Frequency*

We observed the relationship between traffic volume and lane change frequency, as shown in Figure 7. Lane change frequency was measured for each simulation, with the traffic volume varying from 1000 to 3000 vehicles per hour with an interval of 500 vehicles per hour. Speed distribution was set in such a way that all simulated vehicles were moving on the road section within the speed limit (130 km/h). The plot results showed a positive relationship between the two variables, with lane change frequency increasing with the increase in traffic volume. When the number of vehicles increased in a specified period, more vehicles tended to change lanes for overtaking purposes. A previous study [11] had also found a positive correlation between risk factor and traffic flow efficiency in lower traffic demand.

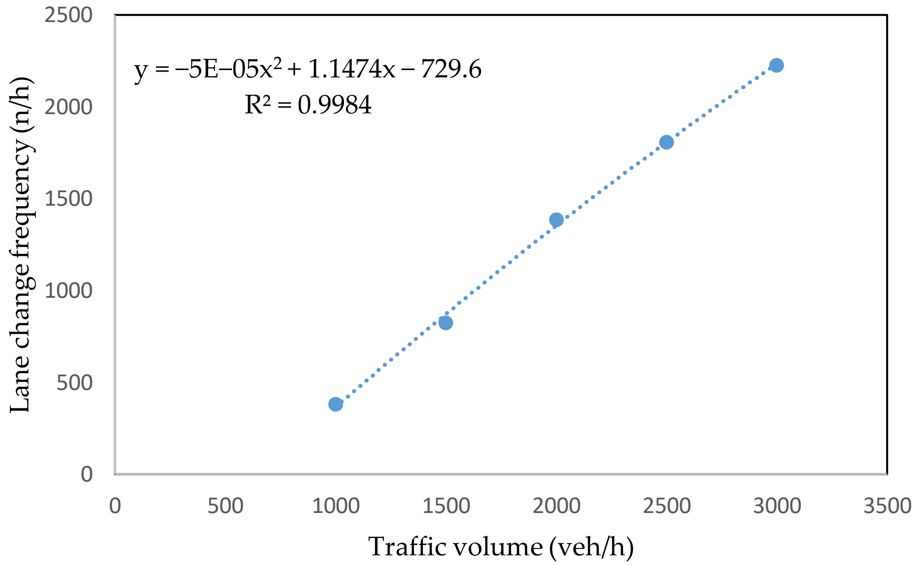

Figure 7. Effect of traffic volume on lane change frequency for a freeway.

3.4. 3D Surface Plots and Regression Model

Previous model [66] results showed that the impact of speed on crashes was associated with volume and between-lane speed variations, which complicated its interpretation. Based on a similar concept, we analyzed the impact of speed (average desired speed and desired speed distribution) on lane change frequency in connection with traffic volume. 3D surface plots were developed to simultaneously observe changes in the shape of lane change frequency with the change in specified traffic parameters, as shown in Figure 8. Figure 8a presents a 3D surface plot to show the impact of the average desired speed on lane change frequency when associated with traffic volume. Figure 8b presents a 3D surface plot to show the impact of desired speed distribution on lane change frequency when associated with traffic volume. The results showed the highest lane change frequency for both cases due to the combined effect of the observed parameters. Xu et al. [30] found that high-speed variance in high-density traffic flow leads to higher crash risk.

Finally, we attempted to develop a regression model between lane change frequency and specified traffic parameters based on observed simulation data. Lane change frequency (*LCF*) was set as a dependent variable, while the independent variables were average desired speed (*ADS*), desired speed distribution (*DSD*), and traffic volume (*TV*). The regression model was developed based on simulation data, and coefficient results were utilized to quantify the effect of traffic parameters on lane change frequency, as shown in Equation (1). The results of this model showed that desired speed distribution had the most significant effect on lane change frequency due to high coefficient values (positive). A previous study [69] found that speed distribution had a vital role in road safety. Subsequently, the average desired speed also had a high effect on lane change frequency with a high coefficient value. However, traffic volume had a small effect on lane change frequency due to a small coefficient value.

$$LCF = (31.36 \times ADS) + (220.8 \times DSD) + (0.67 \times TV) - 4487.28 \tag{1}$$

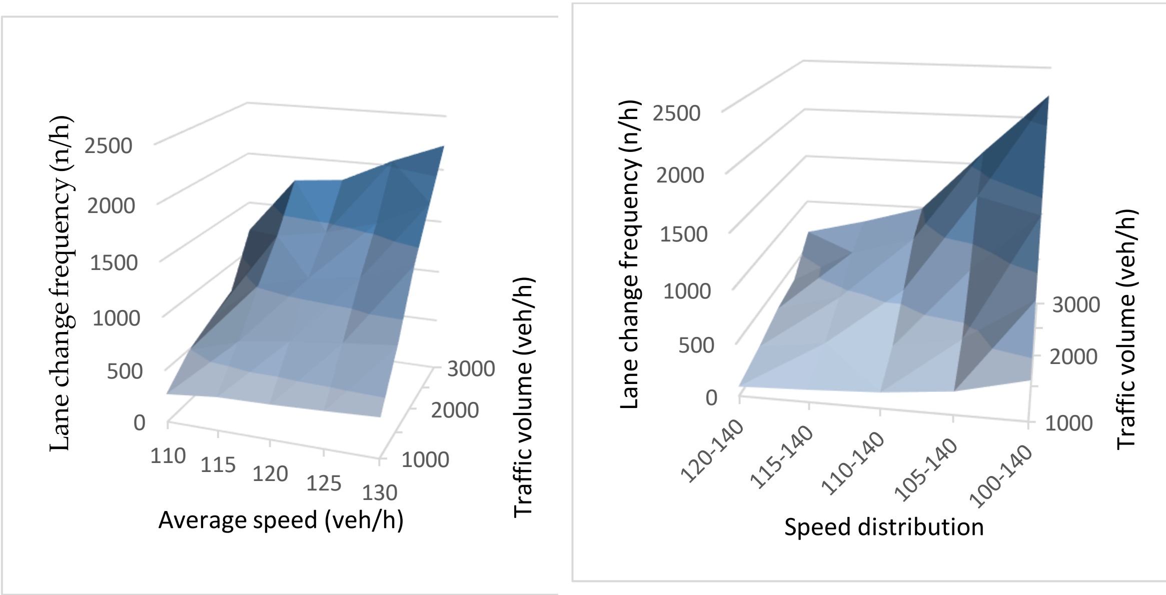

(a) (b)

Figure 8. 3D surface plots.

The results of regression analysis are presented in Table 5. The standard error (SE) is also presented, which represents the average distance that the observed values fall from the regression line. The smaller the standard error, the more representative the sample will be of the overall sample size. The statistical significance of the effect depends on the *p*-value, i.e., if the *p*-value is larger than the selected significance level α, the effect is not statistically significant; however, if the *p*-value is less than or equal to α, then the effect for that particular term is statistically significant. The α value was set as 0.05 in the regression analysis. The results of the model showed that all observed parameters were statistically significant with *p*-values less than 0.05. Moreover, adjusted R^2 was calculated, which represents the percentage of the variation in the response variable that is explained by the model, adjusted for the number of predictors in the model relative to the number of observations.

Table 5. Regression analysis results.

	Coefficients	Standard Error	*p*-Value
Average desired speed	31.36	3.09	0.00
Desired speed distribution	220.8	43.81	0.00
Traffic volume	0.67	0.030	0.00
Intercept	−4487.28	383.26	0.00
Adjusted R^2		92%	

4. Discussion

Identification of the main traffic characteristics causing frequent lane changing could improve our understanding of lane-changing risk and help to develop more effective road safety strategies for freeways. The results of the present study showed that observed traffic parameters had a major impact on lane change frequency. Furthermore, lane change frequency was more greatly affected due to the integrated effect of specified traffic parameters. The regression model results showed that desired speed distribution had the highest effect on lane change frequency. Improvements in drivers' compliance with speed limits and speed management/enforcement strategies can play a vital role in enhancing traffic safety. Regarding the impact of speed changes in speed distribution, several studies have confirmed that speed cameras and vehicle-to-vehicle communication (V2V) systems are effective in reducing both mean speed and excessive speeding [70,71]. However, this study only considered the driving logic "cautious" in the VISSIM model for traffic characteristics close to the real data, such as speed limits, traffic volume, and overtaking rules. Further research can be performed to apply the VISSIM model for other driving logics, such as "all knowing", to analyze lane changing. Finally, lane change frequency should be analyzed in the context of the average traffic speed of traffic flow exceeding the speed limit.

5. Conclusions

This study evaluated the effect of significant traffic parameters on lane changing for a two-lane road section of a freeway. We utilized a traffic simulation software with calibration of the model for driving logic "cautious" to estimate the impact of designated traffic parameters on lane change frequency. The traffic parameters considered in this study were average desired speed, desired speed distribution, and traffic volume. First, VISSIM simulation was performed to measure the effect of average desired speed variation on lane change frequency. The measured simulation data were used to plot the relationship between the average desired speed and lane change frequency. The plot results showed a positive relationship between average desired speed variation and lane change frequency, with lane change frequency increasing with the increase in average desired speed under a predefined speed range. Subsequently, the effect of desired speed distribution on lane change frequency was analyzed. The simulation results showed higher lane change frequency when speed dispersion was set large and lower lane change frequency when speed distribution was set small. Furthermore, the effect of traffic volume variation on lane change frequency was analyzed. The simulation plot results showed a positive relationship between traffic volume and lane change frequency, with lane change frequency increasing with the increase in traffic volume. Based on the simulated data, 3D surface plots were developed between speed (average desired speed and desired speed distribution), traffic volume, and lane change frequency. The plot results showed the integrated effect of the observed parameters on lane change frequency, which was higher than the individual effect. Finally, a regression model was developed between the dependent variable (lane change frequency) and the independent variables (average desired speed, desired speed distribution, and traffic volume) to quantify the effect of traffic parameters on lane change frequency. The regression model results showed that desired speed distribution had the most significant impact on lane change frequency compared to the other observed variables. Overall, the results of this study could help to identify and quantify the effect of significant traffic parameters on lane changing by considering the modern technology of automated vehicles for sustainable traffic safety. Further research can be performed in VISSIM to explore whether changing the significant traffic parameters with diverse distributions for a higher number of lanes has a significant positive effect on lane changing.

Author Contributions: Conceptualization, J.J. and D.F.; methodology, J.J. and D.F.; software, D.F.; validation, D.F.; formal analysis, D.F.; investigation, J.J.; data curation, D.F.; writing—original draft preparation, D.F.; writing—review and editing, D.F. and J.J.; supervision, J.J.

Funding: This research received no external funding.

Conflicts of Interest: The authors declare no conflict of interest.

References

1. World Health Organization (WHO). *The Global Status Report on Road Safety 2018*; WHO: Geneva, Switzerland, 2018.
2. World Health Organization (WHO). *Global Status Report on Road Safety 2009*; WHO: Geneva, Switzerland, 2009.
3. Valette, L. *Road Safety: New Statistics Call for Fresh Efforts to Save Lives on EU Roads*; European Commission Press Release: Brussels, Belgium, 2016.
4. OECD/ITF. *Road Safety Annual Report*; OECD: Paris, France; ITF: London, UK, 2016.
5. KSH. *Road Accidents Involving Personal Injury (2001–2017)*; KSH: Budapest, Hungary, 2018.
6. NHTSA (National Highway Traffic Safety Administration). *National Motor Vehicle Crash Causation Survey*; U.S. Department of Transportation: Washington, DC, USA, 2008.

7. Evans, L. *Traffic Safety*; Science Serving Society, Inc.: Bloomfield Hills, MI, USA, 2004.
8. Choi, E.H. *Crash Factors in Intersection-Related Crashes: An On-Scene Perspective*; NHTSA Technical Report: DOT HS 811 366; U.S. Department of Transportation, National Highway Traffic Safety Administration: Washington, DC, USA, 2010.
9. Papaioannou, P. Driver behavior, dilemma zone and safety effects at urban signalised intersections in Greece. *Accid. Anal. Prev.* **2007**, *39*, 147–158. [CrossRef] [PubMed]
10. Wang, J.; Ding, J.X.; Shi, Q.; Kühne, R.D. Lane-changing behavior and its effect on energy dissipation using full velocity difference model. *Int. J. Mod. Phys. C* **2016**, *27*, 1650013. [CrossRef]
11. Li, X.; Jia, B.; Gao, Z.; Jiang, R. A realistic two-lane cellular automata traffic model considering aggressive lane-changing behavior of fast vehicle. *Phys. A Stat. Mech. Appl.* **2006**, *367*, 479–486. [CrossRef]
12. BERNARD Law group. Accidents Nationwide Associated with Lane-Changing. 2017. Available online: https://www.4injured.com/blog/accidents-lane-changing-risks/ (accessed on 1 August 2019).
13. Elvik, R.; Christensen, P.; Amundsen, A. *Speed and Road Accidents: An Evaluation of the Power Model*; TØI Report Number: 740/2004; Institute of Transport Economics: Oslo, Norway, 2004.
14. Park, S.; Ritchie, S.G. Exploring the relationship between freeway speed variance, lane changing, and vehicle heterogeneity. In Proceedings of the Paper Sub-Mitted to the 83rd Annual Meeting of the Transportation Research Board, Washington, DC, USA, 11–15 January 2004; pp. 11–15.
15. Pirdavani, A.; De Pauw, E.; Brijs, T.; Daniels, S.; Magis, M.; Bellemans, T.; Wets, G. Application of a rule-based approach in real-time crash risk prediction model development using loop detector data. *Traffic Inj. Prev.* **2015**, *16*, 786–791. [CrossRef]
16. Quddus, M. Exploring the Relationship Between Average Speed, Speed Variation, and Accident Rates Using Spatial Statistical Models and GIS. *J. Transp. Saf. Secur.* **2013**, *5*, 27–45. [CrossRef]
17. Xu, C.; Wang, X.; Yang, H.; Xie, K.; Chen, X. Exploring the impacts of speed variances on safety performance of urban elevated expressways using GPS data. *Accid. Anal. Prev.* **2019**, *123*, 29–38. [CrossRef]
18. Levy, D.T.; Asch, P. Speeding, Coordination, and the 55-MPH Limit: Comment. *Am. Econ. Rev.* **1989**, *79*, 913–915.
19. Tanishita, M.; Wee, B. Impact of vehicle speeds and changes in mean speeds on per 2 vehicle-kilometer traffic accident rates in Japan. *IATSS Res.* **2016**, *41*, 107–112. [CrossRef]
20. Elvik, R. *Towards a General Theory of the Relationship Between Exposure and Risk*; TØI Report No: 1316/2014; Institute of Transport Economics: Oslo, Norway, 2014.
21. Garber, J.J.; Gadiraju, R. Factors Affecting Speed Variance and its Influence on Accidents. *Transp. Res. Rec.* **1989**, *1213*, 64–71.
22. Kweon, Y.J.; Kockelman, K.M. Spatially disaggregate panel models of crash and injury counts: The effect of speed limits and design. In Proceedings of the 83rd Transportation Research Board Annual Meeting, National Research Council, Washington, DC, USA, 11–15 January 2004.
23. Lave, C.A. Speeding, Coordination, and the 55 MPH Limit. *Am. Econ. Rev.* **1985**, *75*, 1159–1164.
24. The International Transport Forum. *Speed and Crash Risk*; OECD: Paris, France, 2018.
25. Elvik, R. A re-parameterisation of the Power Model of the relationship between the speed of traffic and the number of accidents and accident victims. *Accid. Anal. Prev.* **2013**, *50*, 854–860. [CrossRef] [PubMed]
26. Elvik, R.; Vadeby, A.; Hels, T.; Van Schagen, I. Updated estimates of the relationship between speed and road safety at the aggregate and individual levels. *Accid. Anal. Prev.* **2019**, *123*, 114–122. [CrossRef] [PubMed]
27. Vadeby, A.; Forsman, A. Changes in speed distribution: Applying aggregated safety effect models to individual vehicle speeds. *Accid. Anal. Prev.* **2017**, *103*, 20–28. [CrossRef] [PubMed]
28. Qu, X.; Kuang, Y.; Oh, E.; Jin, S. Safety evaluation for expressways: A comparative study for macroscopic and microscopic indicators. *Traffic Inj. Prev.* **2014**, *15*, 89–93. [CrossRef]
29. Abdel-Aty, M.A.; Pemmanaboina, R. Calibrating a Real-Time Traffic Crash-Prediction Model Using Archived Weather and ITS Traffic Data. *IEEE Trans. Intell. Transp. Syst.* **2006**, *7*, 167–174. [CrossRef]
30. XU, C.; Liu, P.; Wang, W.; Zhang, Y. Real-time identification of traffic conditions prone to injury and non-injury crashes on freeways using genetic programming. *J. Adv. Transp.* **2016**, *50*, 701–716. [CrossRef]
31. Aarts, L.; van Schagen, I. Driving speed and the risk of road crashes: A review. *Accid. Anal. Prev.* **2006**, *38*, 215–224. [CrossRef]
32. Garber, N.; Ehrhart, A. Effect of Speed, Flow, and Geometric Characteristics on Crash Frequency for Two-Lane Highways. *Transp. Res. Rec. J. Transp. Res. Board* **2000**, *1717*, 76–83. [CrossRef]

33. Fi, I.; Galuska, J. Traffic analysis of two-lane highways. *Period. Polytech. Civ. Eng.* **2011**, *55*, 169–176. [CrossRef]
34. Cunto, F.; Saccomanno, F.F. Calibration and validation of simulated vehicle safety performance at signalized intersections. *Accid. Anal. Prev.* **2008**, *40*, 1171–1179. [CrossRef]
35. TEOpS 16-20. *Traffic Engineering*, Operations & Safety Manual. 2019. Available online: https://wisconsindot.gov/dtsdManuals/traffic-ops/manuals-and-standards/teops/16-20.pdf (accessed on 25 October 2019).
36. Ozbay, K.; Bartin, B.; Yang, H. Derivation and Validation of New Simulation-Based Surrogate Safety Measure. *Transp. Res. Rec. J. Transp. Res. Board* **2008**, *2083*, 105–113. [CrossRef]
37. Park, B.B.; Schneeberger, J.D. Microscopic simulation model calibration and validation, case study of VISSIM simulation model for a coordinated actuated signal system. *Transp. Res. Rec.* **2003**, *1856*, 185–192. [CrossRef]
38. Gettman, D.; Head, L. Surrogate Safety Measures from Traffic Simulation Models. *Transp. Res. Rec.* **2003**, *1840*, 104–115. [CrossRef]
39. Srikanth, S.; Mehar, A.; Praveen, K.G.N.V. Simulation of Traffic Flow to Analyze Lane Changes on Multi-Lane Highways under Non-Lane Discipline. *Period. Polytech. Transp. Eng.* **2017**, *66*, 1–14. [CrossRef]
40. Ciuffo, B.; Punzo, V.; Torrieri, V. Comparison of Simulation-Based and Model-Based Calibrations of Traffic-Flow Microsimulation Models. *Transp. Res. Rec. J. Transp. Res. Board* **2008**, *2088*, 36–44. [CrossRef]
41. Bains, M.S.; Ponnu, B.; Arkatkar, S.S. Modeling of Traffic Flow on Indian Expressways using Simulation Technique. *Procedia Soc. Behav. Sci.* **2012**, *43*, 475–493. [CrossRef]
42. Lee, S.E.; Olsen, E.C.B.; Wierwille, W.W. *A Comprehensive Examination of Naturalistic Lane Changes*; Final Report: DOT HS 809 702; National Highway Traffic Safety Administration: Washington, DC, USA, 2004.
43. Fellendorf, M.; Vortisch, P. Microscopic Traffic Flow Simulator VISSIM. In *Fundamentals of Traffic Simulation, International Series in Operations Research & Management Science*; Barceló, J., Ed.; Springer: New York, NY, USA, 2010.
44. Ma, Z.; Zhang, H.; I-Jy Chien, S.; Wang, J.; Dong, C. Predicting expressway crash frequency using a random effect negative binomial model: A case study in China. *Accid. Anal. Prev.* **2017**, *98*, 214–222. [CrossRef]
45. Potts, I.B.; Harwood, D.W.; Richard, K.R. Relationship of Lane Width to Safety on Urban and Suburban Arterials. *Transp. Res. Rec.: J. Transp. Res. Board* **2007**, *2023*, 63–82. [CrossRef]
46. Wang, X.; Yuan, J. Safety impacts study of roadway network features on suburban highways. *China J. Highw. Transp.* **2017**, *30*, 106–114.
47. Wang, X.; Zhou, O.; Quddus, M.; Fan, T.; Fang, S. Speed, speed variation and crash relationships for urban arterials. *Accid. Anal. Prev.* **2018**, *113*, 236–243. [CrossRef]
48. Mehar, A.; Chandra, S.; Velmurugan, S. Passenger car units at different levels-of-service for capacity analysis of multilane divided highways. *ASCE J. Transp. Eng. USA* **2013**, *140*, 81–88. [CrossRef]
49. Knoop, V.L.; Hoogendoorn, S.P.; Yasuhiro, S.; Buisson, C. Quantifying the number of lane changes in traffic: Empirical analysis. Transportation Research Records. *J. Transp. Res. Board* **2012**, *2278*, 31–41. [CrossRef]
50. Jin, W.L. Macroscopic characteristics of lane-changing traffic. Transportation Research Record. *J. Transp. Res. Board* **2010**, *2188*, 55–63. [CrossRef]
51. Chunying, G. Microscopic simulation system VISSIM and its application to road and transportation. *Highway* **2005**, *8*, 118–121.
52. Al-Ahmadi, H.M.; Jamal, A.; Reza, I.; Assi, K.J.; Ahmed, S.A. Using Microscopic Simulation-Based Analysis to Model Driving Behavior: A Case Study of Khobar-Dammam in Saudi Arabia. *Sustainability* **2019**, *11*, 3018. [CrossRef]
53. Gomes, G.; May, A.; Horowitz, R. *Calibration of VISSIM for a Congested Freeway*; California PATH Research Report, UCB-ITS-PRR-2004-4; Institute of Transportation Studies, University of California: Berkeley, CA, USA, 2004.
54. Siddharth, S.M.P.; Ramadurai, G. Calibration of VISSIM for Indian Heterogeneous Traffic Conditions. *Procedia Soc. Behav. Sci.* **2013**, *104*, 380–389. [CrossRef]
55. Nagy, E.; Sandor, Z. Overtaking ban for heavy goods vehicle in Hungary on the National motorway network. *Pollack Period. Int. J. Eng. Inf. Sci.* **2012**, *7*, 83–95. [CrossRef]
56. Planning Transport Verkehr (PTV). *VISSIM User's Manual*; Version 5.4; PTV Group: Karlsruhe, Germany, 2012.
57. Planning Transport Verkehr (PTV). *VISSIM User Manual*; Version 5.30; PTV Group: Karlsruhe, Germany, 2009.
58. Sukennik, P. *CoExist, PTV Vissim Extension—New Features and Improvements*; PTV Group: Karlsruhe, Germany, 2018.

59. Eboli, L.; Mazzulla, G.; Pungillo, G. How drivers' characteristics can affect driving style. In Proceedings of the 20th EURO Working Group on Transportation Meeting, EWGT 2017, Budapest, Hungary, 4–6 September 2017.
60. SARTRE 3 Report. *European Drivers and Road Risk*; Institut national de recherche sur les transports et leur sécurité: Arcueil, France, 2004.
61. Nilsson, G. *Traffic Safety Dimensions and the Power Model to Describe the Effect of Speed on Safety*; Bulletin 221; Lund Institute of Technology, Department of Technology and Society, Traffic Engineering: Lund, Sweden, 2004.
62. Zhang, C.; Liu, S.; Ogle, J.; Zhang, M. Micro-simulation of Desired Speed for Temporary Work Zone with a New Calibration Method. *Promet Traffic Transp.* **2016**, *28*, 49–61. [CrossRef]
63. AAA. *Aggressive Driving: Research Update*; AAA Foundation for Traffic Safety: Washington, DC, USA, 2009.
64. Martin, J.L. Relationship between crash rate and hourly traffic flow on interurban motorways. *Accid. Anal. Prev.* **2002**, *34*, 619–629. [CrossRef]
65. Gallelli, V.; Iuele, T.; Vaiana, R.; Vitale, A. Investigating the Transferability of Calibrated. Microsimulation Parameters for Operational Performance Analysis in Roundabouts. *Hindawi J. Adv. Transp.* **2017**, *2017*, 3078063.
66. Choudhary, P.; Imprialou, M.; Velaga, N.R.; Choudhary, A. Impacts of speed variations on freeway crashes by severity and vehicle type. *Accid. Anal. Prev.* **2018**, *121*, 213–222. [CrossRef] [PubMed]
67. Montella, A.; Imbriani, L.L.; Marzano, V.; Mauriello, F. Effects on speed and safety of Point-to-Point speed enforcement systems: Evaluation on the urban motorway A56 Tangenziale di Napoli. *Accid. Anal. Prev.* **2015**, *75*, 164–178. [CrossRef] [PubMed]
68. Wang, J.; Gao, C.; Zhu, Z.; Yan, X. Multi-lane Changing Model with Coupling Driving Intention and Inclination. *Promet Traffic Transp.* **2017**, *29*, 185–192. [CrossRef]
69. Hassan, H.M.; Shawkya, M.; Kishta, M.; Gariba, A.M.; Al-Harthei, H.A. Investigation of drivers' behavior towards speeds using crash data and self-reported questionnaire. *Accid. Anal. Prev.* **2017**, *98*, 348–358. [CrossRef] [PubMed]
70. Soole, D.W.; Watson, B.C.; Fleiter, J.J. Effects of average speed enforcement on speed compliance and crashes: A review of the literature. *Accid. Anal. Prev.* **2013**, *54*, s46–s56. [CrossRef] [PubMed]
71. Farooq, D.; Juhasz, J. Simulation Analysis of Contributing Factors to Rider Visibility Issues for Car-Motorcycle Accidents. *Period. Polytech. Transp. Eng.* **2019**, 1–7. Available online: https://www.researchgate.net/publication/332441297_Simulation_Analysis_of_Contributing_Factors_to_Rider_Visibility_Issues_for_Car-Motorcycle_Accidents (accessed on 25 October 2019).

Arabian Journal for Science and Engineering
https://doi.org/10.1007/s13369-019-03809-7

RESEARCH ARTICLE - SYSTEMS ENGINEERING

Use of Microscopic Traffic Simulation Software to Determine Heavy-Vehicle Influence on Queue Lengths at Toll Plazas

Mohammed Bally Mahdi[1] · Lee Vien Leong[2] · Ahmad Farhan Mohd Sadullah[2]

Received: 24 March 2018 / Accepted: 12 March 2019

Abstract
Highways and expressways provide support for the local, regional, and national transportation of services and goods. Moreover, they are indispensable to economic activities as modern lifestyle would be impossible without them. Activities related to work, education, shopping, tourism, and social are generating a demand for trips. Furthermore, the presence of toll plazas at expressways slows down traffic, thus creating traffic congestion during rush hour. Malaysian toll plazas are considered conventional toll collection, which is manual and the most common toll collection method. Manual toll collection is usually the cause of congestion related to the delay experienced by drivers, toll collection procedure, and operators at the manual toll lanes. This paper aims to examine the effect of the percentage of heavy vehicles on the performance of toll plazas in terms of the queue length using the microscopic traffic simulation model called VISSIM. The findings indicate that the percentage of heavy vehicles in traffic flow significantly affects queue lengths at toll plazas.

Keywords Heavy vehicle · Toll plaza performance · Queue length · Traffic simulation model · VISSIM

1 Introduction

The increased use of tollways and their associated toll plazas is a continuing trend in Malaysia because of the expanding number of vehicles going through airports, entrances of major ports, federal routes, and the growing population in towns and major cities. The manual toll collection implemented at toll gates is one of the main causes of traffic congestion along expressways [1]. Every vehicle that passes through a toll plaza experiences certain delays depending on the type of payment, and queues start to build up when traffic volume for one payment type exceeds the capacity of the plaza for one or all of the payment types [2].

Recently, the examination of toll plazas by employing microscopic simulation software has drawn attention because of the intricacy in analyzing the procedure of toll plaza operations. Microscopic simulation software is commonly adopted as a complementary or alternative instrument in diagnostic procedures and methods for road traffic services and for forecasting future performance according to calculated or expected adjustments in probable operational plans or patterns of vehicle travel demand [3,4]. Thus, traffic simulation models should address the important characteristics of the traffic flow dynamics [5].

Microscopic models with 3D visualization are powerful tools for helping planners and traffic engineers solve specific traffic problems. Through 3D visualization, users are provided with virtual and real-world viewpoints (i.e., helicopter, traffic camera, and vehicle) and allowed to view the simulated area in a rich virtual environment, which contains structures representative of the real world [6]. Assessing the performance of toll plazas and the traffic volume effects under different traffic characteristics and toll plaza configurations is always required. Moreover, visualizing and examining the present and forthcoming traffic procedures at toll plazas is critical.

Toll plazas in the Malaysian expressways system are an interesting subject for two reasons. First, traffic along the expressway is heterogeneous with mixed vehicles composed of cars, small lorries, trucks, trailers, and buses. Second, the toll collection system involves both manual and electronic toll collection, and thus payment time and operation vary according to vehicle class. Furthermore, as the automatic

✉ Mohammed Bally Mahdi
engmohbaly@gmail.com

1 Civil Engineering Department, College of Engineering, Muthanna University, Samawah, Muthanna 66011, Iraq

2 School of Civil Engineering, Engineering Campus, Universiti Sains Malaysia, 14300 Nibong Tebal, Penang, Malaysia

Published online: 19 March 2019

vehicle identification (AVI) system has yet to be adopted in Malaysia, heavy vehicles (trucks, trailers, and buses) are prohibited from using electronic toll lanes. This paper addresses the question of how heavy vehicles in a heterogeneous traffic flow affect toll plaza performance and queue lengths in Malaysia.

2 Literature Review

Microscopic traffic simulation is a useful instrument to simulate traffic flow in roadways under homogeneous and heterogeneous conditions [7]. It has been used as an efficient tool for studying traffic problems [8]. Generally, microscopic traffic simulation models can materialize the intricacies of traffic demand and vehicular flow to enhance the understanding of operational performance in toll plazas [9]. Nonetheless, these models are usually not equipped with built-in toll plaza simulations [10]. Accordingly, researchers have attempted to develop their own simulation models for examining toll plaza performance.

Ito examined the traffic congestion in toll plazas in Kochi I.C., Japan, and offered the results of the process simulation [1]. The developed model considers the redesign of the layout of toll plazas and approximates suitable time in combination gates for gate change to achieve enhanced performance. Astarita [11] and Kuang [12] examined mixed toll stations that operate using various systems of toll collection. The developed model of the car-following model can reveal the toll system performance and uphold its ideal design as a traffic condition function. Moreover, the simulation model is an effective tool to analyze traffic in highway stations. Poon and Dia developed a microscopic traffic simulation model called AIMSUN [13], which can assess the performance of toll booths in the current gateway toll plaza design. The model is employed to quantify and examine the effects of different scenarios to increase efficiency in toll areas. These scenarios include increasing the number of heavy vehicles using the toll booths. According to the study, increasing the usage of toll lanes that adopt fully electronic toll collection (ETC) can greatly improve the system's overall efficiency. Drivers who switch from automatic and manual toll payment methods to the ETC method can experience section times five and ten times faster, respectively, then before. Another research [14] developed and calibrated two different simulation models, namely SHAKER and VISSIM. Both the SHAKER and VISSIM models are potential tools for estimating the maximum throughput and capacity of toll plazas. Therefore, planners and engineers can better develop traffic plans for toll plazas and provide valuable processing time and demand data, which can be used to establish capacities based on lane type, payment type, payment amount, and vehicle type. On the basis of users' perception of service quality at toll plazas, Obelheiro developed a method to examine levels of service at toll plazas [15]. The evaluation of model sensitivity shows that "Mean Queue Length at booths" mostly affects the quality perceived at toll plazas. When queue lengths at booths are increased, users' perception of quality is significantly reduced. Moreover, "Percentage of Trucks" significantly affects service quality perception.

This literature review clearly indicates that many research works are available for evaluating toll plazas using different traffic simulation models. However, studies have not been conducted yet on heavy-vehicle influence on the overall performance of toll plazas in terms of queue length at toll plazas in Malaysia.

3 Methodology

In this paper, a simulation model is developed to assess the implementation of mixed mode (cash/ticket and ETC) toll booth collection. In Malaysia, heavy vehicles (trucks, trailers, and buses) should use the mixed mode lanes even when they can use ETC payment. The model seeks to reflect the effect of different factors on payment time at toll booths. To develop the model and obtain results, data were collected from the case study, the service time process was estimated, the model was constructed and calibrated, and different scenarios were run according to different input parameters.

3.1 Microscopic Simulation Model VISSIM

A variety of traffic simulation packages are available for studying traffic operations at toll plazas. Each of these simulation packages has pros and cons for simulating the toll plaza operation. Previous literature research studied specific simulation packages in terms of capabilities of modeling the traffic facilities [16].

The capabilities of these simulation packages differ widely, and selection of the most appropriate model for a given case depends on several factors such as the requirements and characteristics of the site/toll plaza, cost, objectives of the study, and simulation model capabilities for achieving the objectives.

In this study, VISSIM was chosen to simulate the operations at the Juru toll plazas. It was proved that VISSIM was a very well-suited tool to simulate the traffic operations at toll plazas and its performance based on the requirements and the objectives of this study, and also based on various previous studies conducted around the world [2,17–21].

3.2 Data Collection

The paper was interested in simulating the heavy-vehicle influence within traffic flow condition during maximum weekday peak hours. Figure 1 shows that Friday has the maximum traffic flow in weekdays for both entry and exit directions. The collected field data of the Juru toll plaza were separated by morning peak hour and direction because they differed in terms of number of lanes, lane configuration, toll base fee, traffic volume, vehicle composition, and number of approach lanes for each direction. For entry direction (southbound), the morning peak hour was at 11:00–12:00 and had three approach lanes to the plaza. For exit (northbound), the morning peak hour was at 7:00–8:00 and had two approach lanes as shown in Fig. 2.

To simulate the traffic operation at toll plazas, microscopic field data were needed for each individual vehicle arriving and completing the transaction at the toll plaza. The video recording approach was used to collect field data. Thus, CCTV cameras were needed to be installed at the site to record the traffic operations at the Juru toll plazas. The study required to install CCTV systems at both entry and exit directions. The vehicle composition and service time for mixed mode toll lanes are extracted from CCTV recordings during morning peak hour, as part of the efforts to build the simulation model for Juru toll plaza. Six cameras were used to capture the upstream and downstream traffic flow and the operations at the toll plaza. All six cameras were simultaneously started, and each one captured a different situation. Three of the six cameras were used to capture one direction, and the other three were simultaneously capturing the opposite direction. The following data collections were the requirements for the creation of the Juru toll plaza model.

3.3 Toll Plaza Configuration and Payment Type

The model presented in this paper is based on data collected from a closed toll system Juru toll plaza in Bukit Mertajam, Malaysia. Juru toll plaza is a barrier toll plaza at the North–South Expressway. This kind of toll plaza configuration impedes traffic flow on the expressway, especially during peak hours. Figure 3 shows the configuration for Juru toll which has twenty-three toll lanes. Seven toll lanes are allocated for entry direction (enter the expressway) and sixteen toll booths are allocated for exit direction (exit the expressway).

The lanes in the Malaysian toll plazas are mainly divided into two types: First is the single-class lane (specified only for class 1; these lanes are Smart TAG and Touch ’n Go lanes), and the second is the multiclass lane (specified for all

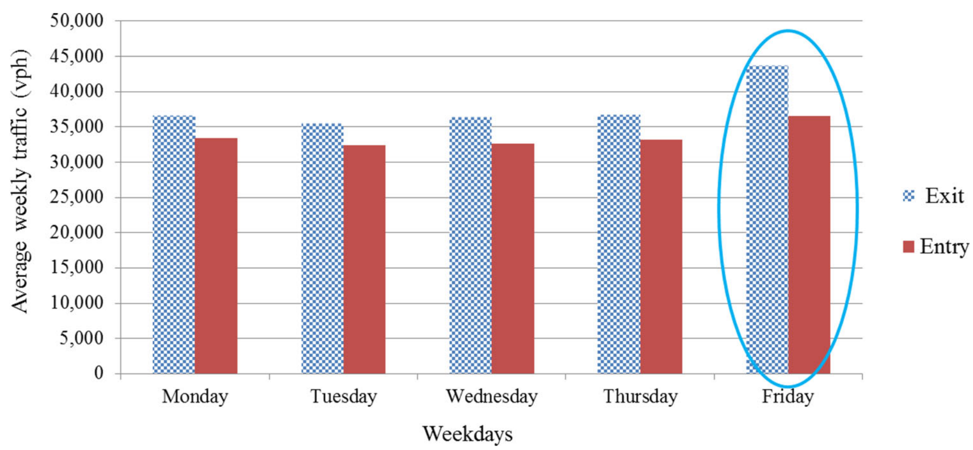

Fig. 1 Average weekly traffic at Juru toll plaza

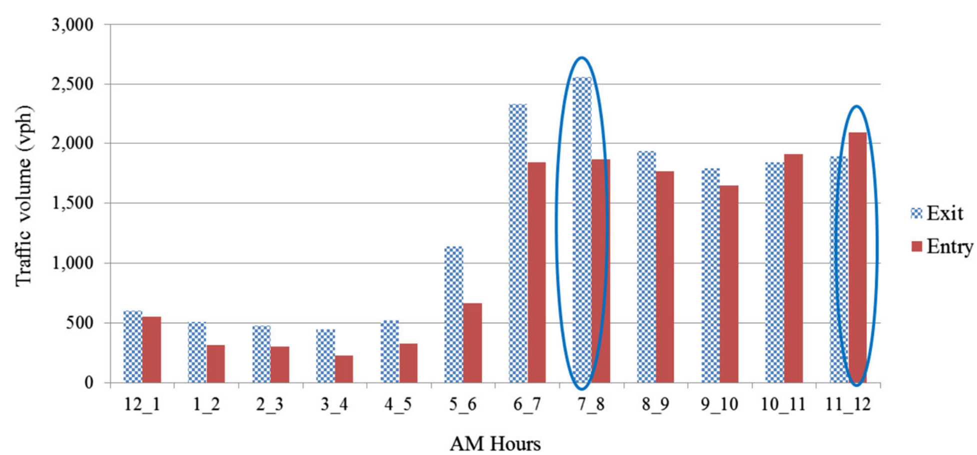

Fig. 2 Friday traffic at AM hours by direction

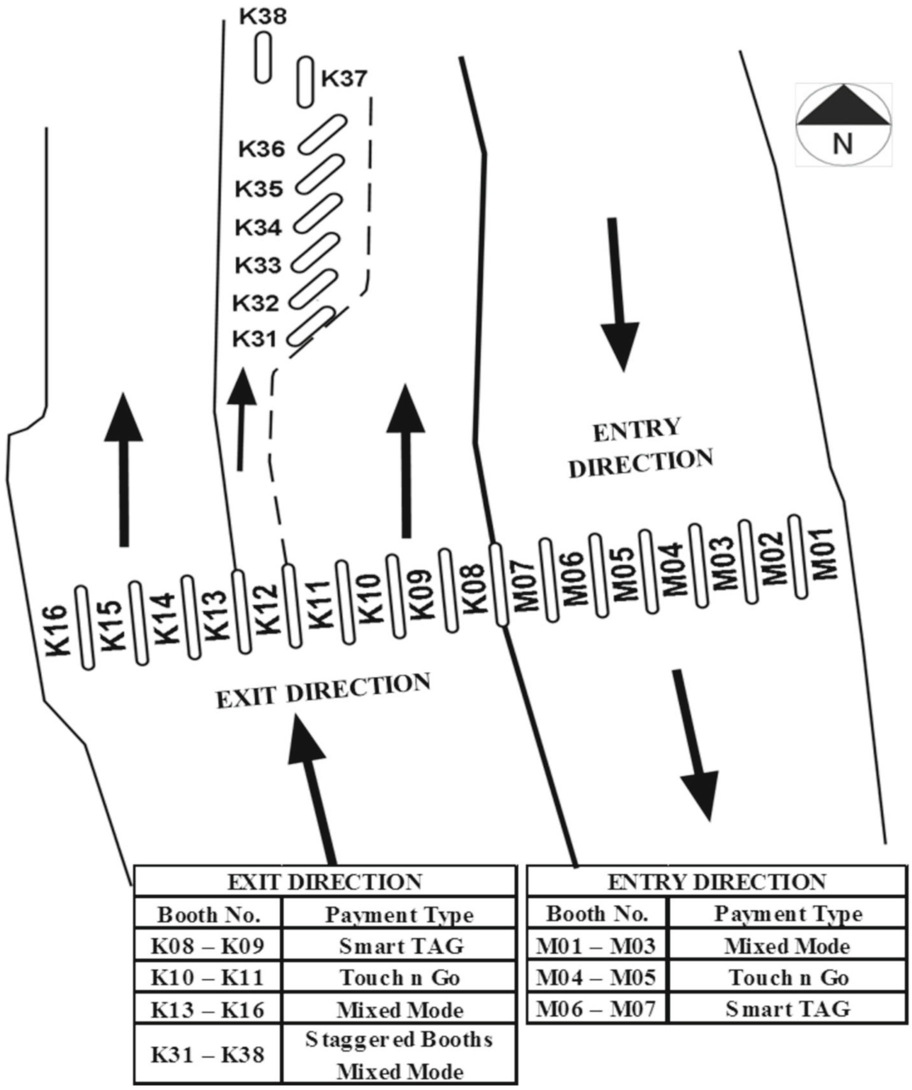

Fig. 3 Juru toll plaza configuration

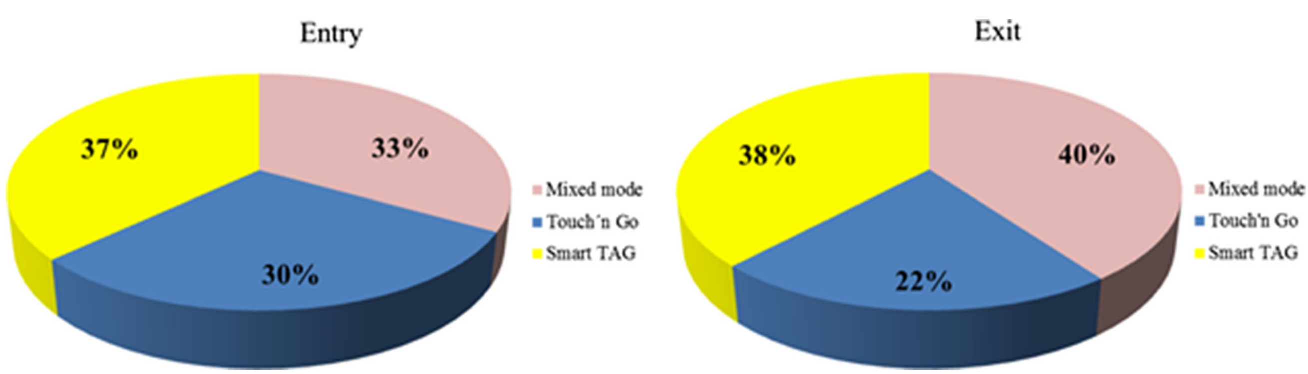

Fig. 4 Percentages of payment type at entry and exit of Juru toll plaza

Vehicle Classification - PLUS			
No	Vehicle class	Icon	Description
1	Class 1		Vehicles with 2 axles and 3 or 4 wheels excluding taxis
2	Class 2		Vehicles with 2 axles and 5 or 6 wheels excluding buses.
3	Class 3		Vehicles with 3 or more axles.
4	Class 4		Taxis
5	Class 5		Buses

(a)

Vehicle type - Simulation model			
No	Vehicle type	Icon	Description
1	Type 1		Car and Taxi
2	Type 2		Small lorry (2 axles and 6 wheels)
3	Type 3		Truck (3 or more axles. With length 8.5-13.0 m)
4	Type 4		Trailer (3 or more axles. With length more than 13.0 m)
5	Type 5		Bus

(b)

Fig. 5 Vehicle classifications; **a** vehicle classification adopted by PLUS, **b** vehicle type used in the simulation model

types of vehicles including heavy vehicles; these lanes are for mixed mode toll collection). Methods of toll payment at toll plazas in Malaysia can be divided into three types. The first and most common method of payment is by cash/ticket in which a toll collector/ attendant is required at the toll booth to collect the cash, dispense the change (if any), and issue the ticket to the patron (upon request). The second method of payment is using the Touch 'n Go card which uses contactless smart card technology (electronic toll collection ETC). Both methods for cash/ticket and Touch 'n Go vehicles need to stop to make the payment. The last method of toll payment is by using Smart TAG which is a nonstop automatic payment system for toll network. The system can make the payment transaction within 20 km/h maximum speed for passing vehicles. Furthermore, Smart TAG and Touch 'n Go toll lanes can be used only by cars, mixed mode toll booths allowable for all vehicles class including the heavy vehicles that use the manual or ETC methods.

Figure 4 shows the percentage of average payment types for Fridays morning peak hour in Juru toll plaza for both directions. At entry direction, mixed mode lanes processed 33% of traffic, Touch 'n Go lanes processed 30%, and Smart TAG lanes processed 37% of the traffic. At the exit direction, the traffic was different where mixed mode lanes processed 40%, Touch 'n Go lanes processed 22%, and Smart TAG lanes processed 38% of the traffic. The study will focus on mixed mode because it presents the traffic composition which contains the heavy vehicles.

3.4 Vehicle Type

Vehicles in the Malaysian expressways (closed system) are divided into five classes according to the vehicle classification adopted by PLUS based on the toll fare and the number of axles and wheels. However, due to reason of passenger cars and taxis having the same vehicle characteristics and thus behaving in the same manner, they were grouped in the same vehicle type in the simulation model. Also, based on field data, huge variations were observed in terms of vehicle length for trailer even though they are classified as vehicles having three or more axles.

The variation in vehicle length for trailers impacts the toll operation. Therefore, vehicles in this class are divided into trucks (heavy vehicles having three or more axles with a vehicle length of between 8.5 and 13.0 m) and trailers (having three or more axles with a vehicle length of more than 13.0 m).

Figure 5a shows the vehicle classification adopted by PLUS, while Fig. 5b shows the vehicle type used in the simulation model.

In VISSIM, vehicles are assigned to certain types and combined with vehicle classes. However, vehicle types needed to be assigned to vehicle categories first. Vehicle categories, by default, contain categories of vehicles with similar traffic interaction. A vehicle type allows the user to form a group of vehicles with the same technical driving characteristics.

Table 1 Vehicle classes that are used in the Juru toll plaza model

No.	Class name		Payment type	Lane type
	Entry	Exit		
1	Car STAG	Car STAG	Smart TAG	Single-class lanes
2	Car TNG	Car TNG	Touch 'n Go	Single-class lanes
3	Entry car ticket	–	Ticket	Multiclass lanes
4	Entry car Tng	–	Touch 'n Go	Multiclass lanes
5	–	Exit car cash	Cash	Multiclass lanes
6	–	Exit car Tng	Touch 'n Go	Multiclass lanes
7	Entry small lorry ticket	–	Ticket	Multiclass lanes
8	Entry Small lorry Tng	–	Touch 'n Go	Multiclass lanes
9	–	Exit small lorry ticket	Cash	Multiclass lanes
10	–	Exit small lorry Tng	Touch 'n Go	Multiclass lanes
11	Entry truck ticket	–	Ticket	Multiclass lanes
12	Entry truck Tng	–	Touch 'n Go	Multiclass lanes
13	–	Exit truck cash	Cash	Multiclass lanes
14	–	Exit truck Tng	Touch 'n Go	Multiclass lanes
15	Entry trailer ticket	–	Ticket	Multiclass lanes
16	Entry trailer Tng	–	Touch 'n Go	Multiclass lanes
17	–	Exit trailer cash	Cash	Multiclass lanes
18	–	Exit trailer Tng	Touch 'n Go	Multiclass lanes
19	Entry bus ticket	–	Ticket	Multiclass lanes
20	Entry bus Tng	–	Touch 'n Go	Multiclass lanes
21	–	Exit bus cash	Cash	Multiclass lanes
22	–	Exit bus Tng	Touch 'n Go	Multiclass lanes

In this step in developing the VISSIM toll plaza model, the traffic composition was created to differentiate different vehicle behaviors in the simulated model. The traffic composition in VISSIM allows the user to insert the relative flows of each link and the desired speed for each vehicle class. In this study, the traffic composition consists of five vehicle classes using three methods of payment.

The difficulty in this stage of the simulation of toll plaza operations was on how to simulate the real vehicle classes in the Juru toll plazas. As previously mentioned, the vehicles at the toll plazas are classified into five classes: cars, small lorries, trucks, trailers, and buses. These classes used three types of payment, namely mixed mode, Touch 'n Go, and Smart TAG. The mixed mode payment in the entry direction is different from the exit direction in terms of procedure, payment type, and service time.

To solve this complexity, the vehicles are classified into two types at the toll plaza according to the toll lane selection: vehicles that select single-class lanes and vehicles that select multiclass lanes. The vehicles that select single-class lanes were cars that used the Touch 'n Go payment and the cars that used Smart TAG payment. Both these two classes are used in the entry and exit directions. The vehicles that selected the multiclass lanes were the vehicles that used the mixed mode payment.

As a result, twenty-two classes of vehicles in the VISSIM model needed to be created to represent the real traffic operation at the toll plazas. Table 1 shows the created vehicle classes in the toll plaza model for the Juru toll plaza.

3.5 Traffic Composition

Traffic composition represents the proportions of different vehicle types in the traffic flow. This is useful to control the way vehicles behave and react in the toll plaza and to incorporate the differences in terms of their operational performance in the simulation model. Traffic compositions are important because vehicle travel routes are assigned for specific vehicle types [22]. In addition, the service time of the mixed mode lane depends upon the arrival pattern of vehicles. Moreover, the traffic composition in the toll plaza modeling concepts is not only focused on the proportions of different vehicle types in the traffic flow but also on the proportion of the traffic flow based on the toll lane types (payment methods).

Figure 6 shows the traffic composition for the entry to the lanes with a traffic volume of 2501 vph, which consists of 85.5% cars, 7.7% small lorries, 1.8% trucks, 3.5% trailers, and 1.6% buses, while the traffic composition at the exit lane with a traffic volume of 2920 vph, which consists of 83.9% cars, 8.5% small lorries, 2.6% trucks, 4.2% trail-

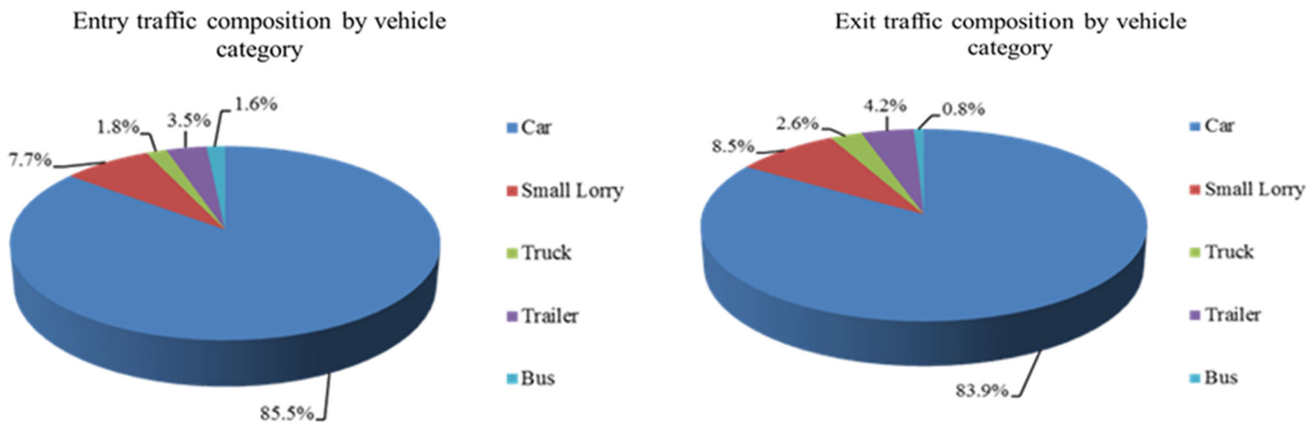

Fig. 6 Traffic composition percentages at Juru toll plaza for entry and exit

ers, and 0.8% buses. The percentage for the heavy vehicle (HGV = Truck + Trailer + Bus) in entry direction is 6.9% and that for the exit direction is 7.6%.

3.6 Desired Speed Distribution

The desired speed distribution is an estimation of the upstream speed of the approaching vehicle toward the toll plaza. The distribution function of the desired speeds is a particularly important parameter because it impacts the link capacity and the queuing at the tollbooths and, thereby, the operation of the toll plazas.

A driver will travel at his desired speed if not hindered by other vehicles or network objects. A driver, whose desired speed is higher than his current speed, will check whether he can overtake other vehicles without endangering anyone. The more the speed of the drivers differs, the more the platoons are created.

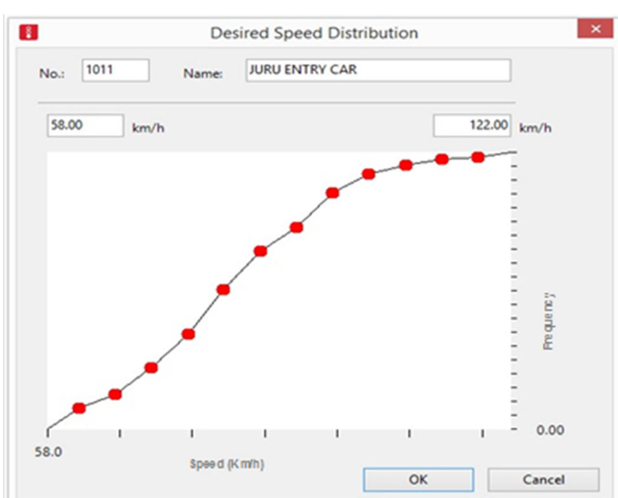

Fig. 7 Desired speed distribution of vehicle class in VISSIM toll plaza model—example

In VISSIM, the desired speed distributions are defined depending on vehicle class, which are used for the command of vehicle compositions. The desired speeds at toll plazas varied according to the toll plaza type, toll plaza location, approach direction, and vehicle class. Thus, the observed speeds from the Juru toll plaza were classified into five categories for both entry and exit directions to meet the needs of the VISSIM toll plaza model. The use of distributions of the values of the desired speeds rather than the average speeds makes the created model more accurate in representing the real traffic operations of toll plaza.

The speed data observations were collected from the Juru toll plazas using a laser speed gun on March 2015. Figure 7 shows an example of the desired speed distribution for the vehicle type in the VISSIM toll plaza model.

3.7 Service Time

Service time, in its general definition, is the time interval between time when the wheels of a vehicle stop rolling at the tollbooth and the time when they start rolling again. In other words, service time is the time a vehicle spends to complete a transaction at the tollbooth; it does not include the delay time in the queue before entering the tollbooth [23,24].

Service time is an important parameter for the evaluation of the operational performance of a toll plaza. Several factors influence the actual service time in electronic toll collection (ETC) and manual toll collection (MTC), such as the type of vehicle making the payment [25–28], the fee value [28], the traffic composition [29,30], the processing efficiency of the electronic toll collection (ETC) technology, and the efficiency of the tollbooth attendant [24]. These factors are helpful in understanding questions such as why cars have different service times from trucks, or why the vehicles of the same class have different service times for same direction of the travel.

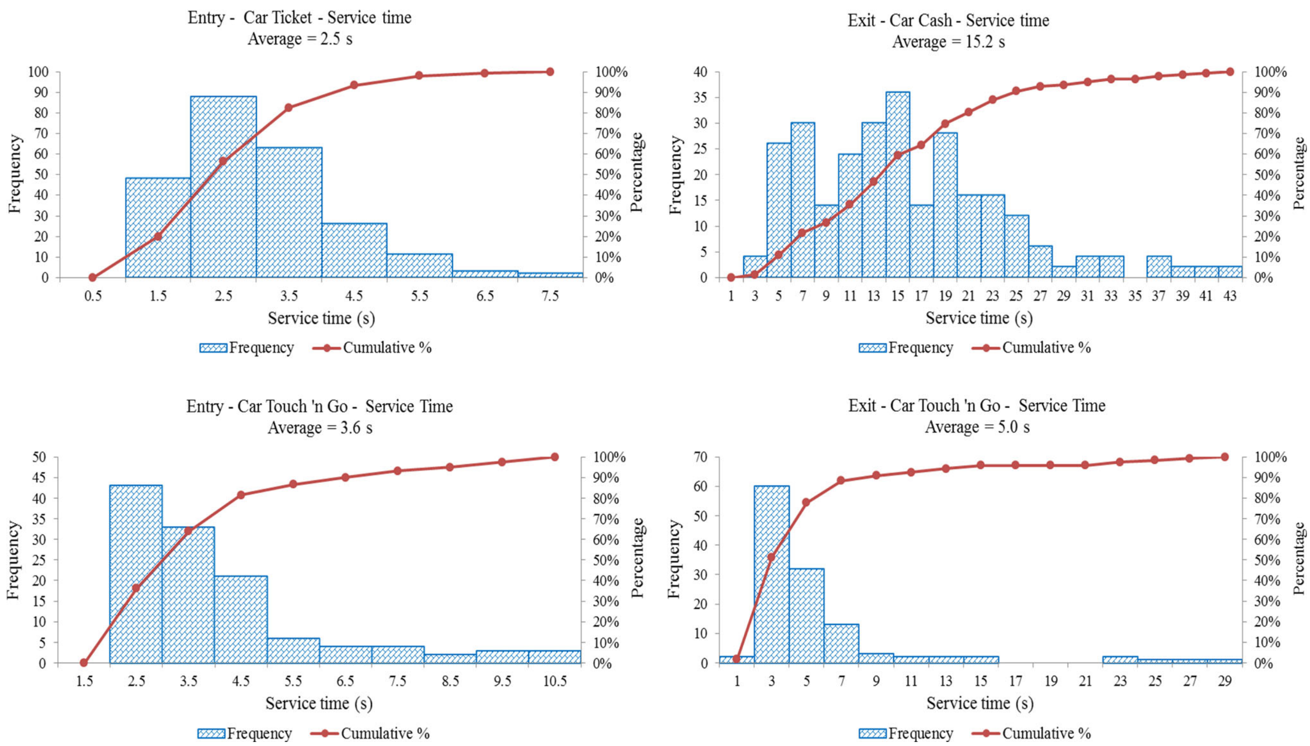

Fig. 8 Frequencies and cumulative curves of service time for car at Juru toll plaza; **a** Entry—ticket and Touch ’n Go, **b** exit—cash and Touch ’n Go

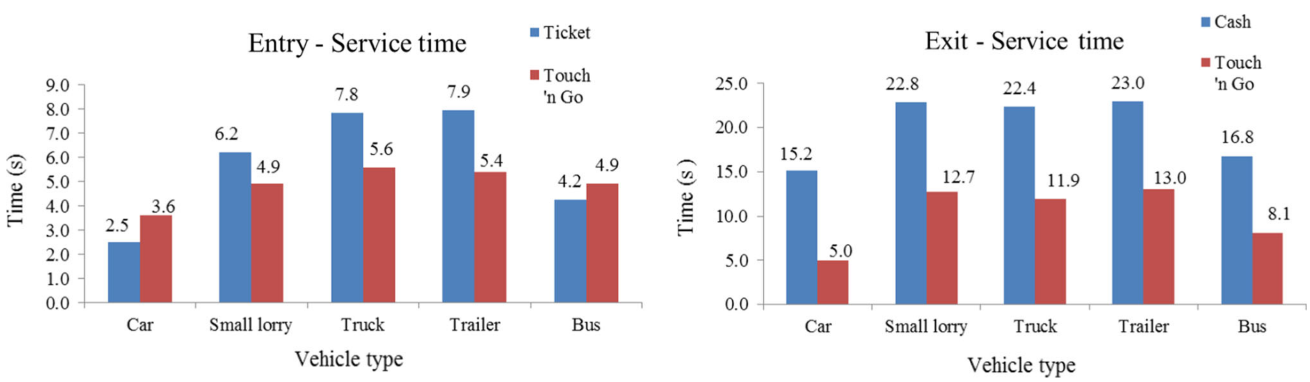

Fig. 9 Service times at Juru toll plaza of mixed mode lanes for ticket and Touch ’n Go based on vehicle type—entry and exit

In a conventional tollbooth, service time is measured from the time the vehicle stops at the tollbooth until it starts moving. For nonstop ETC lanes, the vehicle must decelerate within the speed limit while passing through the toll plaza. Given that the ETC vehicle transacts without stopping at the tollbooth, the service time for the nonstop ETC vehicle in this case is equal to zero [21].

Service time is one of the main input parameters in the toll plaza model, which most significantly influences the performance of toll operation and, thus, the overall toll plaza capacity.

The service time in the mixed mode lanes is the time in seconds that a vehicle spends at a tollbooth to pay a toll until it starts moving. This principle gave the procedure for the observation and extraction of data of the vehicle service time from video recordings for each individual vehicle when it stopped at the tollbooth to make payment.

The determination of the service time at this type of toll plaza (conventional toll plaza) becomes too complex, especially at the multiclass mixed mode toll lane. The complexity comes from the fact that the multiclass mixed mode toll lanes have five types of vehicles, with each type having its own service time. Furthermore, the service time is different, whether at entry or exit, for a particular vehicle type.

According to the VISSIM model requirements, service times need to be represented as cumulative curves. Therefore, Fig. 8 shows an example of the frequencies and cumulative

Fig. 10 Dwell time distribution for vehicle types at multiclass lane—Juru toll plaza—entry—ticket; **a** car, **b** small lorry, **c** truck, **d** trailer, **e** bus

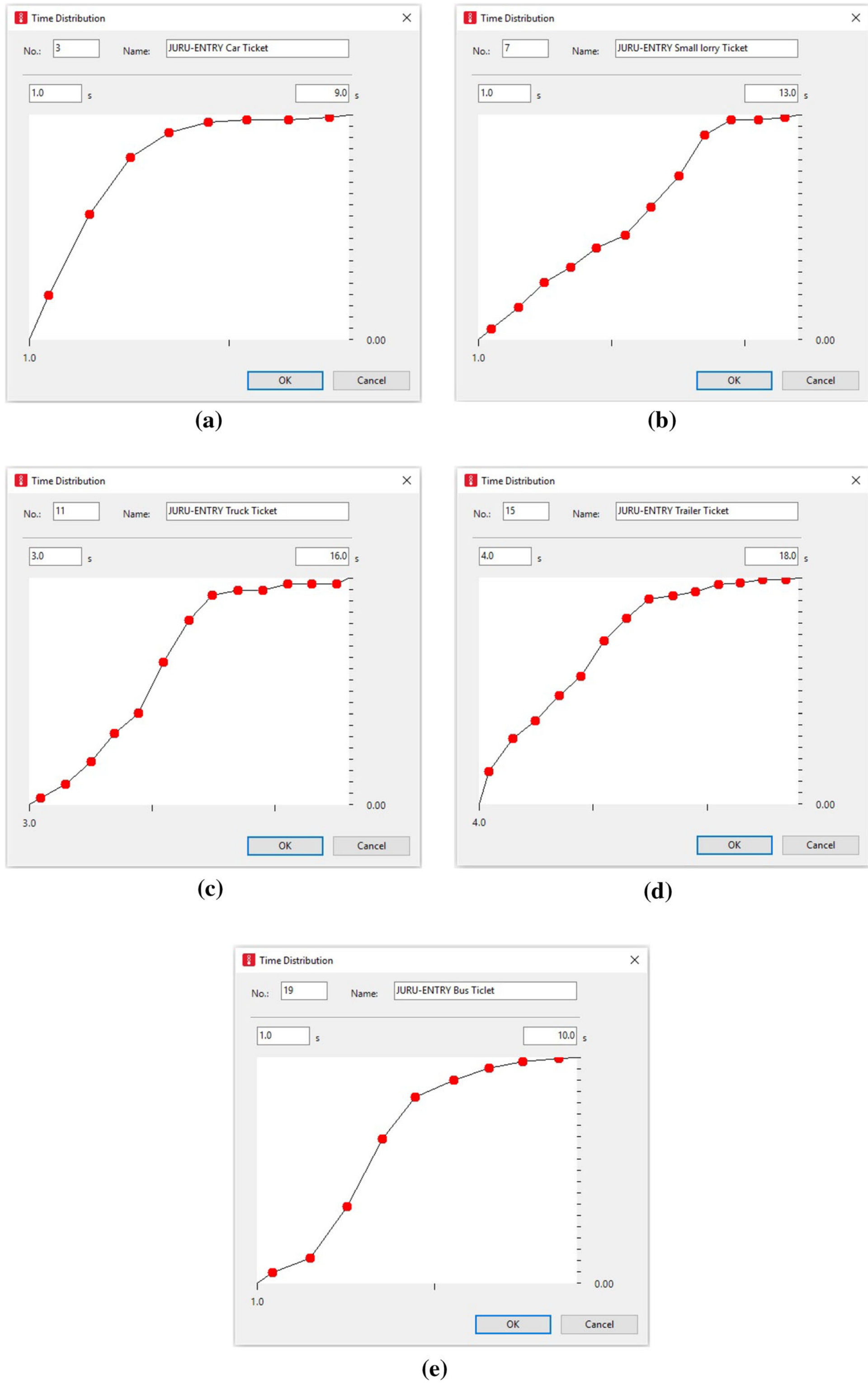

Fig. 11 Flowchart of the calibration process of the simulation

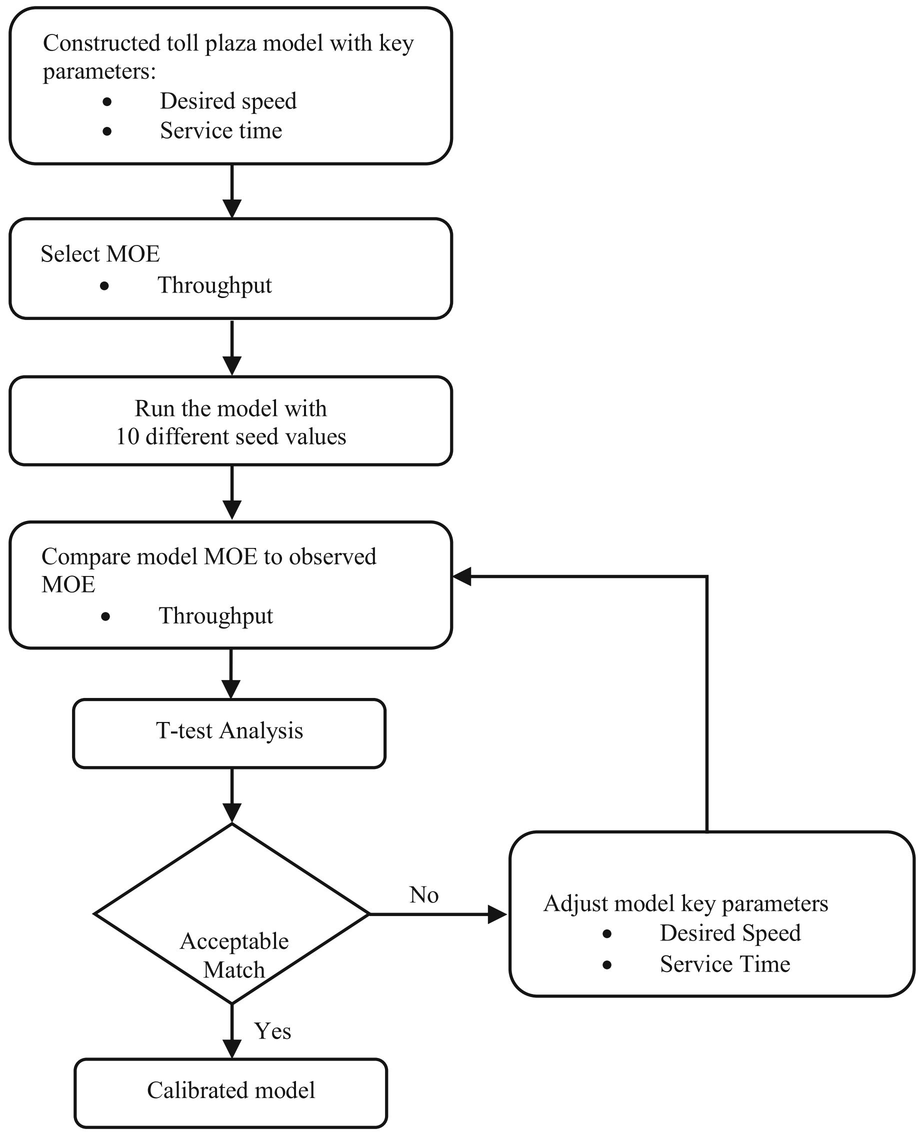

curves of the measured service time for cars in mixed mode lanes.

Figure 9 shows the summary of the service times at entry and exit of mixed mode lanes for ticket and Touch 'n Go based on vehicle type in Juru toll plaza. For entry, the maximum service times for ticket and Touch 'n Go for truck and trailer were (7.8 and 7.9) s and (5.6 and 5.4) s, respectively. For exit, the maximum service times for cash and Touch 'n Go for small lorry, truck, and trailer were (22.8, 22.4, and 23.0) s and (12.7, 11.9, and 13.0) s, respectively.

4 Development of Toll Plaza Models

Once the requirements of the basic features used to build the toll plaza models were completed, the base models of the Juru toll plaza were created with the necessary inputs related to the real toll plazas. The necessary inputs are:

1. The satellite image is used to match the information on the number of lanes in the toll plaza and the geometry of toll plaza area. Additionally, the configurations of the toll plaza are represented by the number of the toll lanes dedicated for each type of payment.
2. The desired speed distribution, which is a particularly important parameter, impacts the link capacity and the queuing at the tollbooths and thereby the operation of the toll plaza.
3. The service time is the distribution for each vehicle type needing to stop to make a payment in the toll lane of the toll plaza. For Juru toll plaza model in this paper, there are twenty service time distributions. For each direction in the mixed mode lanes, there are five types of vehicles

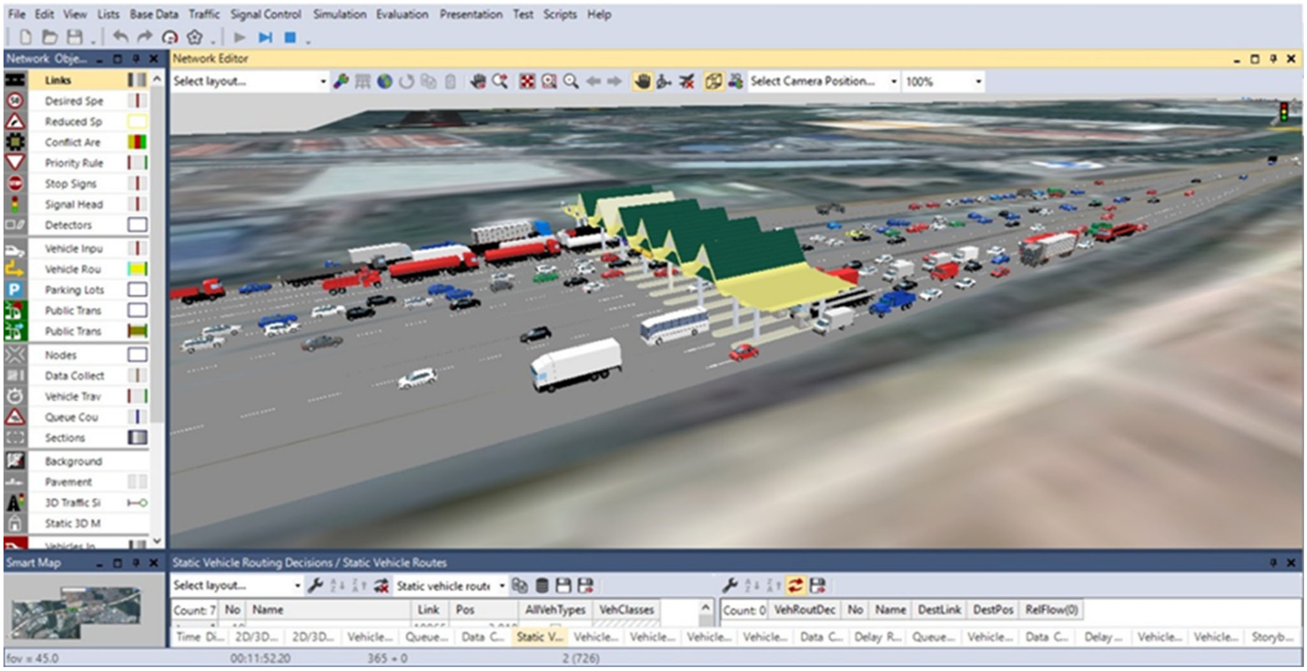

Fig. 12 Screen-captured image of the calibrated model for Juru toll plaza

with two payment types: 10 service time distributions for entry and 10 service time distributions for exit. Figure 10 shows an example of the dwell time distributions (service time) input for vehicle types in the VISSIM model of Juru toll plaza at entry.

5 Calibration of the Model

Calibration is a process of adjusting the model's parameters to improve the model's ability to accurately reproduce traffic operation characteristics [31]. Calibration is performed on various components to replicate observed data to a sufficient level to satisfy the objectives of the model [7].

Calibration is necessary because no single model is equally accurate for all possible traffic conditions. Even the most detailed microsimulation model still contains only a portion of all of the variables that affect real-world traffic conditions. Therefore, every model must be adapted to local conditions [32].

The procedure of the toll plaza model calibration was divided into several steps. The first step was to select the measure of effectiveness MOE (throughput) [33] as the index of comparison between the simulated and observed values. Second, the simulation models for 10 different values were run and the outputs of the selected MOE were obtained [7,13,31]. Then, the statistical paired two-sample t test analysis with 95% level of confidence was used to compare the observed MOE values with the outputs from the simulation results [31].

If the value of the calculated MOE T test was less than the t critical value (from the table), the simulation outputs show a statistical significance of similarity to the observed MOE, and thus, the model of the Juru toll plaza was calibrated. However, when the value of the calculated MOE T test was greater than the t critical value (from the table), a significant difference is seen between the simulated and observed values of the MOE; thus, the model's key parameters need more adjustments depending on the field observation and the simulation reruns for 10 different values. A multiple of 10 simulation runs with different values of the key parameters were done until the calibration was completed.

Figure 11 shows the flowchart of the calibration process, while Figure 12 shows the screen capture of the calibrated model for the Juru toll plaza.

6 Examination of Effect of Heavy Vehicles on Queue Lengths at Juru Toll Plaza

This study aims to construct traffic simulation models of the Juru toll plaza based on the calibration model. Firstly, the newly proposed models are used as scenarios to represent different traffic conditions at the toll plaza, from which the impact of heavy-vehicle percentages on queue lengths along the mixed mode toll lanes is tested. Secondly, the influence of heavy-vehicle percentages on queue lengths along other toll lane types is determined. Finally, the influence of payment types and vehicle types on queue lengths is examined.

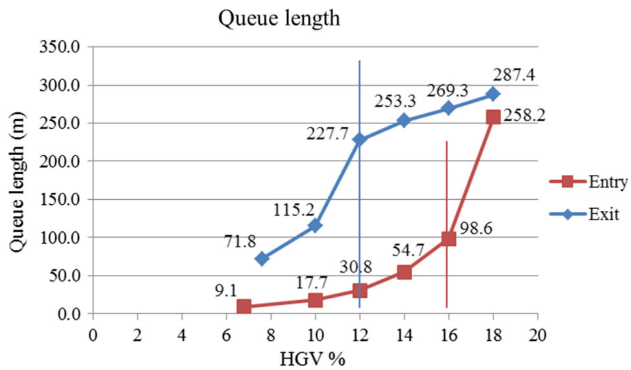

Fig. 13 Impact of heavy-vehicle percentage on queue length along mixed mode lanes of Juru toll plaza

Six scenarios have been identified and simulated to determine the traffic operations of the toll lanes.

1. Scenario 1: base scenario (normal traffic flow)

   Entry: 2501 vph with 6.8% of vehicles are heavy vehicles
   Exit: 2920 vph with 7.6% of vehicles are heavy vehicles

2. Scenario 2: the same traffic volume as in Scenario 1, but heavy-vehicle percentage is increased to 10%, 12%, 14%, 16%, and 18%.

The results obtained in Scenarios 1 and 2 are used to investigate the impact of heavy vehicles on toll plaza operations in terms of queue lengths.

Figure 13 shows the impact of heavy vehicles on queue lengths. Queue length is measured at the end of a 1-h simulation period. At the entry direction (see plotted graphs in Fig. 13), queue length is gradually increased to 16% with increments of heavy-vehicle percentage, after which this queue length is rapidly increased from 98.6 to 258.2 m for 16% and 18% of heavy vehicles, respectively. However, the opposite is observed at the exit direction, in which the queue length is rapidly increased from 71.8 to 227.7 m for 7.6% and 12% of heavy vehicles, respectively, and then the queue length is gradually increased to 287.4 m for 18% of heavy vehicles.

The influence of heavy-vehicle percentage on queue length for other toll lane types is also examined. Figure 14 shows the mixed mode queue lengths for the Touch ’n Go and Smart TAG lanes at the entry and exit directions.

On the basis of the graphs plotted in Fig. 14, heavy-vehicle percentage has no significant influence on other toll lane types at the entry and exit directions.

Figure 15 shows the screen-captured image of the 3D simulation model of the Juru toll plaza, in which the scenario of 18% of heavy vehicles is considered.

With regard to the influence of payment types on queue length with increments of heavy-vehicle percentage, the same case as those of Scenarios 1 and 2 has been adopted, i.e., heavy-vehicle percentages of 6.8%, 10%, 12%, 14%, 16%, and 18% at the entry direction and 7.6%, 10%, 12%, 14%, 16%, and 18% at the exit directions. However, this third case differs in terms of payment type for each vehicle type, particularly for the ticket and Touch ’n Go scheme at entry and the cash and Touch ’n Go scheme at exit. Therefore, new scenarios can be considered. Scenario 1 represents the equality between payment types and vehicle types, that is, the number of vehicles that pay with tickets is equal to the number of vehicles that use Touch ’n Go at entry, and the procedure is the same between cash and Touch ’n Go payment types at exit. In Scenario 2, all vehicle types use Touch ’n Go at entry and exit. In Scenario 3, all vehicle types pay with tickets at entry and cash at exit.

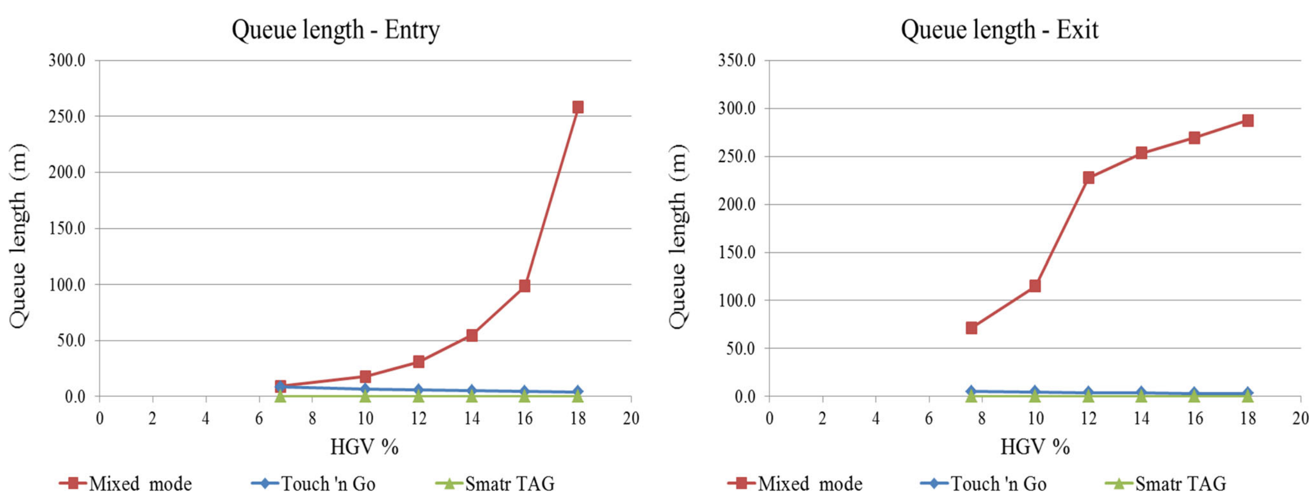

Fig. 14 Queue length results of the Juru toll plaza model at entry and exit directions

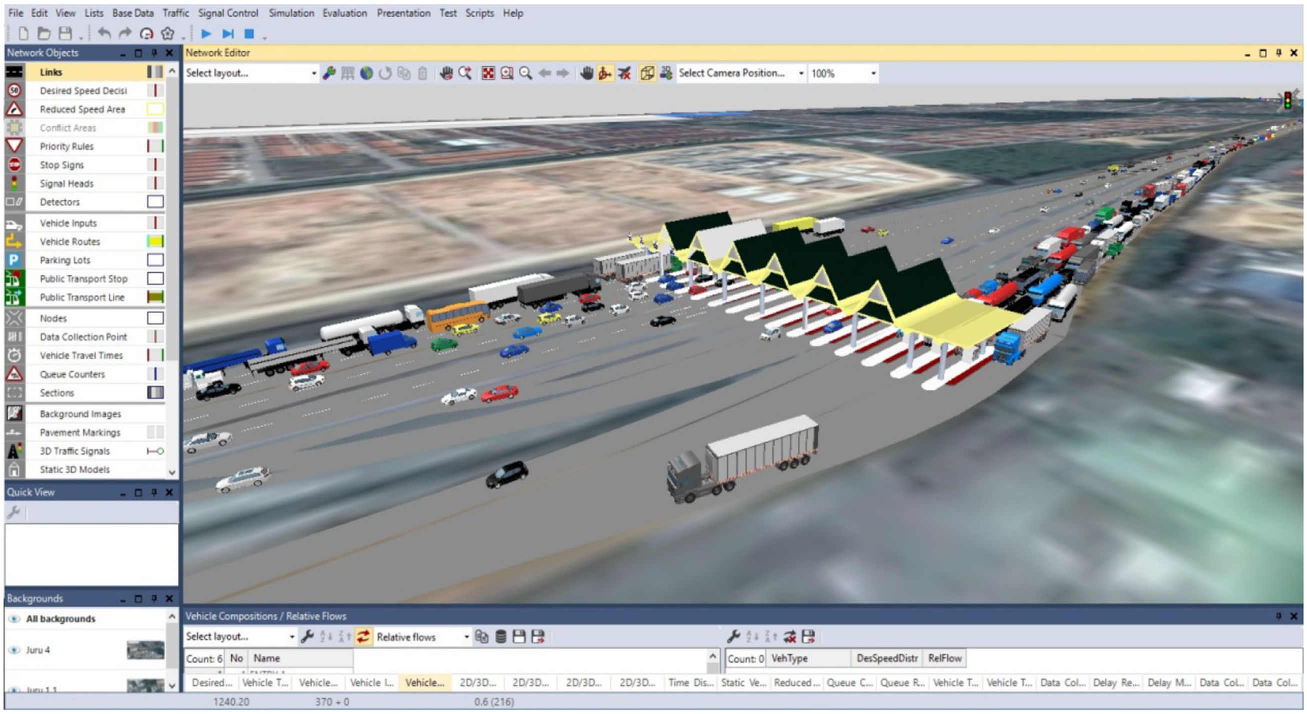

Fig. 15 Screen-captured image of the 3D simulation model of Juru toll plaza

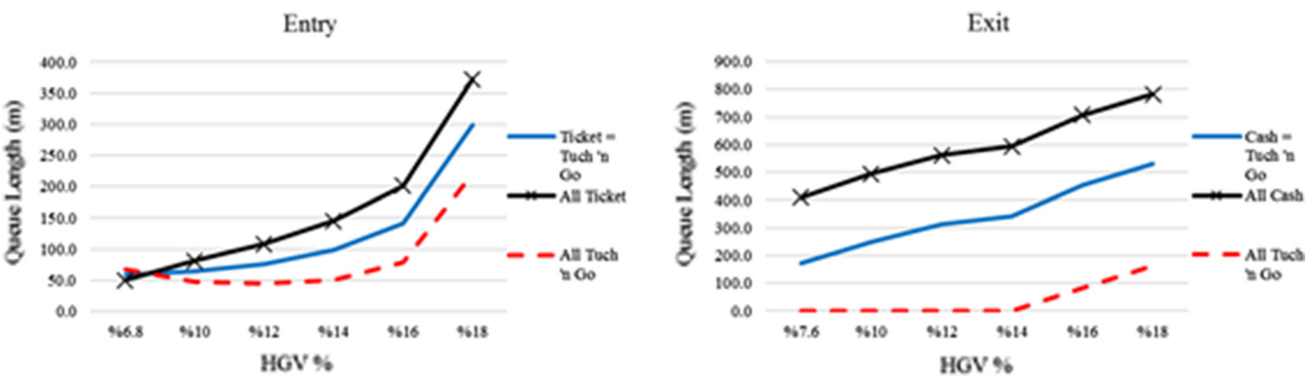

Fig. 16 Influence of payment types on queue length at the entry and exit directions of the Juru toll plaza model

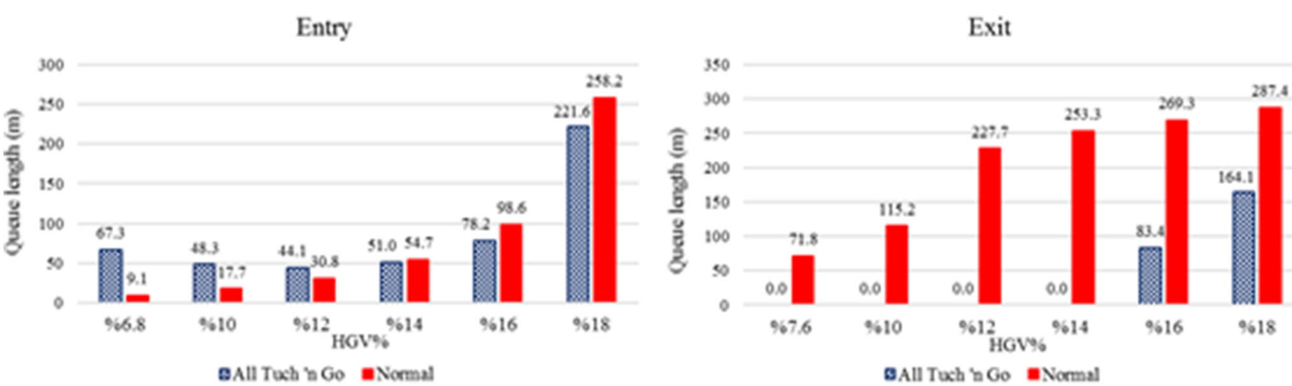

Fig. 17 Comparison between queue lengths after increments of heavy-vehicle percentages and after all vehicles use Touch 'n Go at the entry and exit directions of the Juru toll plaza model

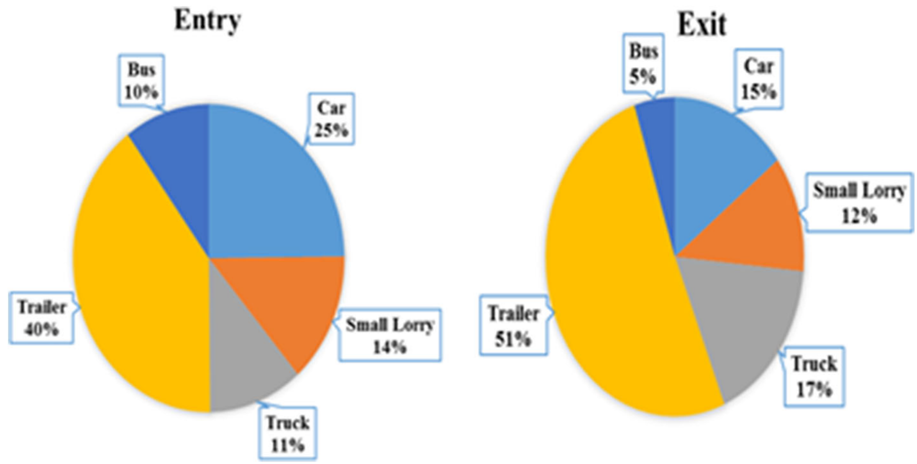

Fig. 18 Influence of vehicle types on queue length at the entry and exit directions of the Juru toll plaza model

As shown in Fig. 16, the best case of queue lengths at the entry and exit directions can be realized when all vehicles use the Touch 'n Go payment type, which is depicted by Scenario 3. Figure 17 shows the comparison between queue lengths in two cases, namely after increments of heavy-vehicle percentage and after all vehicles change to the Touch 'n Go payment type. The results show that the queue lengths after increments of heavy-vehicle percentage can be improved by approximately 80% when all vehicles use Touch 'n Go at exit. However, at the entry directions, the improvement in queue length can be achieved only when heavy-vehicle percentages exceed 14%; in this case, the improvement rate is 17%.

To further determine the influence of vehicle types on queue length with increments of heavy-vehicle percentage, a scenario the same as that of Scenario 1 (i.e., equality between payment types for all vehicle types) has been adopted. In particular, the number of vehicles that correspond to a certain queue length is calculated, and the percentages of all types of queued vehicles are determined. The reason for selecting Scenario 1 is to neglect the impact of payment types on the results. Figure 18 shows that most queue lengths at the entry direction comprise 40% of trailers, 25% of cars, and 14% of small lorries, whereas most queue lengths at the exit direction comprise 51% of trailers, 17% of trucks, and 15% of cars.

7 Conclusions

The main goal of this study is to examine the impact of percentage of heavy vehicles in the Malaysian expressway system on the performance of Juru toll plaza in terms of vehicle queue length. The microscopic simulation software called VISSIM was used to construct the Juru toll plaza model and investigate toll operations. The results of the calibration prove that VISSIM is a suitable tool for simulating heterogeneous traffic flow and can accurately replicate the real-world operations of the toll plaza. Moreover, the results show that the percentage of heavy vehicles in traffic flow has a significant impact on queue length at the Juru toll plaza. The significant impact of heavy-vehicle percentages starts from 16% and 7.6% at the entry and exit directions, respectively. The results also show that heavy-vehicle percentage has no influence on ETC lanes at entry and exit. Most queue lengths have been caused by trailers that represent 40% and 51% of the total queue length at entry and exit, respectively. The best procedure for improving queue length at the entry and exit directions at the Juru toll plaza is by changing the payment type to Touch 'n Go for all vehicle types.

Acknowledgements The authors gratefully acknowledge the financial support from Malaysian Highway Authority (Project No. 304/PAWAM/6050289/L121). Also, the authors wish to express their sincere gratitude to Universiti Sains Malaysia.

References

1. Ito, T.: Process simulation approach to design and evaluation of toll plaza with ETC gates. I. J. Simul. **6**, 14–21 (2002)
2. Aycin, M.; Kiskel, K.; Papayannoulis, V.; Davies, G.: Development of methodology for toll plaza delay estimation for use in travel demand model postprocessor. Transp. Res. Rec. J. Transp. Res. Board **2133**, 1–10 (2010). https://doi.org/10.3141/2133-01
3. Kieninger, D.; Beaulieu, M.; Davis, K.: A guide to documenting Vissim-based microscopic traffic simulation models (2007)
4. Mahdi, M.B.; Leong, L.V.: Assessment of queue length and delay at toll plaza using microscopic traffic simulation. Appl. Mech. Mater. **802**, 387–392 (2015). https://doi.org/10.4028/www.scientific.net/AMM.802.387
5. Rassafi, A.A.; Davoodnia, P.; Pourmoallem, N.: Modeling traffic flow on urban highways: the application of cellular automata and nested logit. Arab. J. Sci. Eng. **37**, 1557–1570 (2012). https://doi.org/10.1007/s13369-012-0277-3
6. Boxill, S.A.: An evaluation of 3-D traffic simulation modeling (2007)
7. Bains, M.S.; Ponnu, B.; Arkatkar, S.S.: Modeling of traffic flow on Indian expressways using simulation technique. Procedia Soc.

Behav. Sci. **43**, 475–493 (2012). https://doi.org/10.1016/j.sbspro.2012.04.121
8. Ratrout, N.T.; Rahman, S.M.; Reza, I.: Calibration of PARAMICS model: application of artificial intelligence-based approach. Arab. J. Sci. Eng. **40**, 3459–3468 (2015). https://doi.org/10.1007/s13369-015-1816-5
9. Al-Deek, H.; Mohamed, A.; Radwan, E.: A new model for evaluation of traffic operations at electronic toll collection plazas. Transp. Res. Rec. **1710**, 1–10 (2000). https://doi.org/10.3141/1710-01
10. Liu, Y.; Liao, H.; Yu, Z.; Cai, M.: Analysis of the operational impact of ETC lanes on toll station. In: Proceedings of the 10th International Conference of Chinese Transportation Professionals, Beijing, China, vol. 48, pp. 566–578 (2011)
11. Astarita, V.; Florian, M.; Musolino, G.: A microscopic traffic simulation model for the evaluation of toll station systems. In: 2001 IEEE Intelligent Transportation Systems Conference Proceedings, pp. 692–697 (2001). https://doi.org/10.1109/ITSC.2001.948744
12. Kuang, X.Y.; Zhou, S.; Xu, L.H.: Simulation and experiment for highway toll station. Appl. Mech. Mater. **178–181**, 1786–1789 (2012). https://doi.org/10.4028/www.scientific.net/AMM.178-181.1786
13. Poon, N.; Dia, H.: Evaluation of toll collection performance using traffic simulation. In: 27th Conference of Australian Institutes of Transport Research (CAITR 2005), Brisbane, Dec, pp. 7–9 (2005)
14. Russo, C.S.: The calibration and verification of simulation models for toll plazas (2008)
15. Obelheiro, M.R.; Cybis, H.B.B.; Ribeiro, J.L.D.: Level of service method for Brazilian toll plazas. Procedia Soc. Behav. Sci. **16**, 120–130 (2011). https://doi.org/10.1016/j.sbspro.2011.04.435
16. Fang, F.C.; Elefteriadou, L.: Some guidelines for selecting microsimulation models for interchange traffic operational analysis. J. Transp. Eng. **131**, 535–543 (2005). https://doi.org/10.1061/(ASCE)0733-947X(2005)131:7(535)
17. Aksoy, G.; Celikoglu, H.B.; Gedizlioglu, E.: Analysis of toll queues by micro-simulation: results from a case study in Istanbul. Procedia Soc. Behav. Sci. **111**, 614–623 (2014). https://doi.org/10.1016/j.sbspro.2014.01.095
18. Ceballos, G.; Curtis, O.; : Queue analysis at toll and parking exit plazas: a comparison between multi-server queuing models and traffic simulation. In: ITE 2004 Annual Meeting Exhibition (2004)
19. Lelewski, A.R.; Berenis, J.A.; Pressimone, G.M.: Analyzing express toll plaza operations using modern simulation models. In: Transportation Research Board Annual Meeting CD (2003)
20. Yilin, L.: The analysis of highway toll station ETC lane capacity. In: Fourth International Conference on Transportation Engineering, pp. 2848–2853 (2013)
21. Zhong, L.; Zhou, Y.; Wu, K.: Analysis of level of service of toll lane allocation of Hong Kong–Zhuhai–Macao bridge. In: 14th COTA International Conference of Transportation Professionals, pp. 3743–3751 (2014)
22. Transportation Research Board: Highway capacity manual (2000)
23. Padayhag, G.U.; Sigua, R.G.: Evaluation of Metro Manila's electronic toll collection (ETC) system. J. East. Asia Soc. Transp. Stud. **5**, 1946–1961 (2003)
24. AL-Deek, H.M.; Radwan, A.E.; Mohammed, A.A.; Klodzinski, J.G.: Evaluating the improvements in traffic operations at a real-life toll plaza with electronic toll collection. J. Intell. Transp. Syst. **3**, 205–223 (1996)
25. Zarrillo, M.L.: Development and applications of TPMODEL: a queuing model describing traffic operations during electronic toll collection (ETC) (1998)
26. Zarrillo, M.L.; Radwan, A.E.: Methodology SHAKER and the capacity analysis of five toll plazas. J. Transp. Eng. **135**, 83–93 (2009). https://doi.org/10.1061/(ASCE)0733-947X(2009)135:3(83)
27. Woo, T.H.; Hoel, L.H.: Toll plaza capacity and level of service. Transp. Res. Rec. **1320**, 119–127 (1991)
28. Oliveira, M.L.; Cybis, H.B.: An artificial neural network model for evaluating workers' performance at tollbooths. In: 1st International Symposium on Freeway and Tollway Operations, vol. 2, pp. 1–38 (2006)
29. Zarrillo, M.L.; Radwan, A.E.; Al-Deek, H.M.: Modeling traffic operations at electronic toll collection and traffic management systems. Comput. Ind. Eng. **33**, 857–860 (1997). https://doi.org/10.1016/S0360-8352(97)00266-0
30. Zarrillo, M.L.; Radwan, I.A.E.; Mak, A.; Dowd, J.; Cyr, W.: Identification of bottlenecks on a toll network of highways. In: Applications of Advanced Technologies in Transportation, pp. 103–110 (2002)
31. Dowling, R.; Skabardonis, A.; Alexiadis, V.: Traffic analysis toolbox volume III: guidelines for applying traffic microsimulation modeling software (2004)
32. Hourdakis, J.; Michalopoulos, P.G.; Kottommannil, J.: A practical procedure for calibrating microscopic by. Transp. Res. Board **1852**, 130–139 (2003)
33. Klodzinski, J.; Gordin, E.; Al-Deek, H.M.: Evaluation of impacts of open road tolling on main-line toll plaza. Transp. Res. Rec. **2012**, 72–83 (2008). https://doi.org/10.3141/2012-09